THESIS FOR THE DEGREE OF LICENTIATE OF ENGINEERING

Wind Turbine Models for Power System Stability Studies

ABRAM PERDANA

Wind Turbine Models for Power System Stability Studies
ABRAM PERDANA

Technical Report at Chalmers University of Technology

Wind Turbine Models for Power System Stability Studies
ABRAM PERDANA
Division of Electric Power Engineering
Department of Energy and Environment
Chalmers University of Technology

Abstract

The purpose of this thesis is to develop dynamic models of wind turbines for power system stability studies. More specifically, the wind turbine models are mainly intended for voltage and frequency stability studies.

In developing the wind turbine models, each part of the wind turbines are examined to define relevant behaviors that significantly influence the power system response. Correspondingly, mathematical models of these parts are then presented with various possible levels of detail. Simplified models for each part of the wind turbines are evaluated against more detailed models to provide a clear understanding on how model simplifications may influence result validity and simulation efficiency. In order to obtain confident results, the wind turbine models are then validated against field measurement data. Two different cases of validation are then presented. Based on the measurement data of two different wind turbines, most typical behaviors of the wind turbines are discussed. Finally, both conformity and non-similarity between simulation results of the wind turbine models and the field measurement data are elaborated.

Two different methods of predicting stator transient current of a wind turbine generator following a fault are presented. The first method implements a modified fifth-order model of an induction generator which is developed to be compatible with the fundamental frequency network model. The second method utilizes an analytical method in combination with the third-order model of an induction generator. A solution for the implementation of wind turbine models that require a simulation time step smaller than the standard simulation time step is also proposed in the thesis.

In order to comprehend behaviors of wind turbines subject to different power system stability phenomena, a number of simulations are performed in the power system simulation tool PSS/E with the standard simulation time step of 10 ms. Each stability phenomenon are simulated using different wind turbine models. The simulation results are evaluated to determine the most appropriate wind turbine model for each particular power system stability study. It is concluded that a fixed-speed wind turbine model consisting of the third-order model of an induction generator and the two-mass model of a drive train is a compromised solution to provide a single wind turbine model for different types of power system stability studies.

The thesis also presents aggregated models of a wind farm with fixed-speed wind turbines. The result of the simulations are validated against field measurement data.

Keywords: wind turbine, modelling, validation, fixed-speed, variable-speed, power system stability, voltage stability, frequency stability, aggregated model.

Acknowledgements

First of all I would like to thank my supervisor Associate Professor Ola Carlson for his excellent supervision and helps during this work. I would like to express gratitude to my examiner Professor Tore Undeland for providing guidance and encouragement.

I owe a debt of gratitude to Urban Axelsson, because of him I could start and realize this work. My acknowledgments go to all members of the reference group, particularly Elisabet Norgren, for their valuable contributions.

I would like to thank my colleagues within the Nordic Project, Jarle Eek, Sanna Uski and Torsten Lund, for their cooperation and contributions. My gratitude also goes to all members of the Nordic Reference Group, especially Poul Sørensen (RISØ, Denmark), Associate Professor Arne Hejde Nielsen (DTU, Denmark), Bettina Lemström (VTT, Finland), Dr. Kjetil Uhlen (SINTEF, Norway) and Dr. Jouko Niiranen (ABB Oy, Finland), for their fruitful discussions during various meetings.

Special thanks go to Professor Torbjörn Thiringer for his valuable comments and suggestions. I also appreciate Nayeem Rahmat Ullah and Marcia Martins for good cooperation throughout my research and valuable suggestions during the thesis writing. Thanks go to Ferry August Viawan for a good companionship. I would also like to thank Associate Professor Pablo Ledesma, Dr. Evert Egneholm, Dr. Jonas Persson and John Olav G Tande for a good collaboration during writing papers. I also thank all the people working at the former Electric Power Engineering Department for providing such a nice atmosphere.

I want to express my gratitude to all my Indonesian friends in Gothenburg for a wonderful brotherhood and friendship.

My ultimate gratitude goes to my parents, Siti Zanah and Anwar Mursid, and my parents in law, Siti Maryam and Dr. Tedjo Yuwono. It is because of their endless pray, finally I can accomplish this work. My most heartfelt acknowledgement must go to my wife, Asri Kirana Astuti for her endless patient, love and support. Finally, to my sons Aufa, Ayaz and Abit, thank you for your love, which makes this work so joyful.

Table of Contents

x

List of Symbols and Abbreviations

Symbols

Boldface characters denote space vectors or matrices. Unless specified, the quantities are in per unit of the corresponding system.

C_p	Aerodynamic coefficient of performance
D_s	Shaft damping coefficient
h	Integration time step size [seconds]
H_g	Generator inertia constant
H_t	Turbine inertia constant
$\mathbf{I}$	Vector of complex current sources
j	Imaginary operator, $\sqrt{-1}$
$\mathbf{i_r}$	Rotor current vector
$\mathbf{i_s}$	Stator current vector
$\mathbf{i_{s0}}$	Stator pre-fault current
J_g	Generator inertia [kg.m^2]
J_t	Turbine inertia [kg.m^2]
K_s	Shaft stiffness
k	Ratio between magnetizing and rotor reactance (X_m/X_r)
L_m	Magnetizing inductance
L_r	Rotor inductance
L_{rl}	Rotor leakage inductance
L_s	Stator inductance
L_{sl}	Stator leakage inductance

P	Active power
P_{mec}	Mechanical power
Q	Reactive power
R_r	Rotor resistance
R_s	Stator resistance
$\mathbf{S}$	Complex apparent power $(P + jQ)$
s_p	Pull-out slip
T_e	Electric torque
T_m	Mechanical torque
T_o	Transient open-circuit time constant
$\mathbf{V}$	Vector of complex bus voltages
$\mathbf{v_e}$	Thevenin voltage source vector
$\mathbf{v_r}$	Rotor voltage vector
$\mathbf{v_s}$	Stator voltage vector
X_m	Magnetizing reactance
X_r	Rotor reactance
X'_r	Rotor transient reactance
X_s	Stator reactance
X'	Transient reactance
$\mathbf{Y}$	The network admittance matrix
β	Pitch angle, in the context of $C_p(\lambda, \beta)$ [deg.]
λ	Tip speed ratio, in the context of $C_p(\lambda, \beta)$
ω_s	Synchronous rotating speed
ω_r	Rotor speed
$\boldsymbol{\psi_s}$	Stator flux vector
$\boldsymbol{\psi_r}$	Rotor flux vector
σ	Leakage factor
θ_t	Turbine rotor angle [rad.]
θ_r	Generator rotor angle [rad.]

Abbreviations

DFIG   Doubly Fed Induction Generator

OLTC   On-Load Tap Changer

Chapter 1

Introduction

1.1 Background and motivations

By mid-2006, the amount of worldwide installed wind power reached 63 GW [1], and another almost 70 GW of new wind power units is expected to be installed by 2009 [2].

Traditionally, wind power generation has been treated as a distributed small generation or negative load. Wind turbines were allowed to be disconnected when a fault is encountered in the power system. Such a perspective, for instance, does not require wind turbines to participate in frequency control and the disconnection of wind turbines is considered as insignificant for loss of production issues.

However, recently the penetration of wind power is considerably high particularly in some countries such as Denmark (18.5%), Spain (7.8%) and Germany (4.3%) [3]. These figures are equivalent to annual production of wind power over the total electricity demand. Consequently, the maximum penetration during some peak hours can be 4-5 times these figures [4].

As the penetration of wind power into the grid increases significantly, which means that the presence of wind power becomes substantial in the power system, all pertinent factors which may influence the quality and the security of the power system operation must be considered. Therefore, the traditional concept is no longer relevant. Thus, wind power generation is required to provide a certain reliability of supply and a certain level of stability.

Motivated by the issues above, many grid operators have started to introduce new grid codes which treat wind power generation in a special manner. In response to these new grid codes, wind turbine manufacturers now add more features to their products in order to cope with the requirements, for instance fault ride-through capability and other features, which enable the wind turbines to contribute to the power system operation more actively.

Meanwhile, as wind power generation is a relatively new technology in power system studies, unlike other conventional power plant technologies, no standardized model is available today. Many studies on various wind turbine technologies have been presented in literature, however most of the studies are more focused on detailed machine study. Only few studies discuss the effect and applicability in power system studies. In many cases, it was found that the model provided is oversimplified or the other way around, far too detailed with respect to power system stability studies.

Hence, the main idea of this thesis is to provide wind turbine models which are appropriate for power system stability studies. Consequently, some factors that are essential for

stability studies are elaborated in detail. Such factors are mainly related to simulation efficiency and result accuracy. Concerning the first factor, a model construction for specific standardized simulation tool is needed. While for the later factor, validation of the models is required.

Development of aggregated models of wind farms is also an important issue as the size of wind farms and number of turbines in wind farms increases. Thus representing wind farms as individual turbines increases complexity and leads to a time-consuming simulation, which is not beneficial for stability studies of large power systems. Hence, this issue is addressed in the thesis.

Wind turbine technologies can be classified mainly into three different concepts: a fixed-speed wind turbine, a variable speed wind turbine with a partial power converter or a wind turbine with a doubly fed induction generator (DFIG) and a variable speed wind turbine with a full power converter. The fixed-speed wind turbine concept uses either a squirrel cage induction generator or a slip ring induction generator. In case of the wind turbine with a full power converter, different generator types can be employed such as an induction generator and a synchronous generator either with permanent magnets or an external electrical excitation. However, at the moment, the majority of installed wind turbines are of the fixed-speed wind turbines with squirrel cage induction generators, known as the "Danish concept." While from market perspective, the dominating technology at the moment are wind turbines with DFIG. The thesis, however, focuses on the fixed-speed wind turbine technology.

1.2 Related research

Models of wind turbines have been reported in several papers and theses. A great detail discussion on wind turbine models can be found in [5, 6]. However, problems that arises in implementing the model into commercial power system simulation tools, such as problems with the simulation time step and compatibility constraints, are not addressed thoroughly. Some key points concerning this issue, such as the inability of the tool to spot phenomena such as the presence of dc-offset and unbalanced events, has been mentioned briefly in [5] yet no detailed explanations and measures are provided. Furthermore, validation of the model against field measurements, especially during grid fault conditions, is still rarely found in the literature.

Regarding aggregated model of wind turbines, different aggregation methods have been proposed in [7, 8] and [9]. However, validation of these models with measurement data is not available in papers.

A discussion concerning fault ride-through capability for a specific type of wind turbine technologies can be found in several papers, such as for a fixed-speed wind turbine in [10, 11] and for a wind turbine with DFIG in [5, 12, 13, 14].

1.3 Contribution

Several contributions of this thesis can be mentioned as follows:

- Requirements for wind turbine models for different types of stability studies are characterized.

- Implementation of wind turbine models into a common power system stability simulation tool with adequate accuracy and considering a number of constraints, such as minimum simulation time step and compatibility of the models and the tool interface, is addressed.

- Wind turbine models as well as aggregated models of wind turbines are validated.

- The response of the models and potential impact to the power system during frequency deviation is presented.

1.4 Thesis outline

The contents of the thesis are organized into 8 chapters. The first chapter presents the background and motivation of the study.

Chapter 2 introduces a definition and classification of power system stability studies and its relevances for wind power generation. Later, the power system stability simulation tool PSS/E, which is used in this study, is described. The chapter describes the numerical integration methods used in the tool and the influence of the methods on simulation time. The knowledge from this discussion is required to find out the most appropriate wind turbine model.

Chapter 3 discusses modelling of a fixed-speed wind turbine. Different levels of detail for wind turbine models are presented. The appropriateness of the models is then examined from the perspective two factors, i.e. simulation efficiency and result validity. The models described in Chapter 3 are then validated against field measurement data, which are presented in Chapter 4

A number of power system stability phenomena are simulated in Chapter 5. Based on simulation results, the most appropriate model for a particular study is then proposed.

An aggregated model of a wind farm consisting of fixed-speed wind turbines is presented in Chapter 6. The study emphasizes dynamic responses of the wind farm during a fault. The model is then validated against field measurement data.

The fault ride-through scheme of different wind turbine technologies are reviewed in Chapter 7 along with a discussion of the impact of these schemes on the system during a fault.

A summary of all findings in the thesis along with proposals for future research are presented in Chapter 8.

1.5 Publications

Major parts of the results presented in this thesis have been published in the following publications.

1. O. Carlson, A. Perdana, N.R. Ullah, M. Martins and E. Agneholm, "Power system voltage stability related to wind power generation," in *Proc. of European Wind Energy Conference and Exhibition (EWEC)*, Athens, Greece, Feb. 27 - Mar 2, 2006.

   This paper presents an overview of voltage stability phenomena in power system in relation to wind power generation. Suitable models of wind power generation for

long- and short-term power system stability studies are proposed. Important aspects, such as fault ride-through and reactive power production capability are also taken into account.

2. T. Lund, J. Eek, S. Uski and A. Perdana, "Fault simulation of wind turbines using commercial simulation tools," in *Proc. of Fifth International Workshop on Large-Scale Integration of Wind Power and Transmission Networks for Offshore Wind Farms*, Glasgow, UK, 2005.

This paper compares the commercial simulation tools: PSCAD, PowerFactory, Simpow and PSS/E for analyzing fault sequences defined in the Danish grid code requirements for wind turbines connected to a voltage level below 100 kV. Both symmetrical and unsymmetrical faults are analyzed. The deviations and the reasons for the deviations between the tools are stated. The simulation models are implemented using the built-in library components of the simulation tools with exception of the mechanical drive-train model, which must be user-modelled in PowerFactory and PSS/E.

3. M. Martins, A. Perdana, P. Ledesma, E. Agneholm, O. Carlson, "Validation of fixed speed wind turbine dynamics with measured data," *Renewable Energy*, accepted for publication.

This paper compares a recorded case obtained from a fixed-speed stall regulated 180 kW wind turbine during a grid disturbance against simulation results. The paper also includes a study of the performance of two induction generator models, neglecting and including the electromagnetic transients in the stator respectively. This paper also discusses the convenience of representing the elastic coupling and the effect of mechanical damping.

4. A. Perdana, S. Uski, O. Carlson and B. Lemström, "Validation of aggregate model of wind farm with fixed-speed wind turbines against measurement," in *Proc. Nordic Wind Power Conference 2006*, Espoo, Finland, 2006.

Models of single and aggregated wind turbines are presented in this paper. The importance of induction generator and mechanical drive train models of wind turbines are examined. The models are validated against field measurement data from Olos wind park.

5. J.O.G. Tande, I. Norheim, O. Carlson, A. Perdana, J. Pierik, J. Morren, A. Estanqueiro, J. Lameira, P. Sørensen, M. O'Malley, A. Mullane, O. Anaya-Lara, B.Lemström, S. Uski, E. Muljadi, "Benchmark test of dynamic wind generation models for power system stability studies," submitted to *IEEE Trans. Power System*.

This paper presents a systematic approach on model benchmark testing for dynamic wind generation models for power system stability studies, including example benchmark test results comparing model performance with measurements of wind turbine response to voltage dips. The tests are performed for both a fixed-speed wind turbine with squirrel cage induction generator and variable-speed wind turbine with doubly feed induction generator. The test data include three-phase measurements of instantaneous voltage and currents at the wind turbine terminals during a voltage dip. The benchmark test procedure includes transforming these measurements to RMS fundamental positive sequence values of voltage, active power and reactive power for

comparison with simulation results. Results give a clear indication of accuracy and usability of the models tested, and pin-point need both for model development and testing.

6. A. Perdana, O. Carlson, J. Person, "Dynamic response of a wind turbine with DFIG during disturbances," in *Proc. of IEEE Nordic Workshop on Power and Industrial Electronics (NORpie) 2004*, Trondheim, Norway, June 14-16, 2004.

A model of a wind turbine with DFIG connected to the power system has been developed in this paper in order to investigate dynamic responses of the turbine during a grid disturbance. This model includes aerodynamics, the mechanical drive train, the induction generator as well as the control parts. The response of the system during grid disturbances is studied. An inclusion of saturation effects in the generator during faults is included as well

Chapter 2

Modelling Aspects of Wind Turbines for Stability Studies

2.1 Power system stability

2.1.1 Definition and classification of power system stability

The term of power system stability used here refers to the definition and classifications given in [15]. The definition of power stability is given as the ability of an electric power system, for a given initial operating condition, to regain a state of operating equilibrium after being subjected to a physical disturbance, with most system variables bounded so that practically the entire system remains intact.

Power system stability can be divided into several categories as follows:

Rotor angle stability This stability refers to the ability of synchronous machines of an interconnected power system to remain in synchronism after being subjected to a disturbance. The time frame of interest is between 3 to 5 seconds and can be extended to 10 to 20 seconds for a very large power system with dominant inter-area swings.

Short- and long-term frequency stability This term refers to ability of a power system to maintain steady frequency following a severe system upset resulting in a significant imbalance between generation and load. The time frame of interest for a frequency stability study varies from tens of seconds to several minutes.

Short- and long-term large disturbance voltage stability This term refers to the ability of a power system to maintain steady voltages following large disturbances such as system faults, loss of generation, or circuit contingencies. The period of interest for this kind of study varies from a few seconds to tens of minutes.

Short- and long-term small disturbance voltage stability This stability refers to system's ability to maintain steady voltages when subjected to small perturbations such as incremental changes in system load. For a large disturbance voltage stability study, the time frame of the study may extend from a few seconds to several or many minutes.

2.1.2 Wind power generation and power system stability

When dealing with power system stability and wind power generation, two questions may be raised: "How does wind power generation contribute to power system stability?" and "Which models of wind turbines are appropriate for power system stability studies?" This thesis is aimed at responding to the latter question. However, in order to motivate importance aspects of wind turbine models in a power system stability study, some cases of system stability problems related to wind power generation are presented in this thesis.

A number of power system stability phenomena may be encountered in relation to the presence of large-scale wind power generation. The contribution of large-scale wind power generation to large system inter-area oscillation has been presented in [16]. The influence of wind power generation on short- and long-term stability has been addressed in [17]. Many investigations into short-term voltage stability issues have also been discussed in literature such as in [5, 18]. An investigation into the impact of increasing wind penetration on frequency stability can be found in [19].

2.2 Simulation tool PSS/E

PSS/E (Power System Simulator for Engineering) is a fundamental frequency-type simulation tool, which is commonly used by power system utility companies for stability studies.

The tool provides an extensive library of power system components, which includes generator, exciter, governor, stabilizer, load and protection models. Many of these have been validated [20]. Additionally, users are allowed to develop user defined models.

As the penetration of wind power generation in the power system is reaching the point where it can not be neglected any longer, there is a need for having reliable wind turbine models in power system stability simulation tools such as PSS/E. ESB National Grid (ESBNG), the Irish Transmission System Operator (TSO), for instance states clearly in its grid codes that companies having wind turbines connected to the grid must deliver the wind turbine models in PSS/E. Moreover, the TSO requires that the model be able to run with an integration time step not less than 5 ms [21]. Although it is not mentioned in the grid codes, Svenska Kraftnät of Sweden similarly covers this issue.

Problems with initialization procedures and a too small integration time step required by the model, which result in considerably long simulation time, are among typical issues related to the implementation of wind turbine models into PSS/E, which are encountered by ESBNG [21]. These two issues will be addressed specifically in this report.

In respect to wind power generation, PSS/E provides several types of wind turbine models. The following wind turbine models are available for users: GE 1.5 MW, Vestas V80, GE 3.6 MW and Vestas V47.

2.2.1 Network representation

In PSS/E, the power system network is modeled in the form of

$$\mathbf{I} = \mathbf{Y} \cdot \mathbf{V} \tag{2.1}$$

where $\mathbf{I}$ represents a vector of complex current sources, $\mathbf{V}$ is a vector of complex bus voltages and $\mathbf{Y}$ is the network admittance matrix [22]. The power flow is non-linear and requires

an iterative process to find the solutions. PSS/E provides different iteration methods for load-flow calculation such as Gauss-Seidel, modified Gaus-seidel, Fully coupled Newton-Raphson, Decoupled Newton-Raphson and Fixed slope decoupled Newton-Raphson iteration methods.

Normally, generating units are represented as voltage sources ($\mathbf{V_{source}}$) behind transient impedances (Thevenin equivalent) as shown in Figure 2.1a. In PSS/E, however, the Thevenin equivalents are replaced with Norton equivalents. This means that the generating units are represented as current sources ($\mathbf{I_{source}}$) in parallel with transient impedances ($\mathbf{Z_{source}}$) as depicted in Figure 2.1b.

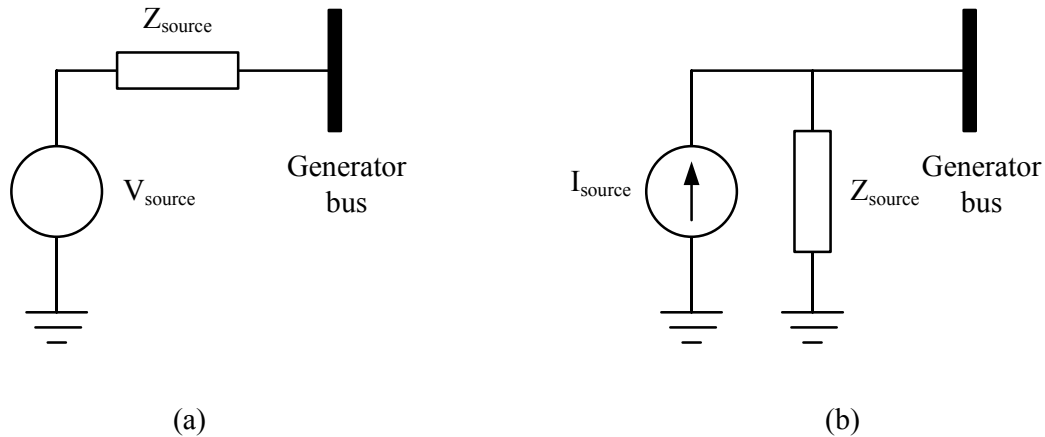(a)   (b)

Figure 2.1: (a) Thevenin and (b) Norton equivalent representation of generating unit in stability studies.

2.2.2   Simulation mode

Basically two modes of simulation can be performed in PSS/E: the standard simulation mode and the extended-term simulation mode.

The standard simulation mode is provided for short-term stability studies, which require detailed representation of power system components. The simulation utilizes a fixed integration time step, which is typically set to half of a system period (equivalent to 10 ms for a 50 Hz system frequency). This simulation uses the modified Euler method, sometimes also referred as the Heun method, as the numerical integration method or solver.

The extended-term simulation mode is designed for long-term stability studies. This simulation allows the user to use a relatively large integration time step. This results in a significant improvement in simulation efficiency compared to the standard simulation mode. In the extended-term simulation mode, the trapezoidal implicit method is used as the integration solver. As a result, the integration time step of the simulation is not required to be less than the smallest time constant of the models as required for the standard simulation mode. This large simulation step is at the expense of the simulation accuracy, since with such a large integration time step, the simulation fails to spot phenomena with a higher frequency relative to a given integration time step. The extended simulation mode requires specific models, which are different from the models used for the standard simulation mode. Consequently, user defined models which are implemented for the standard simulation mode can no longer be used in the extended-term simulation mode.

Despite the long simulation time, it is common to use the standard simulation mode for long-term simulation. By using the standard simulation mode, only one model for different types of stability studies is required. In this study, therefore, only the standard simulation mode is used.

2.3   Supporting tools

Besides PSS/E, other simulation tools are also employed in this study such as PSCAD/ EMTDC and SimPowerSystem provided by Matlab/Simulink. Both of these tools can simulate a three-phase electrical system with instantaneous representation of network model. PSCAD/ EMTDC is mainly used to validate a user written model, which incorporates standardized electrical components such as induction machines, lines and transformers. SimPowerSystem is used to design and optimize controllers and other nonlinear components, such as power electronics, before they are implemented into the standardized power system simulation tool PSS/E. In fact, SimPowerSystem also provides a wide range of built-in models of electrical components, which can be used to validate user written models in PSS/E. By having a model implemented into three different tools, a higher confidence level for the developed models can be achieved.

2.4   Numerical integration methods

In a broad sense, the efficiency of a simulation is mainly determined by the time required to simulate a system for a given time-frame of study.

Two factors that affect simulation efficiency are the numerical integration method used in a simulation tool and the model algorithm. The first factor is explored here, while the later is discussed in the next two chapters. In this section, the two different integration methods used in PSS/E are explored.

The examination of numerical integration methods presented in this section is intended to identify the maximum time step permitted for a particular model in order to maintain simulation numerical stability. Ignoring this limit may lead to a malfunction of a model, caused by a very large integration time step. To avoid such a problem, either the simulation time step must be reduced or the model's mathematical equations must be modified. A typical time step used in simulation tools is shown in Table 2.1.

Table 2.1: Typical simulation time step in commercial simulation tools[20, 23].

PSS/E	PowerFactory
Standard simulation: half a cycle (0.01 sec for 50 Hz and 0.00833 sec for 60 Hz system)	Electromagnetic Transients Simulation: 0.0001 sec
Extended-term simulation: 0.05 to 0.2 sec	Electromechanical Transients Simulation: 0.01 sec
	Medium-term Transients: 0.1 sec

2.4.1 Numerical stability and accuracy

Two essential properties of numerical integration methods are numerical stability and accuracy.

The concept of stability of a numerical integration method is defined as follows [24]: If there exists an $h_0 > 0$ for each differential equation, such that a change in starting values by a fixed amount produces a bounded change in the numerical solution for all h in $[0, h_0]$, then the method is said to be stable. Where h is an arbitrary value representing the integration time step.

Typically, a simple linear differential equation is used to analyze the stability of a numerical integration method. This equation is given in the form

$$y' = -\lambda y, \quad y(0) = y_0 \tag{2.2}$$

This equation is used to examine the stability of the numerical integration method discussed in later sections.

The accuracy of a numerical method is related to the concept of convergence. Convergence implies that any desired degree of accuracy can be achieved for any well posed differential equation by choosing a sufficiently small integration step size [24].

Power system equations as a stiff system

As a part of numerical integration stability, there is a concept of stiffness. A system of differential equations is said to be stiff if it contains both large and small eigenvalues. The degree of stiffness is determined by the ratio between the largest and the smallest eigenvalues of a linearized system. In practice, these eigenvalues are inversely proportional to the time constants of the system elements.

The stiff equations poses a challenge in solving differential equations numerically, since there is an evident conflict between stability and accuracy on one side and simulation efficiency on the other side.

By nature, a power system is considered as a stiff equation system since a wide range of time constants is involved. This is certainly a typical problem when simulating short- and long-term stability phenomena. In order to illustrate the stiffness of power system equations, the system can be divided into three different time constants, e.g. small, medium and large time constants.

System quantities and components associated with small time constants or which represent fast dynamics of the power system are stator flux dynamics, most FACTS devices and other power electronic-based controllers. Among quantities and components with medium time constants are rotor flux dynamics, speed deviation, generator exciters and rotor angle dynamics in electrical machines. Large time constants in power system quantities are found, for instance in turbine governors and the dynamics of boilers.

In book [25], appropriate representation in stability studies for most conventional power system components with such varied time constants is discussed thoroughly. The book also introduces a number of model simplifications and their justification for stability studies. Most of the simplifications, can be realized by neglecting dynamics of quantities with small time constants. Since wind turbines as a power plant are relatively new in power system stability studies, this discussion was not mentioned in the book.

Indeed, like other power system components, wind turbines consist of a wide range of time constants. Small time constants in wind turbine models are encountered, for instance in stator flux dynamics of generators, power electronics and aerodynamic controllers. While mechanical and aerodynamic components as well as rotor flux dynamics normally consist of medium time constants. Hence, it is clear that wind turbine models have the potential to be a source of stiffness for a power system model if they are not treated carefully.

2.4.2 Explicit vs implicit numerical integration methods

Numerical integration methods can be differentiated into two categories: the explicit method and the implicit method. In order to illustrate the difference between the two methods, let us take an ordinary differential equation as below

$$y'(t) = f(t, y(t)) \tag{2.3}$$

Numerically, the equation can be approximated using a general expression as follows

$$y'(t_n) \approx \frac{y(t_{n+1}) - y(t_n)}{h} = \phi \left(\begin{array}{c} t_{n-k}, \ldots, t_n, t_{n+1}, \\ y(t_{n-k}), \ldots, y(t_n), y(t_{n+1}) \end{array} \right) \tag{2.4}$$

where h denotes the integration time step size and ϕ is any function corresponding to the numerical integration method used. Since $y(t_{n+1})$ is not known, the right-hand side cannot be evaluated directly. Instead, both sides of the equation must be solved simultaneously. Since the equation may be highly nonlinear, it can be approximated numerically. This method is called the implicit method.

Alternatively, $y(t_{n+1})$ on the right-hand side can be replaced by an approximation value $\hat{y}(t_{n+1})$. This approach is called the explicit method. There are a number of alternative methods for obtaining $\hat{y}(t_{n+1})$, one of the methods discussed in this thesis is the modified Euler method (sometimes referred to as the Heun method).

As stated previously, PSS/E uses the modified Euler method for the standard simulation mode and the implicit trapezoidal method for the extended term simulation mode. These two integration methods are described in the following.

Modified Euler method

The modified Euler integration method is given as

$$w_{i+1} = w_i + \frac{h}{2} \left[f(t_i, w_i) + f(t_{i+1}, w'_{i+1}) \right] \tag{2.5}$$

where w'_{i+1} is calculated using the ordinary Euler method

$$w'_{i+1} = w_i + h \left[f(t_i, w_i) \right] \tag{2.6}$$

For a given differential equation $y' = -\lambda y$, the stability region of the modified Euler method is given as

$$\left| 1 + h\lambda + \frac{(h\lambda)^2}{2} \right| < 1 \tag{2.7}$$

This means that in order to maintain simulation stability, $h\lambda$ must be located inside the closed shaded area as shown in Figure 2.2. If λ is a real number or if real parts of λ are considerably large compared to its imaginary parts, h can be estimated as

$$h < -\frac{2}{\lambda} \qquad (2.8)$$

However, if a complex number of λ is highly dominated by it's imaginary part, the h must fulfill the following relation

$$h < -\frac{1}{2\lambda} \qquad (2.9)$$

Thereby, a λ dominated by imaginary parts must constitute a smaller simulation time step in order to maintain simulation stability.
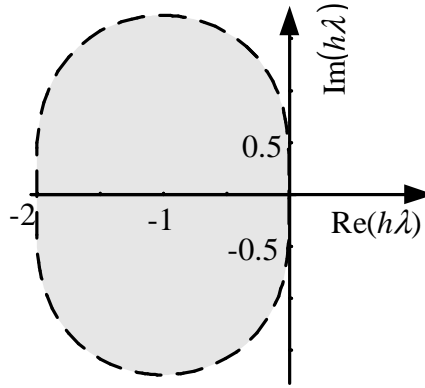

Figure 2.2: Stable region of modified Euler integration method.

Implicit trapezoidal method

The implicit trapezoidal method is classified within A-stable methods. A method is said to be A-stable if all numerical approximations tend to zero as number of iteration steps $n \to \infty$ when it is applied to the differential equation $y' = \lambda y$, with a fixed positive time step size h and a (complex) constant λ with a negative real part [24].

This means that as long as the eigenvalue of the differential system lies in the left-hand side of the complex plane, the system is stable regardless of size of time step h, as shown in Figure 2.3. Besides PSS/E, the implicit trapezoidal method is also implemented into simulation tool PowerFactory [26].

2.5 Conclusion

To provide a reliable wind turbine model implemented into a standard simulation tool, several factors must be taken into account. The first important factor is to clearly define the purpose of the study. Each type of power system study requires a particular frequency bandwidth and a simulation time-frame, depending on how fast the system dynamics need to be investigated. Subsequently, the nature of the system being modeled must be carefully understood and the simulation tool used to simulate the models must be appropriately utilized.
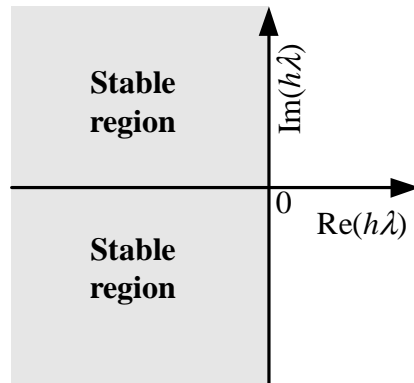
Figure 2.3: Stable region of modified implicit trapezoidal integration method.

Numerical stability of simulation is of particular concern in dynamic modelling. Numerical stability is dependent on the integration method used in a simulation tool and the stiffness of the model's differential equations. The interaction of the two components determines the efficiency of a simulation, which is reflected in the size of the simulation time step. However, if the simulation time step is determined in advance (fixed), as a consequence some models that require a smaller time step cannot run in the simulation without modification.

The upper limit of the time step size allowed for a certain model for a particular integration method to maintain numerical stability can be estimated analytically. The investigation of the numerical stability of the wind turbine models focuses on the modified Euler method, which is used by PSS/E as a main simulation tool in this thesis.

Chapter 3

Fixed-speed Wind Turbine Models

The schematic structure of a fixed-speed wind turbine with a squirrel cage induction generator is depicted in Figure 3.1.
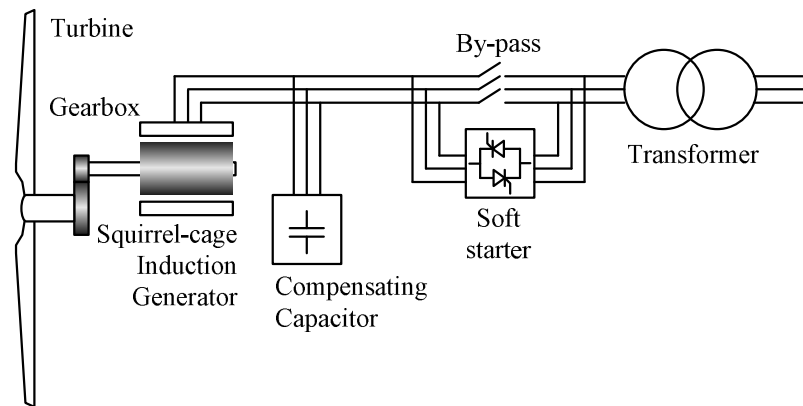

Figure 3.1: System structure of wind turbine with direct connected squirrel cage induction generator.

A fixed-speed wind turbine with a squirrel cage induction generator is the simplest type of wind turbine technology. It has a turbine that converts the kinetic energy of wind into mechanical energy. The generator, which is a squirrel cage induction generator, then transforms the mechanical energy into electrical energy and delivers the energy directly to the grid. Noted that the rotational speed of the generator, depending on the number of poles, is relatively high (in the order of 1000 - 1500 rpm for a 50 Hz system frequency). Such a rotational speed is too high for the turbine rotor speed in respect to the turbine efficiency and mechanical stress. For this reason, the generator speed must be stepped down using a gearbox with an appropriate gear ratio.

An induction generator consumes a significant amount of reactive power (even during zero power production), which increases along with the active power output. Accordingly, a capacitor bank must be provided in the generator terminal in order to compensate for this reactive power consumption so that the generator does not burden the grid.

Because the mechanical power is converted directly to a three-phase electrical system by means of an induction generator, no complex controller is involved in the electrical part of a fixed-speed wind turbine. For an active stall fixed-speed wind turbine, however, a pitch controller is needed to regulate the pitch angle of the turbine.

3.1 The induction generator

An induction generator can be represented in different ways, depending on the model level of detail. The detail of the model is mainly characterized by the number of phenomena included in the model. There are several major phenomena in an induction generator such as:

The stator and rotor flux dynamics The stator and rotor flux dynamics are related to the behavior of the fluxes in the associated windings. As it is known that current in an inductive circuit is considered as a state variable, it cannot change instantaneously. The same behavior applies to the stator and rotor fluxes because the stator and rotor fluxes are proportional to currents.

Magnetic saturation Magnetic saturation is encountered due the nonlinearity of the inductance. Main and leakage flux saturations are associated with the nonlinearity in the magnetic and leakage inductances, respectively.

Skin effect As frequency gets higher, the rotor current tends to be concentrated to the outer part (periphery) of the rotor conductor. This causes an increased in the effective rotor-resistance.

Core losses Eddy current losses and hysteresis are among other phenomena that occur in an induction generator, which are known as core losses.

A very detailed model which includes all these dynamics is a possibility. Nevertheless, such a detailed model may not be beneficial for stability studies because it increases the complexity of the model and requires time-consuming simulations. More importantly, not all of these dynamics give significant influence in stability studies.

A comprehensive discussion on comparison of different induction generator models can be found in [27]. Accordingly, the inclusion of iron losses in the model requires a complicated task and the influence for stability studies is neglected. The main flux saturation is only of importance when the flux level is higher than the nominal. Hence, this effect can be neglected for most operating conditions. The skin effect should only be taken into account for a large slip operating condition, which is not the case for a fixed-speed turbine generator.

Another constraint of inclusion dynamics in the model is the availability of the data. Typically, saturation and skin effect data are not provided by manufacturers. Therefore, in general, it is impractical to use them in wind turbine applications.

All of these argumentations lead to a conclusion that only stator and rotor dynamics are the major factors to be considered in an induction generator model. Accordingly, in this thesis, a model which includes both stator and rotor flux dynamics is considered as the reference model.

In modelling an induction generator, a number of conventions are used in this report, such as:

- The models are written based on *dq*-representation fixed to a synchronous reference frame.

- The *q*-axis is assumed to be 90° ahead to the *d*-axis in respect to direction of the frame rotation.

- The *d*-axis is chosen as the real part of the complex quantities and subsequently the *q*-axis is chosen as the imaginary part of the complex quantities.

- The stator current is assumed to be positive when it flows into the generator. Note that this convention is normally used for motor standpoint rather than for generator standpoint. This convention is preferred because in most literature induction machines exist as motors rather than as generators. Hence, representation of the model using motor convention is used for the reason of familiarity.

- All parameters are given in p.u. quantities.

Furthermore, besides neglecting the effect of saturation, core losses and skin effect as mentioned earlier, the following assumptions are also applicable: (1) no zero-sequence current is present, and (2) the generator parameters in each phase are equal/symmetrical and the windings are assumed to be an equivalent sinusoidally distributed winding. Air-gap harmonics are therefore neglected.

3.1.1 Fifth-order model

As stated earlier, the detailed model of an induction generator involves both stator and rotor dynamics. This model is also referred to as the fifth-order model, since it consists of five derivatives: four electrical derivatives and one mechanical derivative. In some literature, this model is also known as the electromagnetic transient (EMT) model. The equivalent circuit of the dynamic model is represented in Figure 3.2.
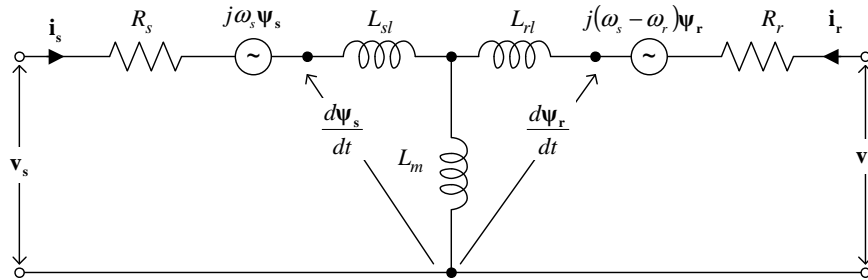

Figure 3.2: Equivalent circuit of an induction generator dynamic model.

The stator and the rotor voltage equations can be expressed according to the well-known representation as follows

$$\mathbf{v_s} = \mathbf{i_s}R_s + j\omega_s\boldsymbol{\psi_s} + \frac{d\boldsymbol{\psi_s}}{dt} \tag{3.1}$$

$$\mathbf{v_r} = 0 = \mathbf{i_r}R_r + j(\omega_s - \omega_r)\boldsymbol{\psi_r} + \frac{d\boldsymbol{\psi_r}}{dt} \tag{3.2}$$

where $\mathbf{v}$, $\mathbf{i}$ and ψ denote the voltage, current and flux quantity, respectively, and ω is the speed. The subscripts $\mathbf{s}$ and $\mathbf{r}$ refer to quantities of the stator and rotor, respectively.

The relation between flux and currents are given by

$$\boldsymbol{\psi_s} = \mathbf{i_s}L_s + \mathbf{i_r}L_m \tag{3.3}$$

$$\boldsymbol{\psi_r} = \mathbf{i_r}L_r + \mathbf{i_s}L_m \tag{3.4}$$

17

where L_m is the magnetizing reactance, L_s and L_r stand for the stator and rotor inductance correspondingly. The two latter parameters are given by

$$L_s = L_{sl} + L_m \tag{3.5}$$

$$L_r = L_{rl} + L_m \tag{3.6}$$

where L_{sl} and L_{lr} are the stator and rotor leakage inductance, respectively.

The electric torque produced by the generator can be calculated as a cross-product of flux and current vectors

$$T_e = \boldsymbol{\psi_s} \times \mathbf{i_s} \tag{3.7}$$

This is equivalent to

$$T_e = \Im \left[\boldsymbol{\psi_s^*} \mathbf{i_s} \right] \tag{3.8}$$

The complex power of the stator is given by

$$\mathbf{S} = \mathbf{v_s} \mathbf{i_s^*} \tag{3.9}$$

Note that there is a certain type of squirrel-cage arrangement, called double squirrel-cage, where the rotor consists of two layers of bar, both are short-circuited by end rings. This arrangement is employed to reduce starting current and to increase starting torque by exploiting the skin effect. Practically, this arrangement is not used in wind power application, therefore it is not discussed in this thesis.

The mechanical dynamics are described according to the following relation:

$$J_g \frac{d\omega_r}{dt} = T_e - T_m \tag{3.10}$$

where T_m is the mechanical torque.

3.1.2 Third-order model

Less detailed representation of an induction generator can be achieved by neglecting the stator flux dynamics. This is equivalent to removing two stator flux derivative from equation (3.1). Subsequently, the stator and rotor voltage equations become

$$\mathbf{v_s} = \mathbf{i_s} R_s + j\omega_s \boldsymbol{\psi_s} \tag{3.11}$$

$$0 = \mathbf{i_r} R_r + j(\omega_s - \omega_r)\boldsymbol{\psi_r} + \frac{d\boldsymbol{\psi_r}}{dt} \tag{3.12}$$

The electric torque and the power equations remain the same as in the fifth-order model.

The disregard of the stator flux transient in the third-order model of induction generator is equivalent to ignoring the dc component in the stator transient current. As a consequence, only fundamental frequency goes into effect. This representation makes the model compatible with commonly used fundamental frequency simulation tools. In some literature, this model is referred to as the electromechanical model.
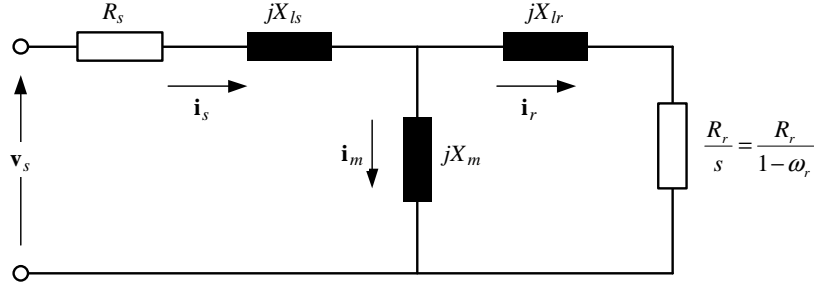
Figure 3.3: Steady state equivalent circuit of induction generator.

3.1.3 First-order model

The simplest dynamic model of an induction generator is known as the first-order model. Sometimes this model is referred to as the steady state model, since only dynamics of the mechanical system are taken into account (no electrical dynamics are involved). The typical steady state equivalent circuit of the first-order model of an induction generator is shown in Figure 3.3.

3.1.4 Induction generator model representation as voltage sources

The models of an induction generator presented in subsections 3.1.1, 3.1.2 and 3.1.3 are basically represented as current sources. In power system stability studies, normally generators are represented as voltage sources behind transient impedance. In order to adapt to this representation, the models must be modified into voltage source components[25].

Fifth-order model

Representation of the fifth-order model as a voltage source behind transient impedance is given as

$$\mathbf{v_s} = \mathbf{i_s}R_s + j\mathbf{i_s}X' + \mathbf{v'_e} + \frac{d\psi_s}{dt} \tag{3.13}$$

$$\frac{d\mathbf{v'_e}}{dt} = \frac{1}{T_o}[\mathbf{v'_e} - j(X_s - X')\mathbf{i_s}] + js\mathbf{v'_e} + j\frac{X_m}{X_r}\mathbf{v_r} \tag{3.14}$$

where X_s, X_r, X_m and X'_s refer to the stator, rotor, magnetizing and transient reactance respectively. T_o is the transient open-circuit time constant of the induction generator. These variables are given by

$$X_s = \omega_s L_s \tag{3.15}$$

$$X_r = \omega_s L_r \tag{3.16}$$

$$X_m = \omega_s L_m \tag{3.17}$$

$$X' = \omega_s(L_s - \frac{L_m^2}{L_r}) \tag{3.18}$$

$$T_o = \frac{L_r}{R_r} \tag{3.19}$$

19

The electric torque can be expressed as

$$T_e = \frac{\mathbf{v}_\mathbf{e}' \mathbf{i}_\mathbf{s}^*}{\omega_s} \tag{3.20}$$

Formula derivation of equations above from the standard fifth-order model can be found in Appendix A.

Third-order model

Similarly, representation of the third-order model as a voltage source behind a transient impedance can be obtained by removing the stator flux derivative in (3.14), while keeping the remaining equations the same.

$$\mathbf{v}_\mathbf{s} = \mathbf{i}_\mathbf{s} R_s + j\mathbf{i}_\mathbf{s} X' + \mathbf{v}_\mathbf{e}' \tag{3.21}$$

Equation (3.21) then can be represented as a voltage source behind a transient impedance as shown in Figure 3.4, which is a standardized representation for power system stability studies. This representation is equivalent to CIMTR1 in the PSS/E built in model.
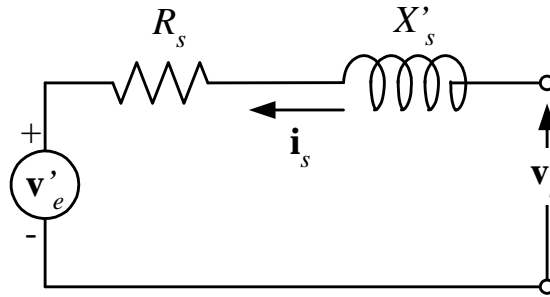

Figure 3.4: Transient representation of the third-order induction generator.

First-order model

For the first-order model of induction generator, all equations for the third-order remain valid except for the transient voltage source which is calculated as

$$\frac{d\mathbf{v}_\mathbf{e}'}{dt} = \frac{jX_m{}^2 R_r \mathbf{v}_\mathbf{s}{}^2}{X_r \left(X_m{}^2 + R_r R_s - sX_s X_r\right)} \tag{3.22}$$

Practically, this model does not contribute short-circuit current to the grid, therefore it is recommended that the first-order model of an induction generator is represented as a negative load rather than as a generator.

3.1.5   Result accuracy

To provide a comparison of different induction generator models, two simulation cases were performed. In the first case, the response of the models subjected to a grid fault was investigated. The second case investigated the influence of frequency deviation on the behavior of

the models. In the comparison study, the fifth-order model was assumed to be a "reference model." This was justified by the description given in Section 3.1 and later by the validation result presented in Chapter 4.

Fault response

In the following, the fault response of the three different models of induction generator is compared. Each model is examined using the same network topology, which is a simple two-buss test grid as depicted in Figure 3.5. The equivalent circuit parameters of the generator are given in Appendix F.
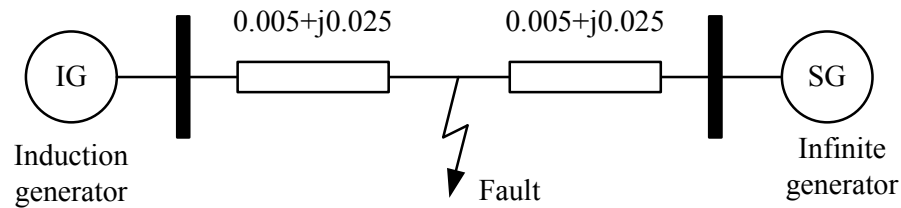

Figure 3.5: Test grid.

The mechanical input is held constant throughout the simulation. A fault is applied at the middle of the transmission line connecting the two busses with a duration of 150 ms. In order to provide a fair comparison, the fifth-order model is simulated in a standard electromagnetic transient program PSCAD/EMTDC, which simulates the case using an instantaneous three-phase network model. Whereas the lower order models are simulated using a standard stability program PSS/E using a fundamental frequency network model. The response of the three different models subjected to the fault is shown in Figure 3.6.

Figure 3.6a shows the trace of the stator voltage. The fault causes the voltage drops to 0.1 pu. The voltage profiles of the three different models during the fault are similar, despite a slower voltage decays for the fifth-order and the third-order models and a small oscillation on the stator voltage for the fifth-order model due to the nature of the network. However, the differences become obvious during the voltage recovery following the fault clearing, this will be described later.

Figure 3.6b shows the stator current response of the three different models. Note that for the fifth-order model, the current presented is one of the phase currents that contains the highest dc-offset. The current for the third-order and the first-order models presented in the figure correspond to positive sequence current components.

During the first few cycles after the fault initiated, the third-order model predicts a lower transient current than the fifth-order model. The current response of the first-order model even shows an opposite tendency of the current response of the other models. This over-optimistic estimation of current response is to be considered when an instantaneous over-current protection system of wind turbine is incorporated into the model. In fact, it is sufficient for the protection to take into effect when at least one of the phases hits the limit.
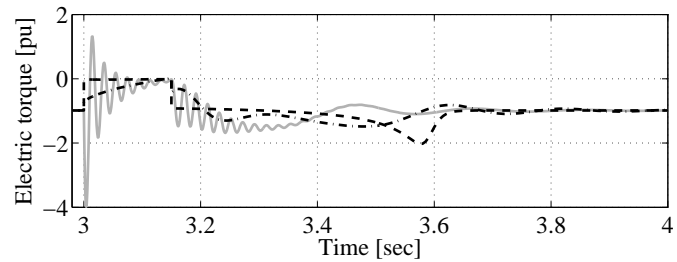
It should be noted however, that if the role of instantaneous over-current protection is disregarded, the peak transient current will become a trivial issue. This is because the rotor time constant of a typical induction generator is considerably small and therefore the transient current decays very rapidly.
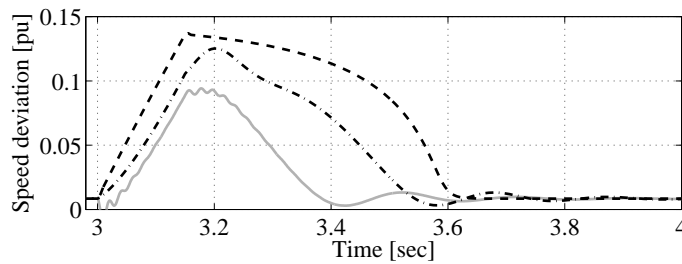
21
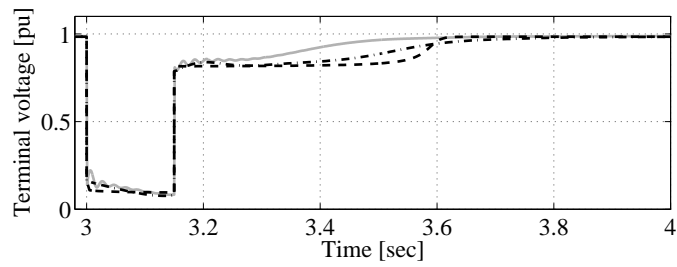
(a) Terminal voltage
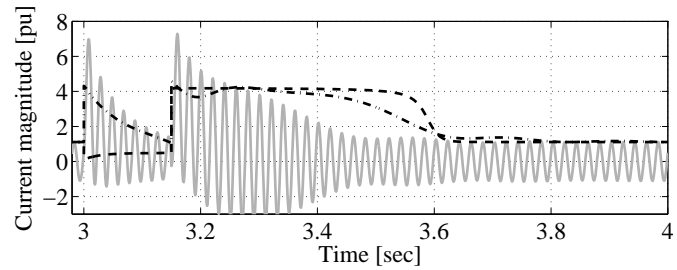
(b) Current

(c) Electric torque

(d) Speed deviation

Figure 3.6: Comparison of different induction generator models: fifth-order (solid), third-order (dash-dotted) and first-order (dashed). Observe that the time scale of each figure is not the same.

Figure 3.6c demonstrates the electric torque response of the three different models. Similar to the current responses, the torque responses of the three different models are also noticeably different. This is because the electric torque is directly influenced by the current. Oscillations of the electric torque can be clearly observed in the fifth-order model. The oscillations occur because of the presence of dc-offset components in the stator current. During the first half cycle these components create the effect of counteracting torque or so-called

braking torque. In contrary, during the next half cycle they give an acceleration effect to the rotor with less amplitude, and so forth.

In the third-order model, the torque oscillations are omitted, which result in a lower total effective electric torque. This leads to a larger speed deviation. Since no electrical transient is involved in the first-order model, once the stator voltage drops to nearly zero, the electrical torque virtually falls to zero as well. Consequently, the speed of the first-order model is accelerated much rapidly than in the other models.

The peak value of the electric torque during transient is actually more pronounced issue in the mechanical stress investigation rather than in power system stability studies. Therefore this issue is not discussed in this thesis.

Figure 3.6d shows the rotor speed response of the models. In general, the rotor speed course can be characterized by an increase in speed due to reduced electric torque during the fault. As mentioned earlier, the effect of braking torque in the fifth-order model gives a noticeable speed drop immediately after the fault occurs.

The response of the model after the fault clearing can be explained as follows:

Directly after the voltage is recovered, the current undergoes a transient which results in an overshoot of the electrical torque. This overshoot leads to a sudden decrease in rotor acceleration. This effect is practically the same as the braking torque mentioned earlier. As this effect is absent in the third- and first-order model, the generator speed continues to accelerate for a short period after the fault clearing.

The relation between reactive power and slip of an induction machine is given as follows:

$$Q = |\mathbf{v_s}|^2 \frac{R_r^2(X_m + X_s)^2 + s^2(X_r X_s + X_m(X_r + X_s))^2}{R_r^2(X_m + X_s) + s^2(X_m + X_r)(X_r X_s + X_m(X_r + X_s))} \tag{3.23}$$

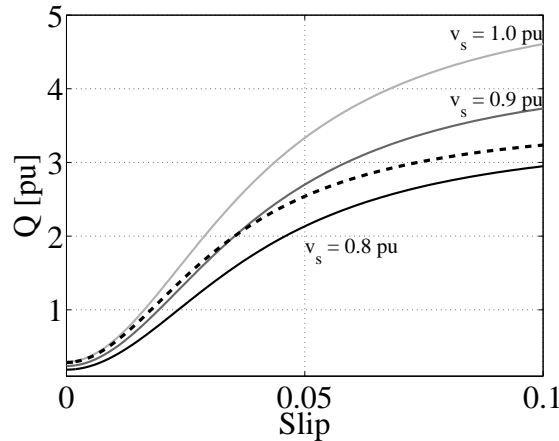The relation above can be graphically depicted as shown in Figure 3.7.

Figure 3.7: Typical relation between reactive power and slip of induction generator for different terminal voltages (solid) and considering non-stiff grid with line impedance of 0.05 pu (dashed).

Figure 3.7 shows that the reactive power consumption of the generator increases non-linearly with slip. This high reactive power consumption results in a prolonged terminal voltage recovery, as noticed in Figure 3.6a.

It is worth mentioning that the zero-crossing switching mode of the breaker opening at the fault clearing event, which is not included in the simulation, in reality provides a less severe current transient than the one shown in the simulation.

It should be noted that the rotor speed response dissimilarity between the models is driven by a number of major factors, such as the magnitude of the voltage dip, fault duration, rotor resistance and rotor inertia. Figure 3.8 illustrates the contribution of each factor to the speed response discrepancy of the different models. The reference generator parameters are given in Appendix F. Note that the term of maximum speed deviation used in Figure 3.8 is equivalent to the negative slip of the generator.

(a) Reference

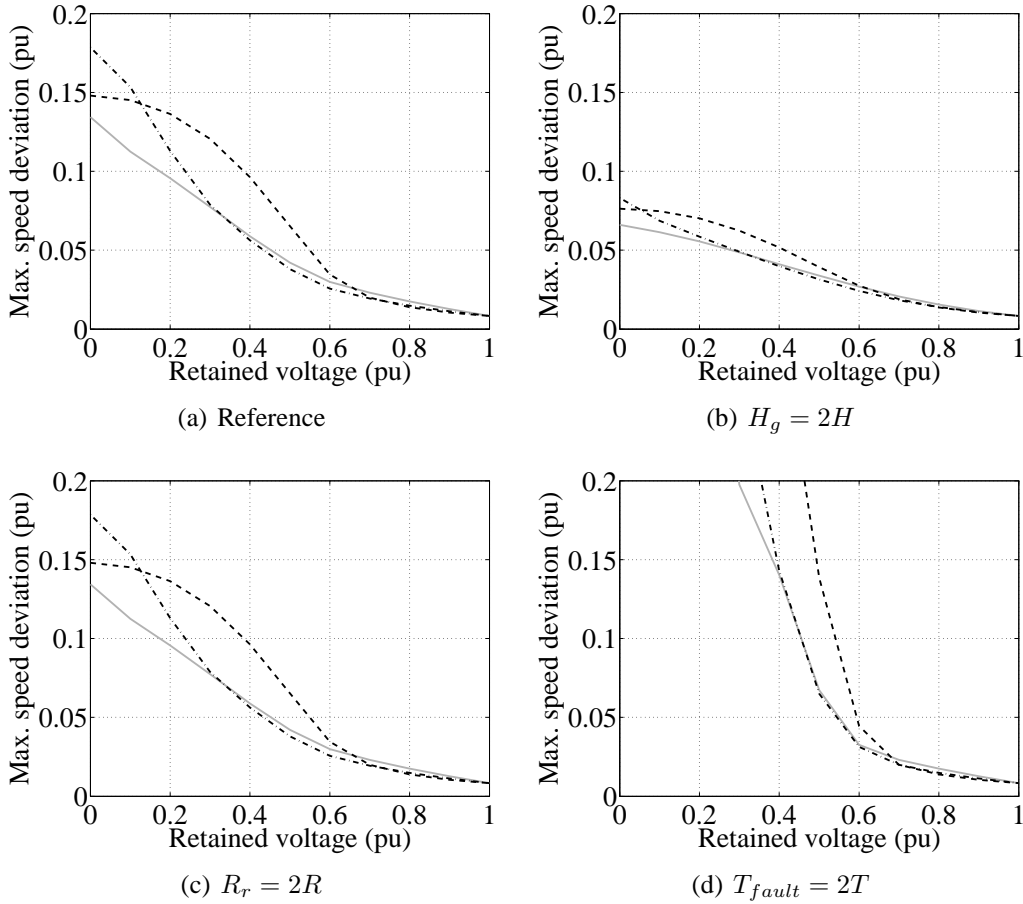(b) $H_g = 2H$

(c) $R_r = 2R$

(d) $T_{fault} = 2T$

Figure 3.8: Influence of generator inertia, rotor resistance and fault duration on rotor speed deviation for different retained voltages of different induction generator models: fifth-order (solid grey), third-order (dash-dotted) and first-order (dashed).

Based on simulations of a number of different generator parameters (which are not presented in this thesis), it can be said that the third-order model can predict the maximum speed deviation sufficiently accurately for a retained voltage more than 0.4 pu.

It should be noted that the inertia used in the simulation above considers only generator rotor inertia. In reality, the actual inertia is larger because the rotor inertia must also include some parts of the gearbox which are connected stiffly to the rotor. As the inertia becomes larger, the difference in speed deviation between the models (especially between the third-order and the fifth-order models) becomes insignificant. This is clearly shown in Figure 3.8b.

Off-nominal frequency response

In the following discussion, the response of the models to off-nominal frequency operation is investigated. The simulation is conducted by applying frequency deviation to the input voltage. The profile of the applied frequency is depicted in Figure 3.9. Note that this frequency deviation profile is used merely to illustrate the response of the generator models rather than to simulate a realistic frequency response that typically occurs in a power system. During the simulation the mechanical power is kept constant at 793 kW.
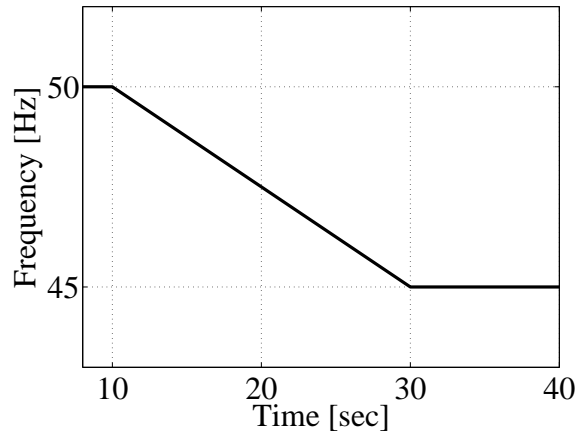

Figure 3.9: Frequency deviation input of the stator voltage.

Since frequency deviation is considered as a slow phenomenon, only power response of the induction generator is observed. Figure 3.10 shows that the traces of active and reactive power during the frequency reduction in the three different models are noticeably different.
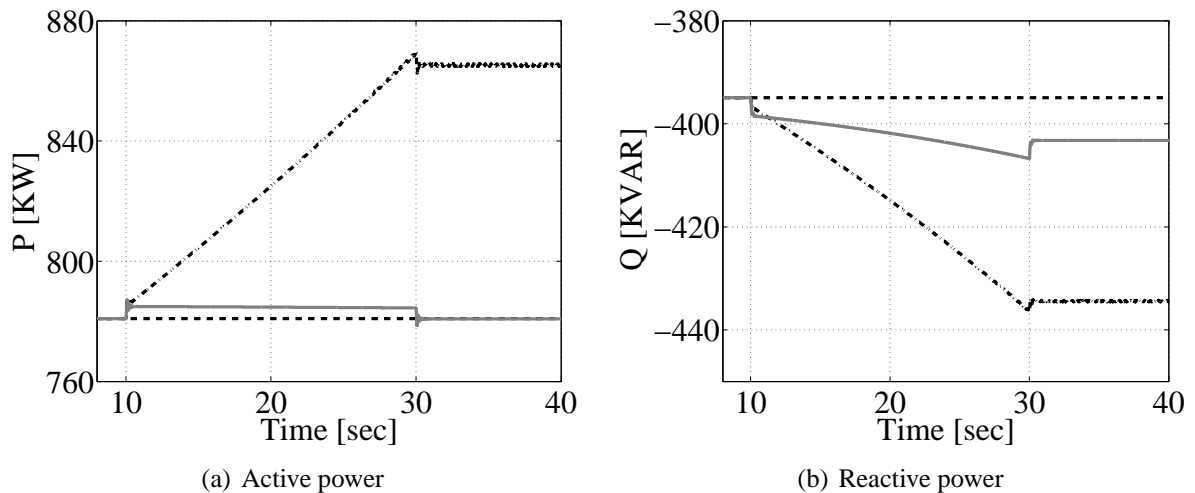

(a) Active power

(b) Reactive power

Figure 3.10: Active and reactive power response of different induction generator models subjected to a frequency deviation: fifth-order model (solid-grey), third-order model (dash-dotted) and first-order model (dash).

Concerning the fifth-order model, the response of active and reactive power can be explained as follows:

25

As the stator voltage frequency constantly decreases at the rate of 0.25 Hz/sec, the generator speed also decreases at roughly the same rate. Since the input power is constant, the fraction of energy contained in the rotating rotor is released due to reduced generator speed. This energy is then subsequently transferred into electrical energy, which is noticed by an increase in active power. Once the frequency is stable at 45 Hz, the active power is back close to the nominal level.

The trace of reactive power is practically determined by two factors. The first factor is directly related to the active power according to the well-known PQ characteristic curve. The second factor is determined by the effective reactance of the generator due to different operating frequencies. As the frequency becomes lower, the effective reactance is reduced as well. During the transition of the frequency from 50 Hz to 45 Hz the increased in reactive power consumption is the sum of these two factors. After the frequency becomes stable at 45 Hz, the reactive power increase is governed only by reduced reactance due to the frequency drop.

The difference in the active power response between the fifth-order and the third-order models during frequency deviation is caused by the absence of the stator flux derivative in the third-order model. During off-nominal frequency, depending on the size of the deviation, the stator flux derivative can be considerably large. Consequently, any neglect of this factor leads to an incorrect prediction of electric torque as well as copper losses, which leads to an incorrect response to active power output. From a more fundamental perspective, it is found that the third-order model cannot even hold the energy conservation law, as the input power can be larger than the sum of the output power and losses. This is shown in Figure 3.10a. Once the frequency is stable at 45 Hz, the output power is around 865 kW while the actual input power is approximately 793 kW. The reactive power response of the third-order model can be explained using the same method as for the fifth-order model.

Regarding the first-order model, as the model disregards all electrical dynamics and the reactance values are constant, the response of the model is totally unaffected by the frequency change. This was clearly indicated by the constant active and reactive power during the frequency change.

3.1.6   Integration time step size

As mentioned in Chapter 2, the maximum integration time step of a model can be calculated analytically using the concept of stability region. The study starts by analyzing the maximum integration time step allowed for each model in order to keep the simulation within the numerical stability limit. This can be done, first, by deriving a linearized model of each induction generator model. Subsequently, the largest eigenvalues of the system matrix are to be calculated. By substituting this eigenvalue into (2.7) the maximum allowed integration time step can be found.

Fifth-order model

The simplified linearized model of the fifth-order model can be made by assuming that the slip is constant around the operating point. Hence, only an electrical system is considered. This can be justified since the electrical system time constants are much smaller than me-

chanical system time constants. This result in a linear model, which is given as

$$
\begin{bmatrix} \dot{\psi}_s \\ \dot{\psi}_r \end{bmatrix} = -\begin{bmatrix} \frac{R_s}{\sigma L_s} + j\omega_s & -\frac{R_s L_m}{\sigma L_s L_r} \\ -\frac{R_r L_m}{\sigma L_s L_r} & \frac{R_r}{\sigma L_r} + j s \omega_s \end{bmatrix} \begin{bmatrix} \psi_s \\ \psi_r \end{bmatrix} + \begin{bmatrix} \mathbf{v_s} \\ \mathbf{v_r} \end{bmatrix}
\tag{3.24}
$$

where σ is the leakage factor and is given by

$$
\sigma = 1 - \frac{L_m^2}{L_s L_r}
\tag{3.25}
$$

For an illustration, the induction generator parameters given in Appendix F are used. The largest eigenvalue of the system matrix is

$$
\lambda_1 = -8.99 - 313.81i
$$

Substituting this value into (2.7), and solving the equation for h, we have

$$
h < 0.00206 \text{ s}
$$

Hence, the maximum time step required (h_{max}) is approximately 0.00206 s.

The analytical result is then compared with the simulation result performed in the simulation tool Matlab/Simulink. A small disturbance in the form of a 1% voltage dip is applied to the generator terminal and then the current is observed. As demonstrated in Figure 3.11, the simulation is pretty stable for a time step less than the critical value ($h = 0.0015$ s), this can be noticed by the fast decay of the current. If the time step is increased so it reaches the critical value ($h = h_{max} = 0.00206$ s), the current starts to oscillate constantly, later when the value just exceeds the critical value ($h = 0.0021$ s) the simulation becomes unstable (current magnitude tends to increase continuously). Accordingly, this simulation result shows the validity of the analytical calculation.

Third-order model

By removing the stator flux derivative from (3.24), the system equations become

$$
\dot{\psi}_r = \left(\frac{R_r}{\sigma L_r} + j s \omega_s \right) \psi_r + \mathbf{v_r}
\tag{3.26}
$$

Now the maximum eigenvalue is determined by

$$
\lambda = \frac{R_r}{\sigma L_r} + j s \omega_s
\tag{3.27}
$$

Typically, the first term on the right-hand side of (3.27) is a small constant variable. Hence, the eigenvalue is governed mainly by the last term of the equation, which is slip dependent.

By substituting λ into (2.7) and by varying the value of the slip, the relation between maximum time step h_{max} and the slip can be presented as shown in Figure 3.12.

Suppose the generator given in Appendix F runs at 0.8% of slip, then according to the relation between slip and the maximum time step given in Figure 3.12, the corresponding maximum time step will be 0.158 s. Again, this Figure is examined using a simulation and the result is shown in Figure 3.13. Similar to the previous simulation of the fifth-order model, the calculation result agrees with the simulation result where the simulation becomes unstable when the time step just exceeds h_{max}.
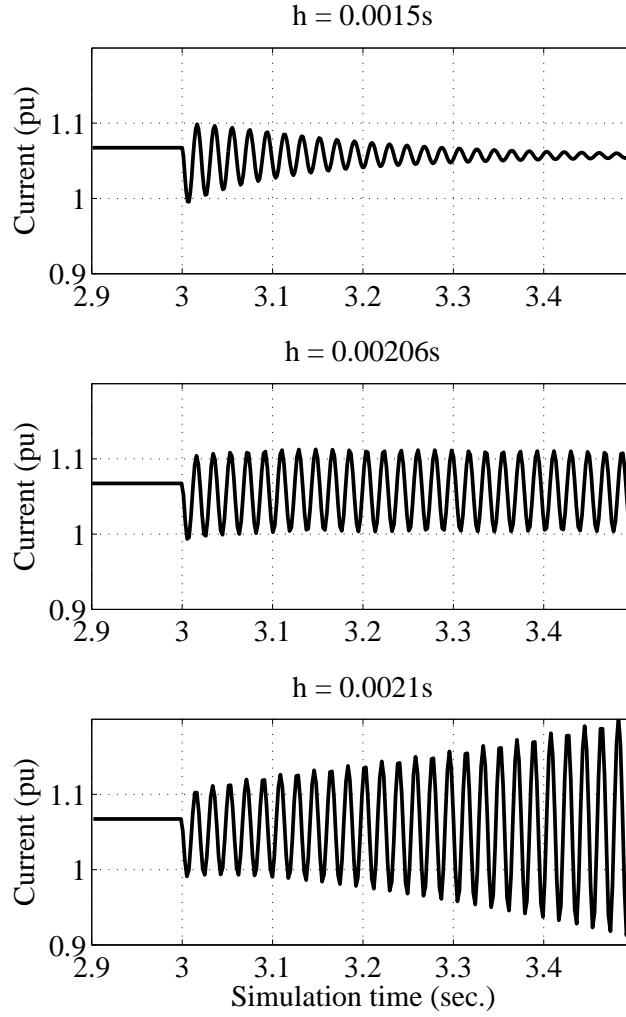
27

Figure 3.11: Influence of time step on numerical stability of the fifth-order model of induction generator.

First-order model

In the first-order model, the only state variable is rotor speed. According to [28], the linearized model of the first-order model is given by

$$T_e = p \left(\frac{L_m}{L_s} \right)^2 \frac{|\mathbf{v_s}|^2}{\omega_s^2 R_r} (\omega_s - \omega_r) \tag{3.28}$$

$$\dot{\omega}_r = -p \left(\frac{L_m}{L_s} \right)^2 \frac{|\mathbf{v_s}|^2}{J_g \omega_s^2 R_r} \omega_r + K \tag{3.29}$$

Equation (3.29) indicates that the maximum time step of the first-order model depends on many factors, such as stator voltage, magnetizing and stator inductance, rotor resistance and rotor inertia. Using a similar calculation with the same generator parameters as in the previous models, the maximum time step for the first-order model is found to be 0.028 s.
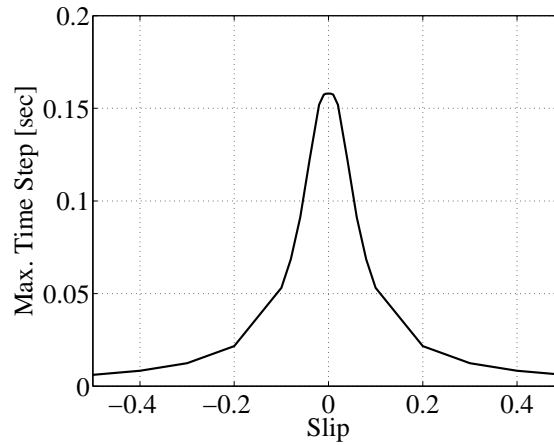
28

Figure 3.12: Maximum integration time step for third-order model of induction generator as function of slip.

This value is smaller than the maximum time step in the third-order model. From simulation efficiency standpoint, this means that use of the first-order model is not always beneficial compared to the third-order model.

3.1.7 Modified fifth-order model for fundamental frequency simulation tools

The advantage of the fifth-order model in terms of result validity, which has direct consequences on the action of over-speed and instantaneous over-current protection, has been addressed in Subsection 3.1.5. Therefore, from this perspective it would be beneficial to employ the fifth-order model for stability studies.

However, the fifth-order model cannot be implemented directly into a fundamental frequency network model owing to the involvement of stator flux dynamics, which is equivalent to the presence of a dc-offset in the stator current, as explained in subsection 3.1.1. In fact, the fundamental frequency network model is the most commonly used in stability simulation tools rather than the instantaneous network model. This is because by utilizing the fundamental frequency network model, a much more efficient simulation time can be attained.

Accordingly, in order to interface the fifth-order model of an induction generator with the fundamental frequency network model, the dc-offset component in the stator current of the fifth-order model must be removed. This can be done by using a procedure proposed in the following.

Dc-offset removal contained in the stator current

As expressed in (3.13), the Thevenin equivalent of the fifth-order model is depicted in Figure 3.14.

Considering Figure 3.14, according to the superposition theorem for electric circuits, the stator current is composed of two components which correspond to two voltage sources: (1) the rotor flux linkage $\mathbf{v}'_e$ and (2) the rate of change of the stator flux $d\psi_s/dt$.

The stator current delivered into the network $\mathbf{i}_{sf}$ includes only the first component, while the second component is removed. By doing so, the grid recognizes only the fundamental
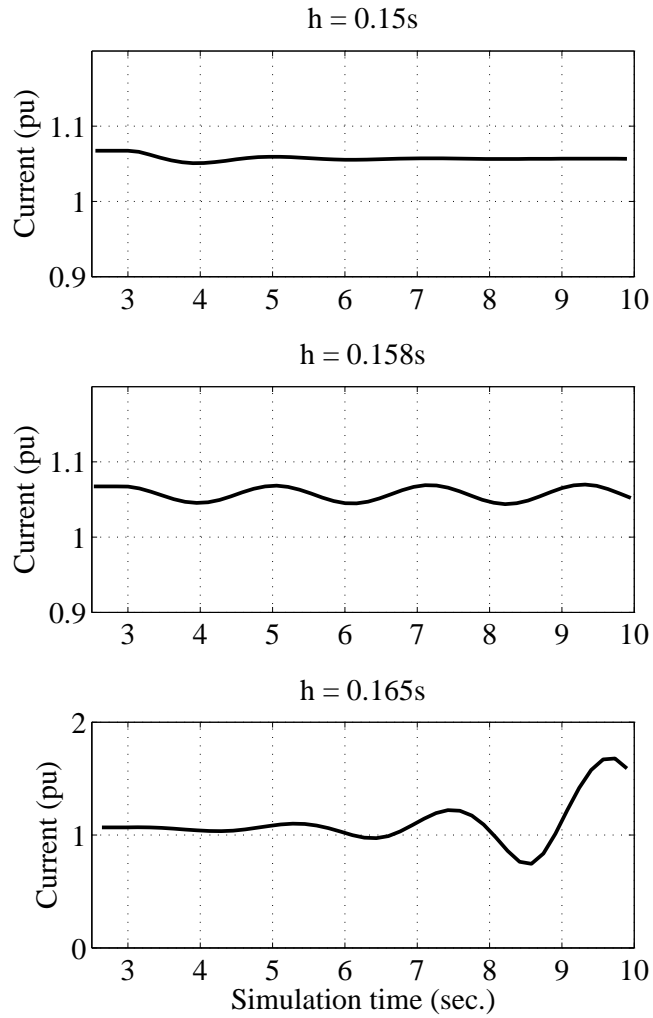
29

Figure 3.13: Influence of time step on the numerical stability of the third-order model of induction generator.

frequency component of the stator current. The grid injected stator component is calculated using the following equation

$$\mathbf{i_{sf}} = \frac{\mathbf{v_s} - \mathbf{v'_e}}{R + jX's} \tag{3.30}$$

Figure 3.15 illustrates the stator current and the stator current component that is injected into the grid.

The electrical torque of the generator remains to be calculated using the actual stator current. This leads to a more accurate prediction of the rotor speed.

Model adaptation with a larger simulation time step

As described in subsection 3.1.6 the fifth-order model demands a considerably small integration time step (approximately 2 ms) in order to maintain numerical stability, while the
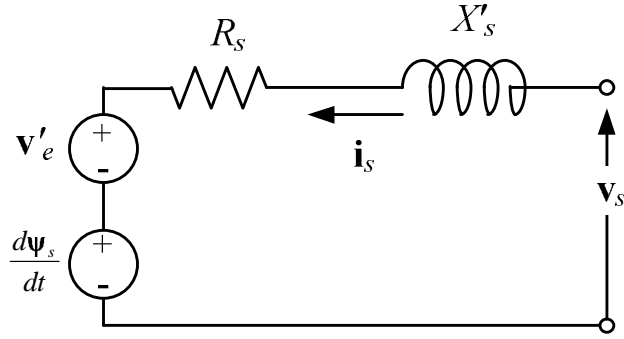
Figure 3.14: Transient representation of the fifth-order induction generator. Observe that the current direction is expressed according to motor convention.
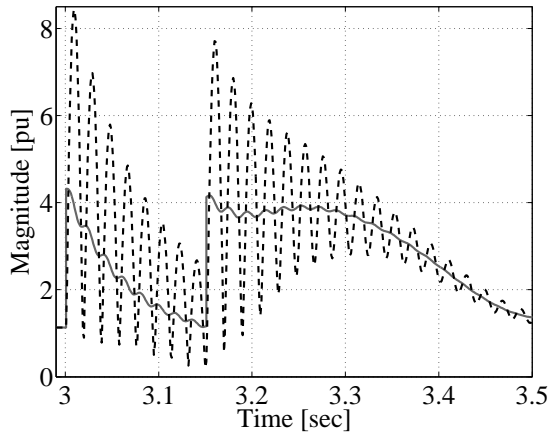

Figure 3.15: Actual stator current magnitude (dash) and stator current component injected into the grid (solid).

standard integration time step for stability studies is much larger (10 ms). This poses a challenge to keep the model running at such a constraint. This thesis proposes utilizing an internal integration loop. This means that for each standard integration time step, the model executes an internal loop procedure iteratively at a smaller time step size. The Heun integration method is chosen in this study because this method is relatively simple yet provides relatively good accuracy.

At each internal loop execution, the model performs a derivative calculation, performs an integration and advances the internal time sample. This sequence is carried out continuously until it reaches the next standard integration time sample. The stator voltage, as an input to the model, is updated by the network calculation every standard time step. The internal integration loop can be performed by assuming the stator voltage is constant at each standard time step. However, when the stator voltage changes rapidly and continuously, such in the case of a large frequency deviation, this assumption is no longer valid. Hence, the value of the stator voltage at each internal integration time step must be estimated. The estimation is derived from the rate of change (slope) of the voltage from the last two standard simulation time samples (t_{n-2} and t_{n-1}). Subsequently, the rate of change of the voltage at current time sample (t_n) can be estimated. By doing so, the estimated value of the stator voltage of the following integration interval (from t_n to t_{n+1}) can be obtained.

**Result validation against PSCAD/EMTDC model**

The modified model described above is implemented in the simulation tool PSS/E. The validity of the model is then compared with a full order model in PSCAD/EMTDC as demonstrated in Figure 3.16. The response of the third-order model is also included in the figure to show the advantage of the modified model compared to the third-order model. The Figure shows that the modified fifth-order model is able to provide a much accurate rotor speed than the third-order model.

As shown in Figure 3.17, the peak value of the stator current in the modified fifth-order model is higher than the stator current of the PSCAD/EMTDC model. This is because of the different natures of the network model between the two simulations. For the fundamental frequency network model, the voltage quantities (magnitude and angle) change immediately after fault initiated, this is not the case for the instantaneous network model. Figure 3.18 shows that the voltage angle of the instantaneous network model does not change instantly, this makes the transient current somewhat lower. Nevertheless, the modified model tends to provide a more conservative estimation in regard to transient current response.

Figure 3.19 shows that the accuracy of the model in predicting peak current is characterized by the generator and grid parameters, as well as fault magnitude. The model estimates transient current better at a higher value of the stator resistance because of the smaller time constant. The prediction is also better for a more severe voltage dip. Speed and the voltage transient behavior prediction is highly accurate at any given generator and grid parameters, as well as fault magnitude.
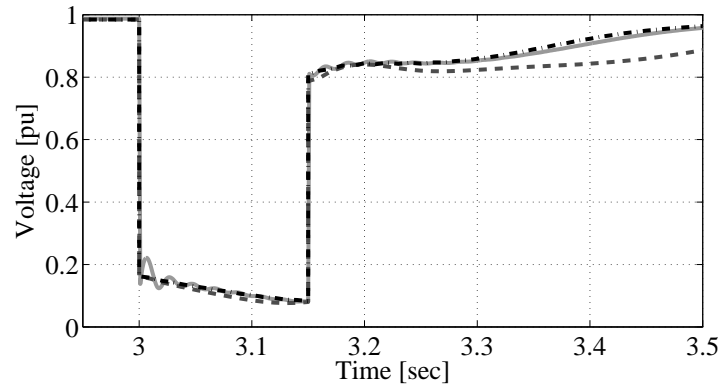
(a) Voltage
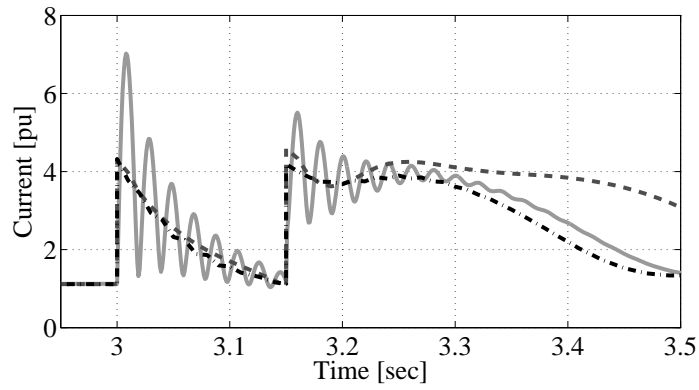
(b) Grid injected current
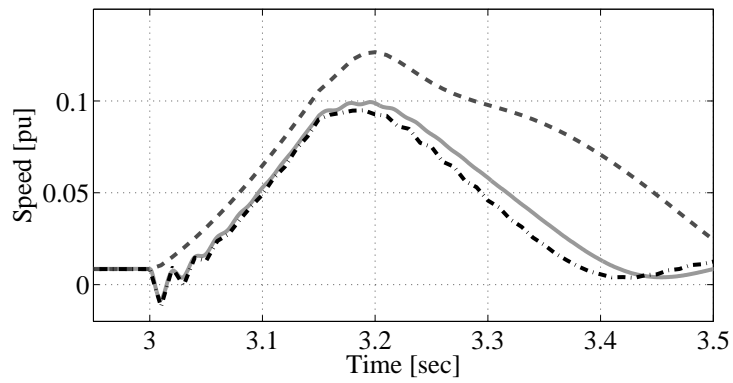
(c) Speed

Figure 3.16: Fault response of induction generator models: the fifth-order model with instantaneous network model in PSCAD/ETMDC (solid-grey), the modified fifth-order model in combination with phasor network model in PSS/E running at 10 ms time step (dash-dot) and the typical third-order model in PSS/E (dash).
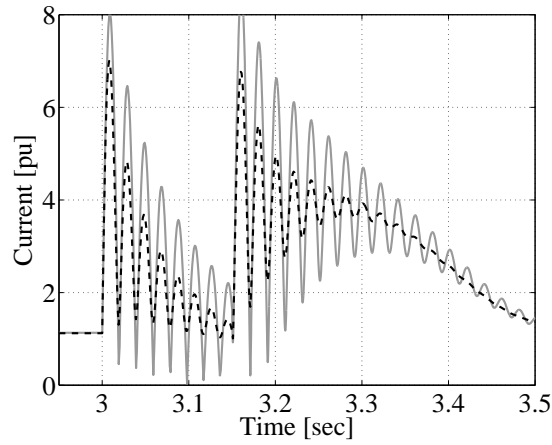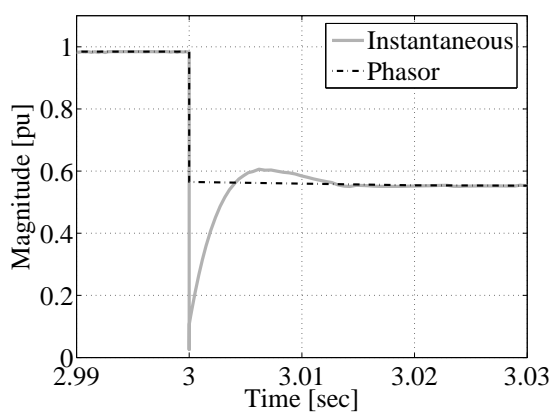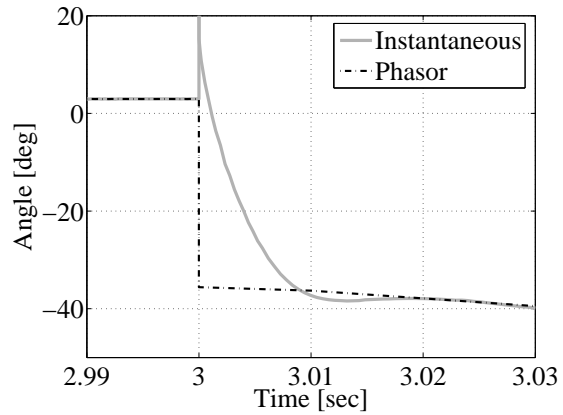
Figure 3.17: Stator peak current: the modified fifth-order model in PSS/E (solid-grey) and the fifth-order model in PSCAD/EMTDC (dash-black).

(a) Voltage magnitude

(b) Voltage angle

Figure 3.18: Voltage quantities during switching in the instantaneous and fundamental frequency network models.
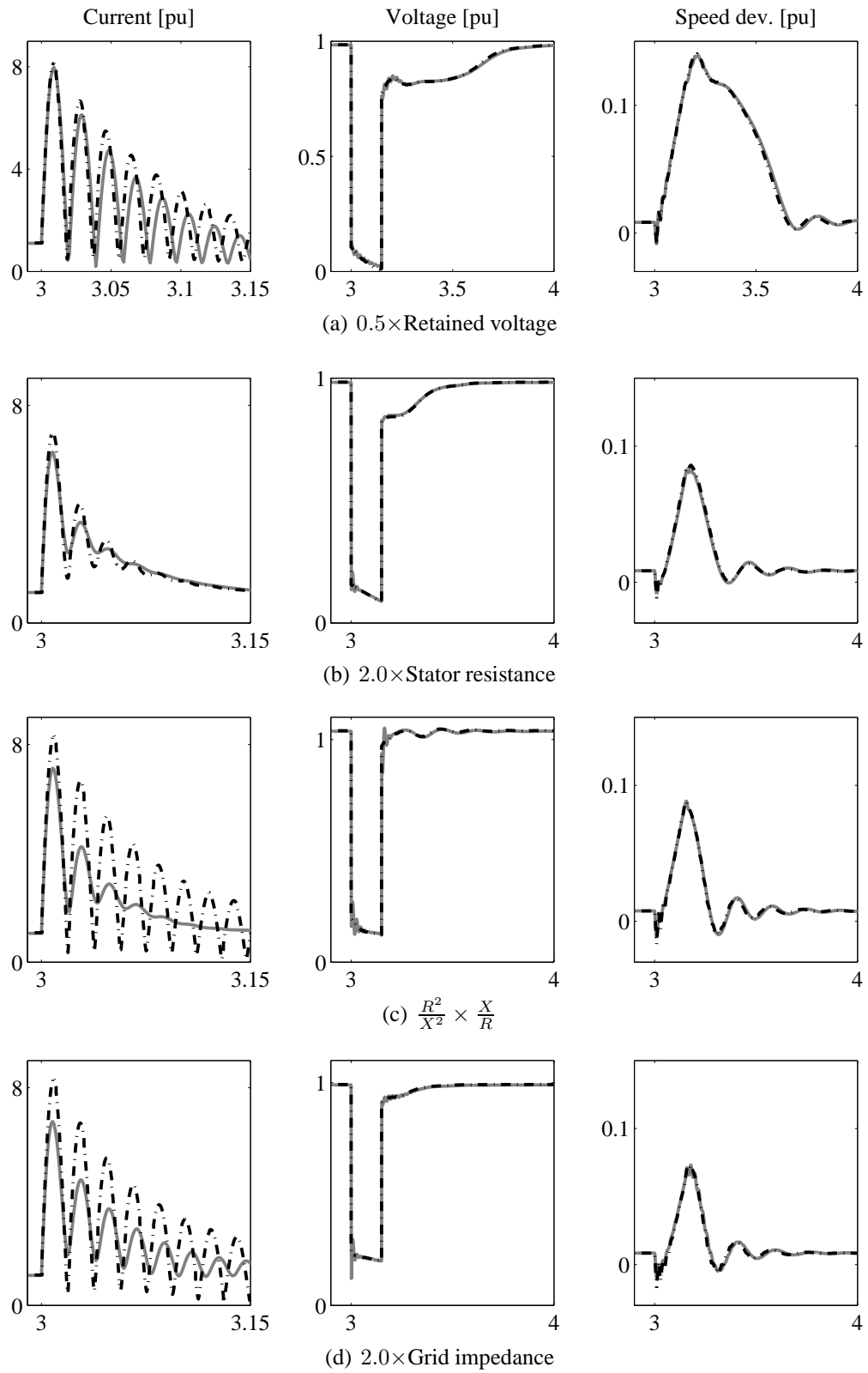
Figure 3.19: Accuracy of the modified fifth-order model for fundamental frequency simulation tools for different generator and grid parameters.

35

3.1.8 Third-order model with calculated peak current

Another method of estimating peak transient current can be carried out based on the short-circuit analysis given in [29]. Accordingly, a short-circuit on the terminal of an induction generator is identical with applying negative stator voltage $(-\mathbf{v_s})$ on the terminal of the generator. Assuming that the generator is free of currents and voltages before the negative voltage is applied, this applied voltage creates a transient current component. Later, the steady-state pre-fault current is then added to the transient current in order to obtain the actual short-circuit current of the generator.

The transient current component in per unit is given by

$$\mathbf{i_s} \approx -\frac{\mathbf{v_s}}{jX_r}e^{j\tau} - \frac{\mathbf{v_s}}{jX_r'}e^{-s_p\tau}\left(k^2 e^{j\tau} - 1\right) \tag{3.31}$$

where $\mathbf{i_s}$ is the stator transient current, $\mathbf{v_s}$ is the pre-fault stator voltage and τ is the time. Note that τ is in per unit $(\tau = \omega t)$. Transient reactance X_r' is obtained using the following relation

$$X_r' = X_{sl} + \frac{X_m X_{rl}}{X_m + X_{rl}} \tag{3.32}$$

Subsequently, the pull-out slip s_p is calculated as

$$s_p = \frac{R_r}{X_r'} \tag{3.33}$$

and k is given by

$$k = \frac{X_m}{X_r} \tag{3.34}$$

In order to simulate a fault that results in a voltage dip, Equation (3.31) can be modified into

$$\mathbf{i_s} \approx -\frac{\Delta\mathbf{v_s}}{jX_r}e^{j\tau} - \frac{\Delta\mathbf{v_s}}{jX_r'}e^{-s_p\tau}\left(k^2 e^{j\tau} - 1\right) \tag{3.35}$$

where $\Delta\mathbf{v_s}$ is the stator voltage change/reduction.

Considering that the pre-fault current is $\mathbf{i_{s0}}$, the actual current after the voltage dip becomes

$$\mathbf{i_s} \approx \mathbf{i_{s0}} - \frac{\Delta\mathbf{v_s}}{jX_r}e^{j\tau} - \frac{\Delta\mathbf{v_s}}{jX_r'}e^{-s_p\tau}\left(k^2 e^{j\tau} - 1\right) \tag{3.36}$$

Figure 3.20 shows the transient current of an induction generator during a voltage dip using analytical and simulation methods.

This estimation method can be used as a complement to the third-order model. The third-order model assures compatibility with the fundamental frequency simulation tool while the estimation method predicts the peak current during a transient. Since the estimation method calculates peak current algebraically and takes place only during the fault, this combination offers faster computational time compared to the fifth-order model.

However, this method assumes the pre-fault steady state condition is fully known. Hence, for a transient that occurs during a non-steady state condition cannot be accurately predicted by this method.
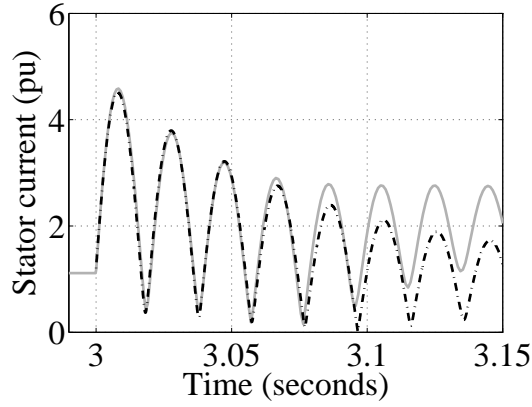
Figure 3.20: Transient current of induction generator during voltage dip: using simulation method (solid-grey) and calculation/analytical method (dash-dotted).

3.2 Turbine rotor aerodynamic models

Simulation of power extraction from a wind stream, which is converted into mechanical shaft power can be performed using different approaches. The relation between mechanical power input and wind speed passing a turbine rotor plane can be written according to the following expression

$$P_{mec} = 0.5\rho\pi R^2 \upsilon^3 C_p(\lambda, \beta) \tag{3.37}$$

where P_{mec} is the mechanical power input, ρ is the air density, R is the rotor blade radius, υ is the wind speed and C_p is the coefficient of performance of the turbine rotor which is a function of pitch angle β and tip speed ratio λ. The tip speed ratio is obtained from $\lambda = (\omega_t R)/\upsilon$, where ω_t is the rotational speed of the turbine.

There are different possible alternatives for modelling the aerodynamic system of a wind turbine such as using the blade element method, $C_p(\lambda, \beta)$ lookup table and the wind speed-mechanical power lookup table.

3.2.1 The blade element method

According to the blade element method (sometimes called the blade element theory or the blade element momentum) [30, 31] a turbine blade is divided into several cross-sections along the radius. The total forces applied to the blade are the sum of force on each section. Two major force components that act on each blade segment are (see Figure B.2): (1) lift force, which occurs because of the pressure difference between the upper and the lower side of the blade, the force direction is orthogonal to the equivalent wind speed, and (2) drag force, which acts on the same direction of the equivalent wind speed. Further description and formula used in the blade element method can be found in Appendix B

3.2.2 $C_p(\lambda, \beta)$ lookup table

The blade element method yields a rather good result in agreemenet with the measurement [30]. The disadvantage of the method is that the model requires time-consuming computational efforts. As an alternative, a static representation of $C_p(\lambda, \beta)$ can be used. Since

the generator receives mechanical torque as an input, the mechanical power must be divided by the corresponding generator rotor rotational speed. During standstill, however, the torque is unidentified since the generator rotor speed is zero. To overcome this problem, it is common to use the torque coefficient lookup table or $C_q(\lambda, \beta)$. This can be done by dividing each elements in $C_p(\lambda, \beta)$ lookup table with tip speed ratio λ.

3.2.3 Wind speed - mechanical power lookup table

When the wind speed and the rotor speed dynamics are considered as slow throughout a study, the relation between wind speed and mechanical power can be presented as a two-dimensional lookup table. This model is suitable for long-term power system stability studies where the dynamics of the aerodynamic system can be neglected without neglecting the influence of the wind speed fluctuation on mechanical and electrical output power.
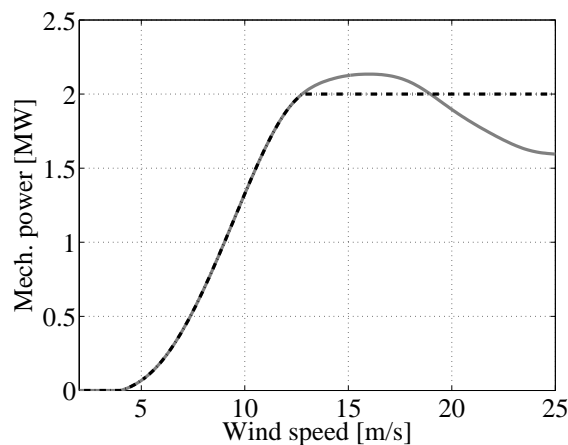

Figure 3.21: Mechanical power input as a function of wind speed for typical 2 MW fixed speed wind turbine: passive stall (grey solid) and active stall (black dash-dotted).

3.2.4 Active stall controller

Limiting mechanical input power so that rated power is not exceeded is an essential aspect for large wind turbines. This can be done in different ways, such as using passive stall control, pitch control and active stall control.

The passive stall control utilizes the geometry of the rotor blades which can limit the lift force when the wind speed becomes too high by creating turbulence on the rotor blade side which is not facing the wind. The pitch controlled wind turbine limits the output power by turning (pitching) the rotor blades slightly out of the wind.

The active stall control is similar with the pitch control in the way that it uses pitch mechanism to limit the output power. When the input power reaches the rated power of the generator, the stall controller moves the blade in such a direction that increases the angle of attack, which is in the opposite direction from what the pitch controller does.

The active stall mechanism allows the wind turbine to operate at almost constant output power for wind speeds above rated speed. Another advantage of the active stall mechanism is that this mechanism can avoid an active power overshoot beyond the rated power.

The active stall controller is depicted in Figure 3.22. First, the actual power of the turbine is measured and compared with the active power reference value, which is the rated power of the turbine. The error between the reference and the actual values of active power is passed through a PI-controller to provide the pitch angle reference value. In order to limit the pitch rate, the pitch reference value is passed through a pitch rate limiter. The limited-rate reference value is fed into a pitch actuator. The pitch actuator is modeled as a first-order time-lag system in order to model the hydraulic system of the actuator.
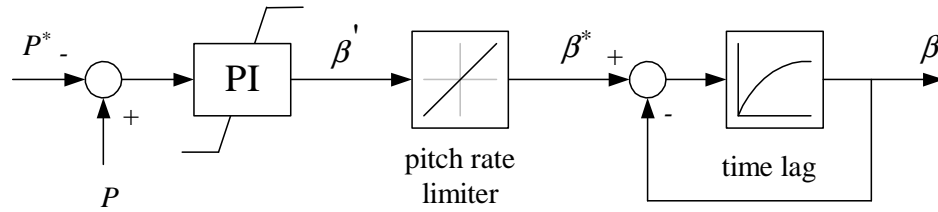

Figure 3.22: Pitch control for active stall wind turbine.

Only a small change in pitch angle is required for the active stall mechanism in order to reduce the power output. Hence, the travel of the pitch angle is considerably shorter than a pitch control mechanism. As shown in Figure 3.23, the active stall operating curve is represented as line OA and the pitch operating curve is represented as line OB. Both lines have the same length. Point A corresponds to $C_p \approx 0.05$ and point B corresponds to $C_p \approx 0.1$. This means that with the same angle movement, the active stall can reduce the power twice as much as for the pitch control mechanism. In stall regulation, normally the pitch angle is adjusted within the range of 0° to -10°.
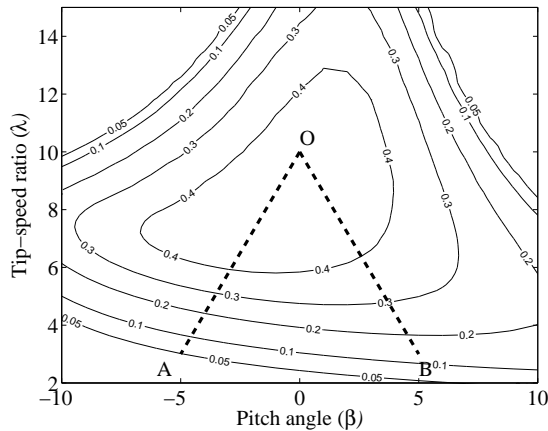

Figure 3.23: Contour diagram of a $C_p(\lambda, \beta)$ curve. The contour lines show constant C_p values. Operation area of an active stall and a pitch regulation are shown in the figure as line OA and line OB, respectively.

In order to avoid unnecessary continuous changes in pitch angle, which may wear the pitch mechanic, the pitch is moved by utilizing a "sample and hold" controller in combination with a threshold controller block [32]. This mechanism allows the pitch to move only for every specified period of sample time and if the difference between the new and the old set point exceeds a certain minimum value. For power system stability studies, however, this mechanism can be excluded from the model.

3.3 Mechanical system

Different mechanical dynamics/effects take place in a wind turbine that may induce dynamics in the electrical part, such as (1) a 3p effect, (2) tower vibration effect, and (3) soft shaft drive train dynamics. The first effect is caused by a non-homogenous wind speed across the turbine rotor plane and the presence of a tower (tower shadow). For power system stability studies, the 3p effect as well as tower vibration are of secondary importance because the oscillation magnitude generated by these dynamics is negligible. Hence, only dynamics on the drive train due to non-stiffness of the gearbox are taken into account in the study.

As shown in Figure 3.24, the structure of a mechanical drive train consists of two inertias [33]. The first inertia is made of the lumped inertia of the turbine, part of the gearbox and the low-speed shaft. The second inertia consists of the generator rotor mass, the high-speed shaft including a disk brake and part of the gearbox. The two inertias are connected to each other through a spring, which mainly represents the stiffness of the gearbox and the mechanical shaft.
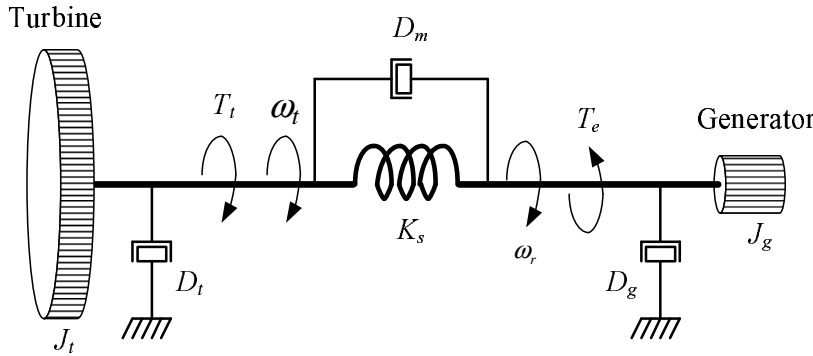

Figure 3.24: Drive train structure of a wind turbine.

Three different damping components are present on the mechanical model:(a) the turbine self damping (D_t), (b) the generator self damping (D_g) and (c) the mutual damping (D_m). The aerodynamic resistance takes place in the turbine blade, the generator self damping represents mechanical friction and windage and the mutual damping represents balancing dynamics which occur because of different speeds between the generator rotor and the turbine shaft. The mathematical equations of the two-mass model of a drive train, by neglecting the turbine and the generator self damping, are given as

$$2H_t \frac{d\omega_t}{dt} = T_t - K_s(\theta_r - \theta_t) - D_m(\omega_r - \omega_t) \tag{3.38}$$

$$2H_g \frac{d\omega_r}{dt} = -T_e + K_s(\theta_r - \theta_t) + D_m(\omega_r - \omega_t) \tag{3.39}$$

$$\frac{d\theta_t}{dt} = \omega_t \tag{3.40}$$

$$\frac{d\theta_r}{dt} = \omega_r \tag{3.41}$$

where H_t and H_g are the turbine and the generator inertia constant, respectively. K_s is the shaft stiffness, ω_t and ω_r denote the turbine and the generator rotor speed, respectively. θ_t and θ_r denote the turbine and the generator rotor angle, respectively.

The model can be simplified by removing the shaft stiffness. Hence, there is only a single inertia which is the sum of the generator rotor and the turbine inertia. The mathematical equation of this simplified model can be expressed as follows:

$$2(H_t + H_g)\frac{d\omega_r}{dt} = T_t - T_e \qquad (3.42)$$

3.4 Soft starter

Soft starters are always employed in recent wind turbines to limit the inrush current during starting operation of induction generators. This can be done by controlling the voltage applied to the generator stator in such way so the voltage increases progressively during the starting operation. The voltage control is done by cutting the stator voltage waveform using thyristors at an appropriate firing angle. In a more advanced soft starter, the starting current can be limited at a predefined value offering smoother interaction with the power system.

A soft starter consists of three pairs of anti-parallel thyristors as shown in Figure 3.25.
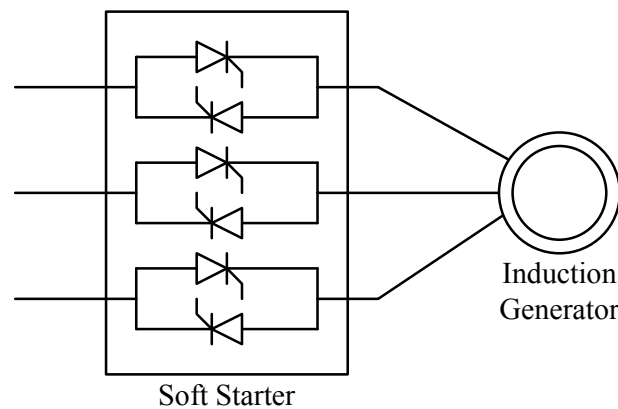

Figure 3.25: Soft start arrangement.

The starting process of a soft starter can be described as follows [27]: First, the turbine is let to accelerate by means of wind speed so that the generator speed reaches approximately 5-30% below the synchronous speed. The soft starter then starts to operate by providing ramping-up for the rms stator voltage. Once the generator speed reaches its rated value or the current is at steady state, the bypass contactor is closed. Subsequently, the capacitor banks are connected either gradually (several steps) or at once.

The generator response during starting operation using a soft starter is shown in Figure 3.26. The firing angle of the soft starter in the simulation is set to $180°$ in the beginning and is increased linearly to $0°$ in 2 seconds. Since the rms-voltage is not proportionally linear to the firing angle, the rms-voltage increases in non-linear mode. The current drawn by the generator is also highly non-liner due to several factors such as the non-linearity of the generator, especially during starting operation. The current flowing through the soft-starter is also a function of the power factor. Consequently, the current is not proportional to the voltage.

For power system stability studies, the soft start operation is modeled as a controller voltage source in parallel to the generator. A comparison between the rms-model and the

41

(a) Instantaneous voltage
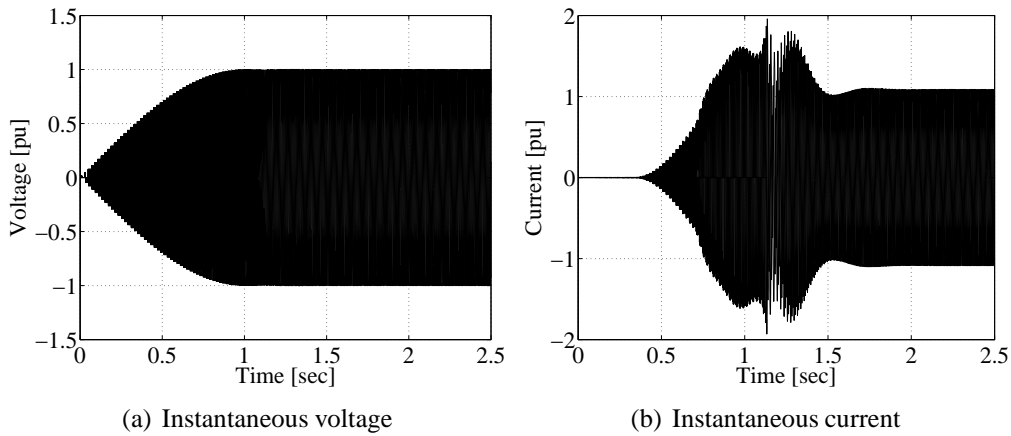
(b) Instantaneous current

Figure 3.26: Simulation of detailed model of soft-starter.

detailed-model of the soft starter is shown in Figure 3.27. The figure shows that the response of the rms-model is not similar to the detailed-model, however the rms-model can still estimate the magnitude of the peak current during starting operating within an acceptable range (with an error rate of approximately 13%). Simulation results of a soft starter operation with a ramp-up time of 200 ms, which is typical for a stall-controlled wind turbine, are shown in Figure 3.28. The rms-model is able to estimate the peak inrush current sufficiently accurate (with an error rate of approximately 10%).
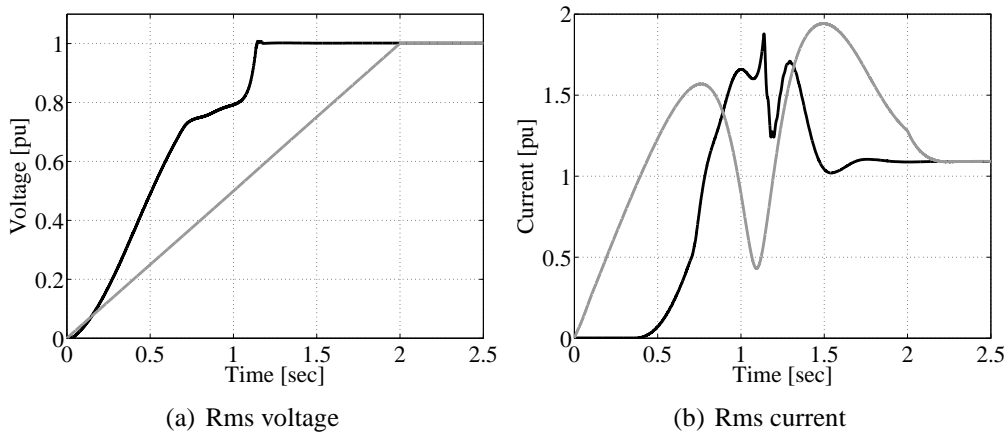

(a) Rms voltage

(b) Rms current

Figure 3.27: Simulation result of soft-starter: detailed model (black) and rms model (grey) with ram-up time 2 seconds.

Alternative method of reducing starting current in wind turbine

An insertion of external resistors during starting operation can be another alternative method to reduce the starting current of a wind turbine. In this method, the capacitor bank can be connected directly before the starting event in order to provide sufficient reactive power during the starting process. A more detailed discussion regarding this method can be found in [27].
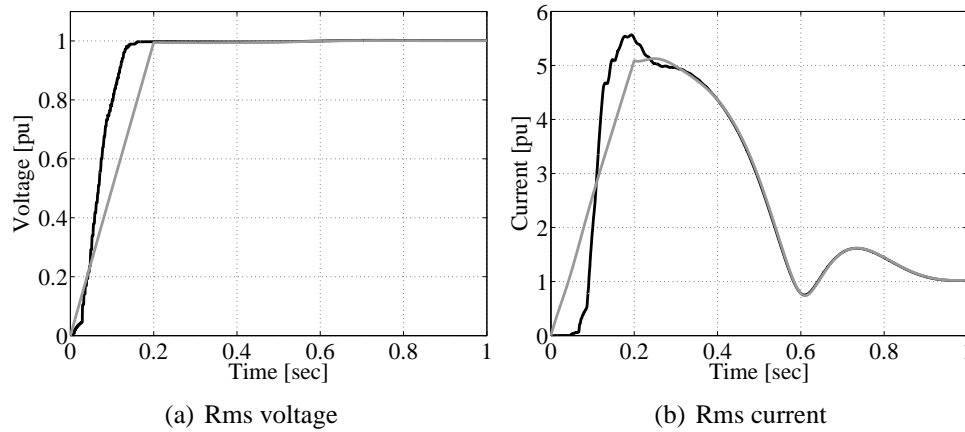
(a) Rms voltage	(b) Rms current

Figure 3.28: Simulation result of soft-starter: detailed model (black) and rms model (grey) with ramp-up time 200 ms.

3.5 Protection system

Different types of protection relays in a wind turbine, which are relevant for power system stability studies, are:

- **Under-voltage protection**: An under-voltage protection system is provided to disconnect the wind turbine in the event of a sustained voltage dip. This may occur when the wind farm fails in its attempt to recover following a system fault, or in case of the wind farm being isolated from the rest of the transmission system.

- **Over-voltage protection**: An over-voltage protection system is provided to protect the wind turbine from damage and to prevent a cluster of wind turbines or a wind farm from supplying an unstable island. The protection setting must be set carefully in order not to trip over the normal operating voltage range of the transmission system, including the voltage transient caused by normal switching.

- **Other protections**: Other than under voltage and over-voltage protection, typically a wind turbine is also equipped with over-current protection, under and over frequency protection and turbine trip protection for fault or grid disturbances.

Figure 3.29 shows a typical over/under-voltage protection setting for Vestas OptiSlip V80 wind turbine [34].

The protection devices mentioned above may need some modifications in order to fulfill grid requirements that demand the wind turbine to stay connected during grid disturbances.

3.6 Initialization

Dynamic simulation flow in power system simulation tool PSS/E is presented in Figure 3.30. As depicted in the figure, the dynamic simulation is started by incorporating the dynamic model data into the simulator. Thereafter, state variables and other variables of the dynamic simulation models must be initialized based on the initial load flow data, which has been prepared in advance. If the initialization is not carried out correctly, the system will start
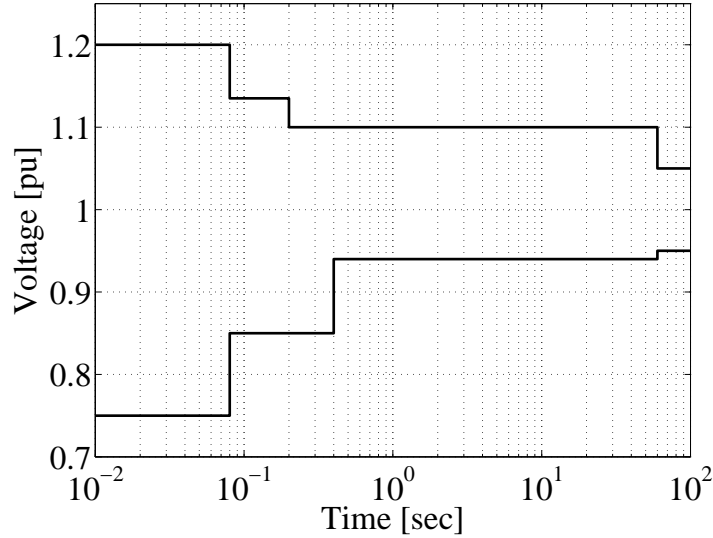
Figure 3.29: Under-voltage and over-voltage protection setting for Vestas OptiSlip V80 [34].

at the unsteady condition. In some cases, it may move toward the equilibrium condition after some time. However, the desired state as obtained from the initial load flow may not be achieved. In the worst situation, instead of moving toward convergence, the system may become unstable and finally the simulation halts.

As part of dynamic models, the wind turbine model must be initialized. The initialization procedure is presented in the following.

3.6.1 Initialization procedure

For a large induction generator representing a large wind farm, for instance, initialization of the generator is highly important. In such a case, inaccurate initialization may lead to numerical instability. The induction generator initialization can be done by solving simultaneous equations that consist of (3.1), (3.2), (3.3), (3.4) and (3.9) to find unknown variables $\mathbf{i_s}$, $\mathbf{i_r}$, ψ_s, ψ_r and s. Note that all of the derivatives in these equations are set to zero.

Since Equation (3.9) is a quadratic expression, the solutions are not in the form of simple expressions. Using mathematical tools, such as Maple or Mathematica, the solution for slip can be obtained analytically. Alternatively the solution can be obtained numerically by using the Newton-Raphson method. Nevertheless, whether solved analytically or numerically, the initialization procedure should be implemented internally into the dynamic model in order to be practical to use.

Once the initial value of these variables are known, the mechanical power input can be calculated using (3.8) and (3.10). Depending on the aerodynamic model used, the corresponding wind speed input can be derived using one of the methods given in (3.2).

The drive train model can be simply initialized using the following equation:

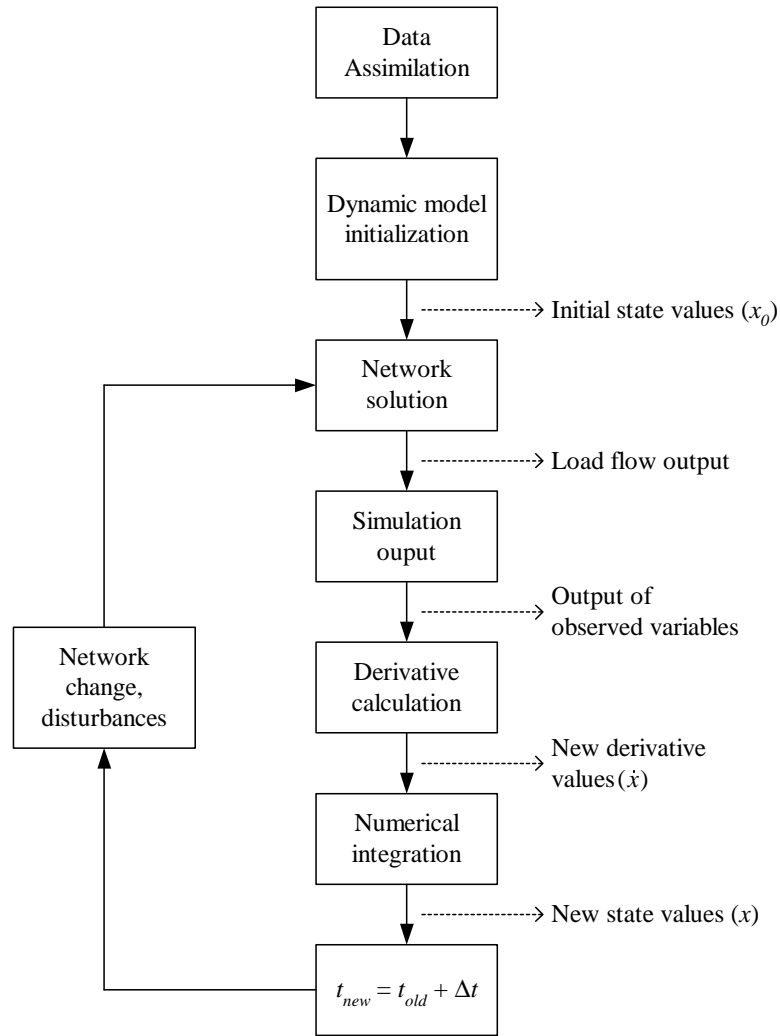$$\Delta\theta = \frac{T_t}{K_s} = \frac{T_e}{K_s} \tag{3.43}$$

44

Figure 3.30: Dynamic simulation flow.

3.6.2 Mismatch between generator initialization and load flow result

In the load flow, active and reactive power injected into the generator bus are given (known variables). Subsequently, the bus voltage is then calculated. In contrast to the generator model, the active and reactive power are calculated by first knowing the stator voltage, which is equivalent to the bus voltage. For this reason, there is a mismatch between the actual reactive power calculated in the generator model and the reactive power provided by the load flow calculation. There are several methods that have been proposed to overcome this problem:

Method 1: An iteration procedure is performed between the power flow and the dynamic model calculation back and forth until a steady state condition is reached. This method is prone to a numerical instability when it is used for a power system with a large amount of induction generator.

Method 2: An artificial admittance is inserted into the generator terminal. The value of the admittance is determined by the difference between the reactive power on the bus (reactive load) obtained from the load flow calculation and the actual reactive power absorbed by the generator Q_s. This method is applied in some power system simulation tools, such as

PSS/E [22]. However, a large mismatch between the initial value in the power flow and the actual value may lead to an incorrect result in a stability study. Special attention is needed particularly when the initialization is performed for a generator with active power production far from unity/rated power. In such a case, reactive power is very sensitive to the voltage level on the generator terminal as illustrated in Figure 3.31. The situation will be more critical for a weak grid due to strong coupling between the generator reactive power and the generator terminal voltage (bus voltage).
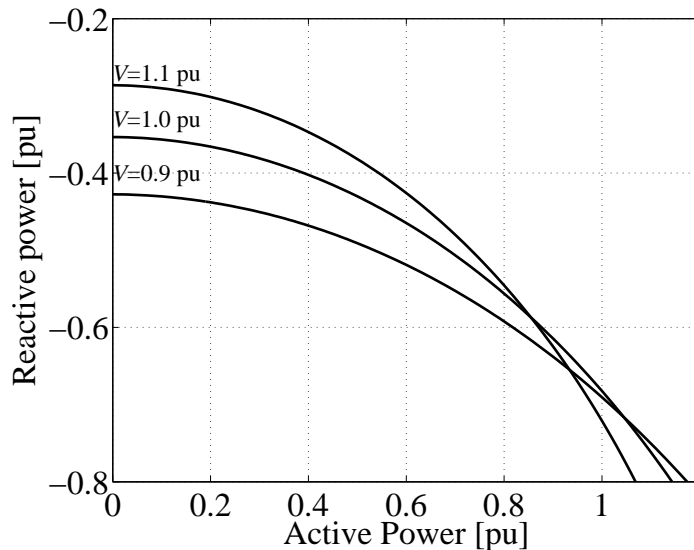

Figure 3.31: Voltage sensitivity of PQ curve for typical induction generator.

Method 3: The steady state induction generator model is included in the initial step of the power flow calculation [35]. This method gives more accurate result i.e. the reactive power in load-flow is close to the actual reactive power calculated using the dynamic model. However since this method must implement additional equations into the network/load flow calculation, it is impractical for most simulation tools.

It is recommended, however, to utilize the PQ-characteristic curve of the generator to approximate a set point of the reactive power in the load flow. The artificial admittance as applied in Method 2 should be avoided whenever possible.

Inaccurate estimation of the initial value of the generator reactive power may lead to unexpected simulation results as illustrated in Figure 3.32. The actual reactive power of the simulated generator at unity power output is 0.7 pu, whereas the reactive power given by the load flow data is 0.3 pu. The difference between the two reactive power is compensated by inserting 0.4 pu of susceptance. The presence of the susceptance results in over optimistic results for the generator response during fault as compared to a generator that is appropriately initialized.

3.7   Model implementation in PSS/E

This sections presents detail of model implementation in the power system stability simulation tool PSS/E. The block diagram of the implementation of a fixed-speed wind turbine model in PSS/E is depicted in Figure 3.33.
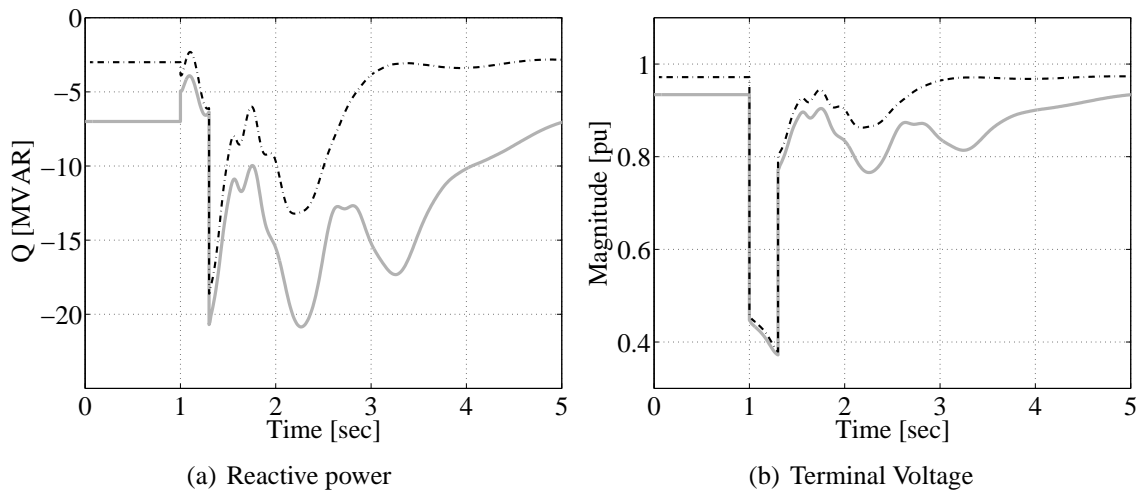
(a) Reactive power

(b) Terminal Voltage

Figure 3.32: Fault simulation with correctly initialized induction generator (solid-grey) and inaccurate estimation of initial reactive power with admittance insertion (dash-dot).
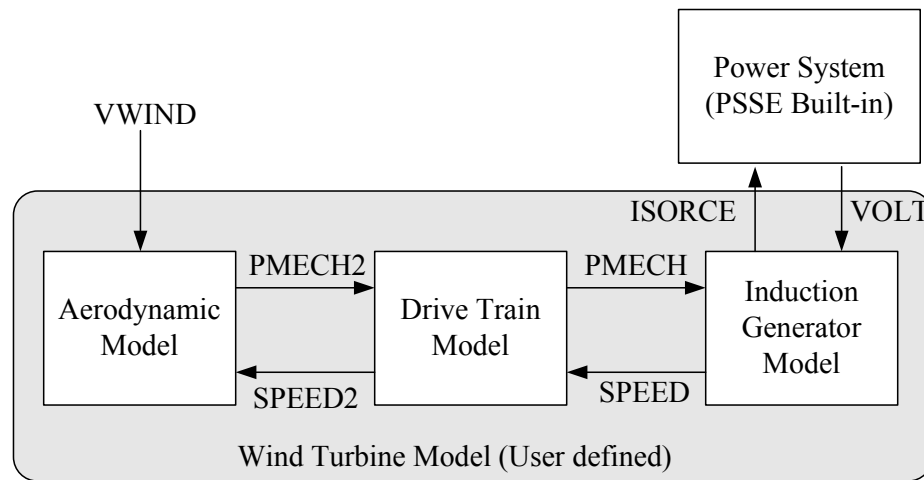

Figure 3.33: Model structure of fixed-speed wind turbine in PSS/E.

The aerodynamic model converts wind speed (VWIND) into the turbine mechanical power (PMECH2) and feeds it into the drive train model. Using the generator rotor speed (SPEED) and the turbine mechanical power (PMECH2) as inputs, the drive train model calculates the shaft mechanical power (PMECH) and the turbine speed (SPEED2). Interaction between the wind turbine user defined model and the network model in PSS/E is performed as follows: The induction generator takes voltage (VOLT) at the bus where the generator is connected. Subsequently, the output of the generator is fed into the network model by putting an appropriate value of the Norton equivalent current source (ISORCE) connected in parallel to the transient impedance (ZSORCE) of the generator. Note that the generator inputs and outputs may differ from the common representation suggested in some literature, such as the input of an induction generator is normally mechanical torque rather than mechanical power. The reason is that the input and output parameters in this model are made to comply with the standard built-in model in PSS/E, which uses mechanical power as an input.

3.8   Conclusion

Among fixed-speed wind turbine parts, the generator is the most critical part from a modelling point of view. This is because the induction generator plays the role as an interface to the network model, which later may influence both result validity and overall simulation efficiency.

Representation of an induction generator using the first-order model has no advantage in terms of accuracy and simulation efficiency. Hence, it is not an option for power system stability studies.

The representation of the third-order model of an induction generator offers a compatibility with the network model and provides more efficient simulation time. The main drawbacks of the third-order model is its inability to predict peak transient current and, to some extent, its less accurate estimation of speed. However, at a relatively high inertia, the third-order model is sufficiently accurate. The inaccuracy of the current response of the third-order model can be compensated by utilizing the analytical method. Despite its ability to provide a valid result, the fifth-order model poses some constraints, such as incompatibility with the network model and that it requires time-consuming simulation owing to a very small time step. A modified model with time step adjustment was proposed in this chapter and may overcome these constraints.

The second important part of a fixed-speed wind turbine model is the drive train, which at the least must be represented in a two-mass model.

Chapter 4

Validation of Fixed Speed Wind Turbine Models

In this chapter, the models of a fixed-speed wind turbine with a squirrel cage induction generator were validated against field measurement data. The aim of these validations is to assure the validity of the models for power system stability studies. Two cases were used for validations, which were based on measurement data from the Alsvik wind turbine and the Olos wind turbine. The measurement data consist of the voltage and current of the wind turbines, which extend from a few cycles preceding faults until a few seconds after the faults are cleared.

The main parts of this chapter have been presented in Paper 3 [36], Paper 4 [37] and Paper 5 [38].

4.1 Validation of the models against Alsvik field measurement data

4.1.1 Measurement setup and data description

The measurement data were taken from the Alsvik wind turbine. The measurement set-up is depicted in Figure 4.1. The relevant data of the measured wind turbine are given in Appendix C. All per unit parameters in the data were calculated on a 210 kVA, 400 V base system.
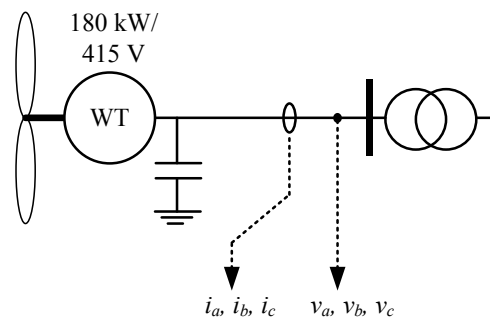

Figure 4.1: Alsvik measurement set up.

The recorded data consist of phase voltages (v_a, v_b and v_c) and phase currents (i_a, i_b and

i_c), which were measured on the low-voltage side of the step up transformer of the wind turbine unit. The measurement data were recorded at a sampling frequency of 256 Hz. As this sampling frequency is relatively low, any dynamics that involve unsymmetrical grid quantities cannot be observed accurately. For this reason, a symmetrical grid condition was assumed in the validation procedure. This means only the positive sequence components of the grid were simulated.

The magnitude of the voltage, as shown in Figure 4.2, was obtained from the available measurement data according to the following relation:

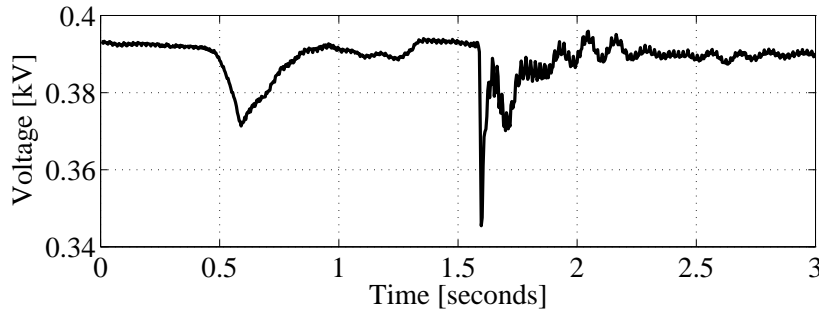$$v_{p-p} = \sqrt{v_a^2 + v_b^2 + v_c^2} \tag{4.1}$$

Figure 4.2: Voltage magnitude data calculated from measured phase voltage.

By referring the system to a particular frequency, which is 50 Hz in this case, the phasor angle of the voltage can be derived and is shown in Figure 4.3. It is shown in the figure that, following the fault event, the phasor angle changes continuously. This indicates that the system frequency slightly changed at the time.
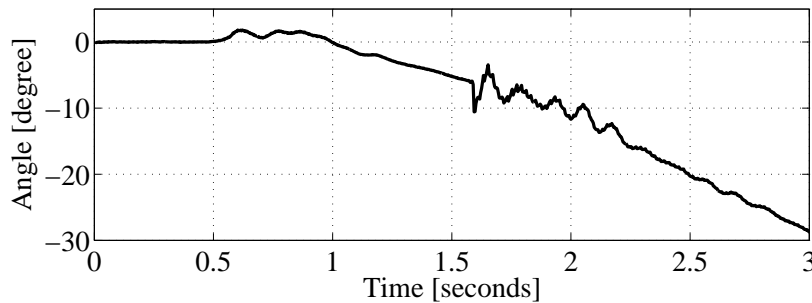

Figure 4.3: Angle deviation.

The active and reactive power of the turbine were calculated from the measured voltage and current using the following expressions:

$$P = v_a i_a + v_b i_b + v_c i_c \tag{4.2}$$

$$Q = \frac{1}{\sqrt{3}}\{(v_a - v_b)i_c + (v_b - v_c)i_a + (v_c - v_a)i_b\} \tag{4.3}$$

The calculated active and reactive power are depicted in Figure 4.4.

(a) Active power output
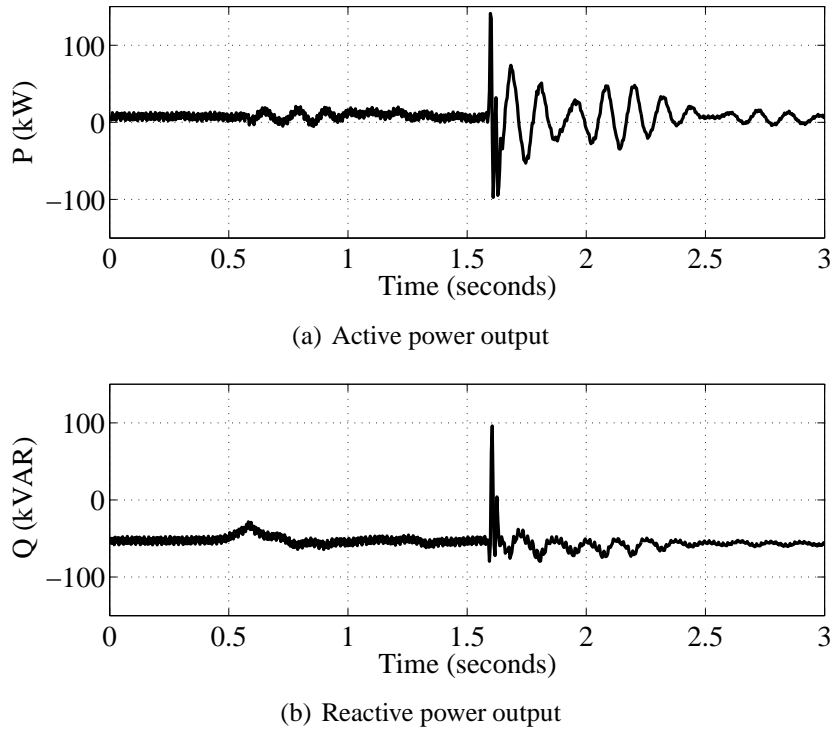

(b) Reactive power output

Figure 4.4: Calculated active and reactive power.

According to Figures 4.2, 4.3 and 4.4, initially, the wind turbine was running at very low power output, which was around 0.05 pu. The induction generator absorbed reactive power of 0.33 pu. However, there was no information regarding the reactive power compensation at the time. Two different transients may be observed:

1. At time 0.5 s the terminal voltage dropped by approximately 5%, followed by a slow recovery and slight frequency oscillations due to angle oscillations. The active power suffered oscillations of around 10 kW in amplitude and around 8 Hz in frequency. The reactive power absorption decreased as a result of the voltage decay, and slightly increased after the transient in order to recover the rotor flux.

2. At time 1.6 s there was a sharp voltage drop of about 10% below the nominal value, followed by voltage and angle oscillations. There were also high active power oscillations of more than 50 kW in amplitude with a frequency of approximately 8 Hz. The behavior of the reactive power after the disturbance was mainly governed by voltage oscillations. A more careful observation in Figure 4.4 shows that there was a slight increase in reactive power consumption after the fault.

Since the second transient had a more rapid and larger voltage drop than the first transient, the second transient was considered to be representative enough to explain responses of the wind turbine. Consequently, only the second transient is discussed in the following sections.

4.1.2 Simulation

The simulations were performed using the simulation tool Matlab/Simulink. The terminal voltage was used as an input of the wind turbine model. Since the voltage data resolution

is poor, it cannot be used directly as an input for the simulation. Instead, a new set of input data must be generated by interpolating both the voltage and the angle data sample given in Figures 4.2 and 4.3 assuming that the three-phase voltages are fully symmetrical. By doing so, a new voltage data set can be obtained as presented in Figure 4.5.
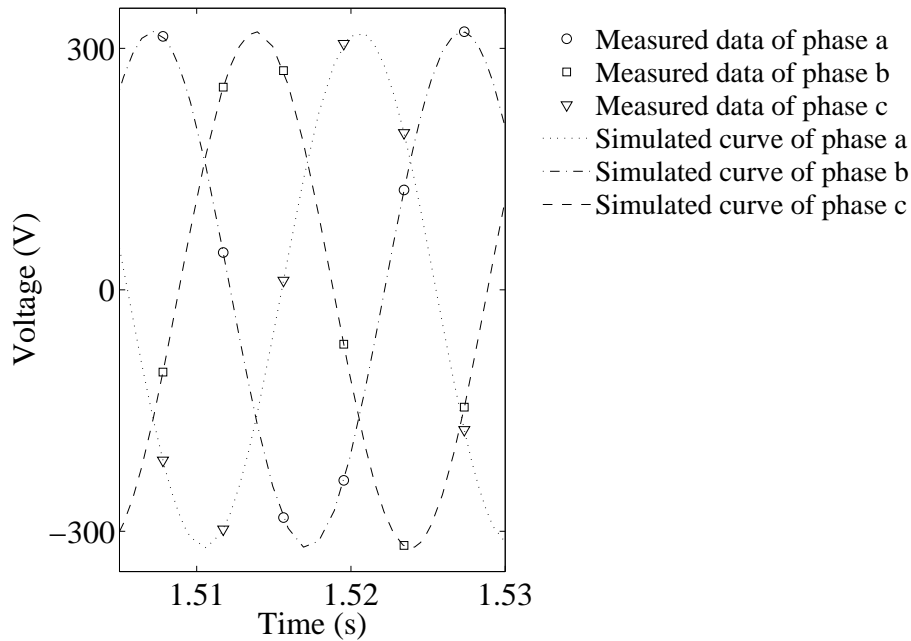

Figure 4.5: Discrete actual data obtained from measurement compared with continuous voltage data used for simulation.

Figure 4.6 shows detail of the active and reactive power oscillations obtained from the measurement data and the simulation using the fifth-order model of an induction generator and the two-mass model of the drive train without a mechanical damping. It can be seen that, in spite of the presence of 50 Hz oscillations, the results provided by the model show fairly good agreement with the measurement data.

The following are a number of considerations obtained from Figure 4.6a:
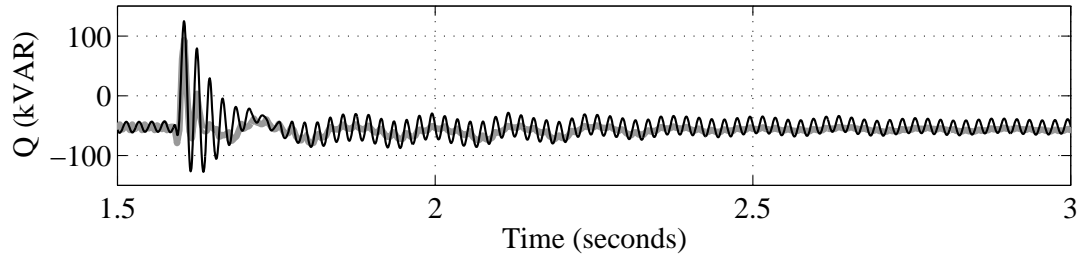
- The power oscillations in the measurement data and the simulation results have a similar frequency.

- The fast transients in the first few cycles in the simulation and the measurement data have a similar magnitude.

- The amplitude of the simulated and the measured power oscillations are similar during the first oscillations following the fault event. Later, the simulated oscillations are higher than the measured ones.

From Figure 4.6b, it can be seen that:

- There is a good accordance between the measured and the simulated reactive power, despite a small shift in the reactive power after the second disturbance. This shift could be due to the disconnection of some compensating capacitors as a result of the disturbance. However, this event was not recorded, so it is not possible to confirm this supposition.
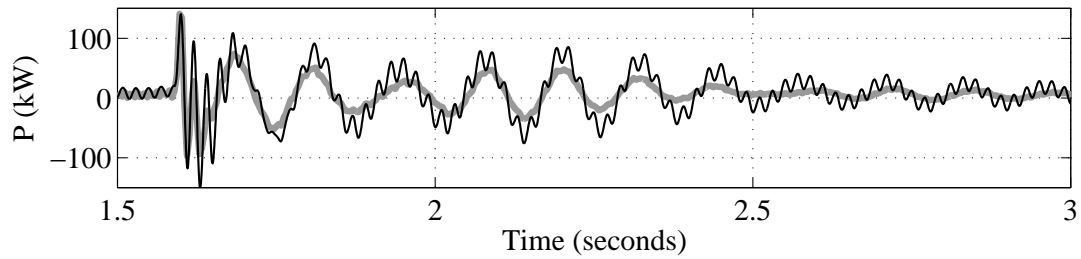
(a) Active power output

(b) Reactive power output

Figure 4.6: Active and reactive power responses of fifth-order model of induction genera-tor and two-mass model of drive train without mechanical damping (black) compared with measurement data (grey).

50 Hz oscillations are apparent in the active and reactive power output due to the presence of a dc-offset in the voltage data. This dc-offset may occur due to the inaccuracy of the resistor used to find the neutral point of the measurement sensor.

Removing dc-offset from the measurement data

In order to remove 50 Hz oscillations in the active and reactive power, the dc offset contained in the measurement data was filtered out. Simulation results of the model after removing the dc-offset from the voltage data are presented in Figure 4.7.

The result is now relatively free from 50 Hz oscillations in the active and reactive power. The 50 Hz oscillations that remain at the beginning of the fault, are caused by unsymmetrical voltage during that period.

Influence of generator models

In the following, the third-order model of an induction generator is used. The result is then compared with the fifth-order model in order to examine the influence of the generator model on simulation results.

As can be seen in Figure 4.8, the third-order model fails to predict the peak (electromag-netic) transient current that occurred immediately after the fault event. This is because the stator flux derivative component is not involved in the third-order model. However, in gen-eral, the third-order model of induction generator is able to capture the electro-mechanical transients of the wind turbine.
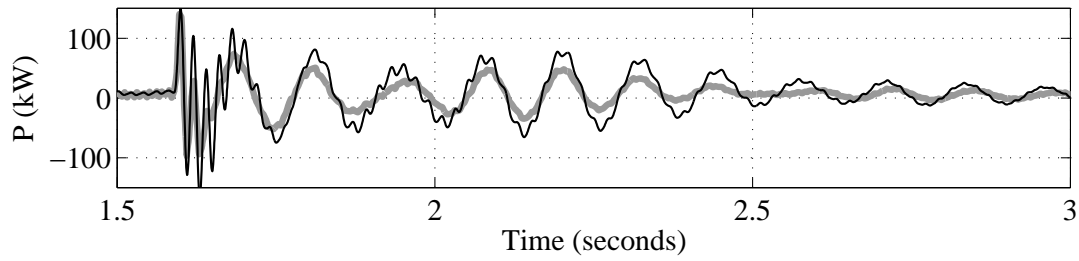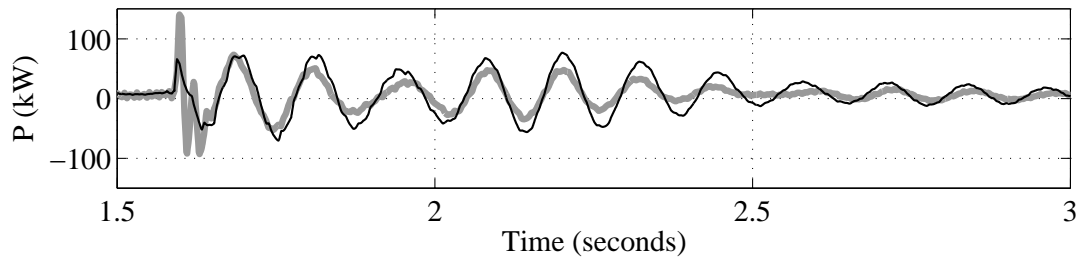
(a) Active power output
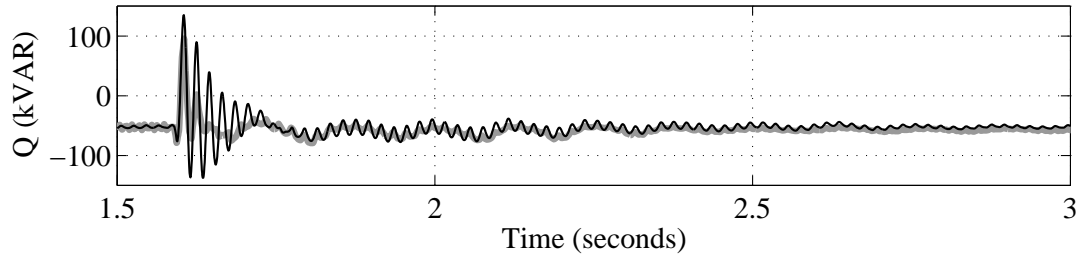
(b) Reactive power output

Figure 4.7: Active and reactive power responses of fifth-order model of induction generator and two-mass model of drive train with dc-filtered input voltage and without mechanical damping (black) compared with measurement data (grey).

(a) Active power output

(b) Reactive power output

Figure 4.8: Active and reactive power responses of third-order model of induction generator and the two-mass model of drive train with dc-filtered input voltage and without a mechanical damping (black) compared with the measurement data (grey).

Influence of drive train models

As seen in Figure 4.9, if the drive train of the wind turbine is represented as the one-mass model, the simulated active power oscillation frequency differs from the measurement data.

This is because by using the single-mass model of a drive train, soft shaft oscillations are omitted. The remaining oscillations apparent in the active power were governed by a rapid fluctuation of the angle deviation as shown in Figure 4.3. The result shows that the one-mass model predicts more optimistic results than the two-mass model.

(a) Active power output

(b) Reactive power output

Figure 4.9: Third-order model of induction generator and single-mass model of drive train (black) compared with measurement data (grey).

Introducing a mechanical damping

Poorly damped active power oscillations in Figure 4.8 suggest the convenience of introducing a mechanical damping constant into the drive train model. Figure 4.10 shows simulation results of the model including a mechanical damping constant of 3 pu.

It is shown in Figure 4.10 that after introducing the mechanical damping constant, the model is able to predict the magnitude of active power oscillations more accurately. While reactive power oscillations are virtually unaffected by the mechanical damping since reactive power is more dependent on voltage oscillations as discussed previously.

However, the mechanical damping constant is often not provided in wind turbine data. Nevertheless, since the model without the mechanical damping constant provides more conservative results, the exclusion of the mechanical damping constant from the model is not critical for power system studies.

4.2 Olos measurement data

4.2.1 Measurement setup and data description

The second measurement data were taken from the Olos wind farm situated in the northern part of Finland. The farm consists of 5x600 kW wind turbines with an operating voltage of
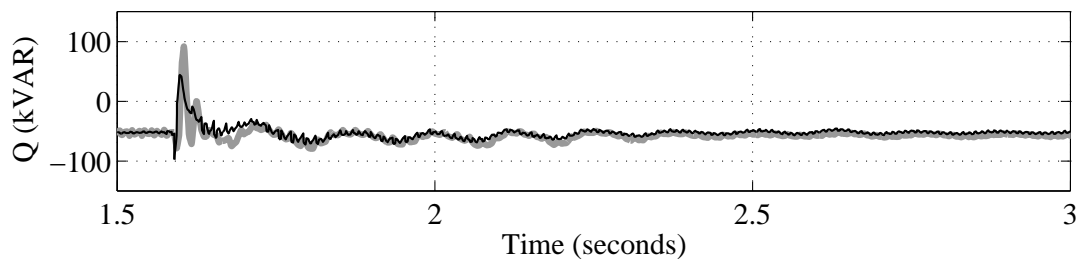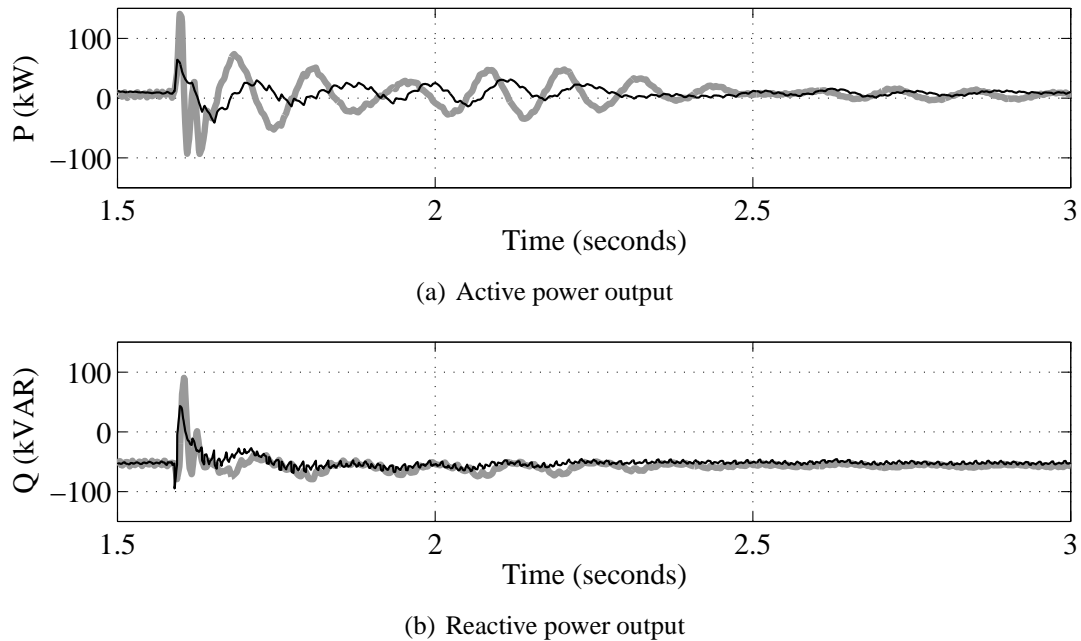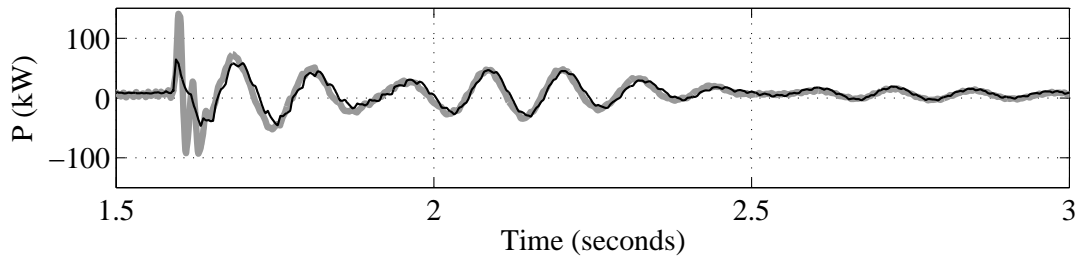
(a) Active power output

(b) Reactive power output

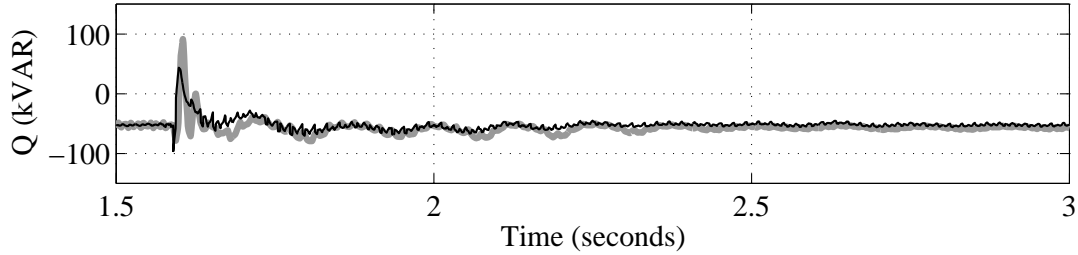Figure 4.10: Active and reactive power responses of third-order model of induction generator and two-mass model of drive train with dc-filtered input voltage and mechanical damping constant (black) compared with measurement data (grey).

690 V. Each turbine is connected to a 21 kV grid by means of a step-up transformer with a rating capacity of 800 kVA. The generator is equipped with two separate sets of windings, which correspond to 600 kW/4-poles or high-speed operation mode and 120 kW/6-poles or low-speed operation mode. During the measurement, the generator was operating in the high-speed operation mode. Each wind turbine is equipped with a 3-step capacitor bank with a reactive power compensation of 50 kVAr for the low-speed operation mode, and with a reactive power compensation of 50+50+62.5 kVAr for the high-speed operation mode. In this study, only turbine number 2 is investigated.
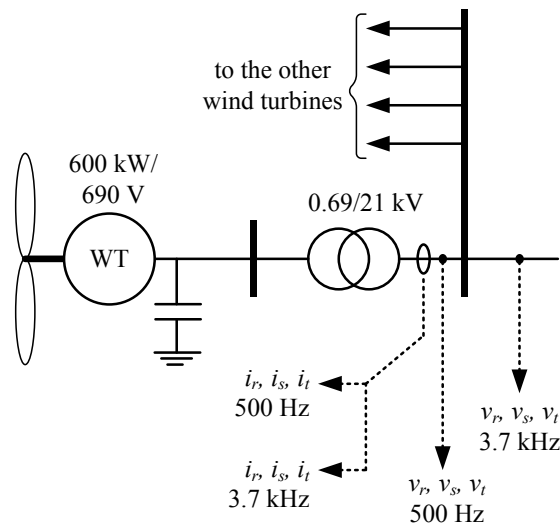

Figure 4.11: Olos single turbine measurement set up.

56

The measurement data contain phase voltages and phase currents. Using the measurement data, the instantaneous active and reactive power can be computed using Equation (4.3). The measurements were performed at two different sampling frequencies: 500 Hz and 3.7 kHz. In the following, the two different sampling frequency measurement data are presented and discussed separately.

500 Hz measurement data

The measurement data with a 500 Hz sampling frequency are explained as follows: The phase voltages and currents of the turbine are shown in Figure 4.12. The active and reactive power of wind turbine 2 presented in Figure 4.13 were calculated from the measured currents and voltages according to (4.2) and (4.3), respectively. Note that the latter equation is only valid for calculating reactive power in balanced 3-phase quantities. Therefore, it must be kept in mind that the instantaneous reactive power calculated for unbalanced conditions, as presented in several figures in the remaining parts of this chapter, is intended merely for comparisons between simulation results and measurement data rather than for providing exact values.
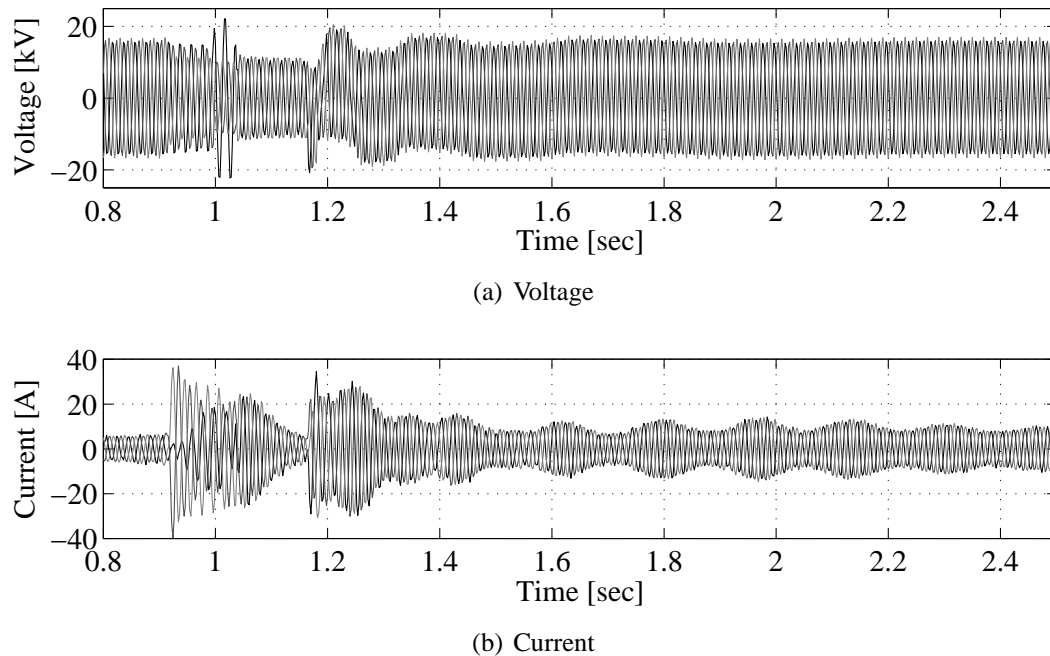
(a) Voltage

(b) Current

Figure 4.12: Measured voltage and current of a single turbine at Olos wind farm with 500 Hz sampling frequency.

Initially, wind turbine 2 was producing active power at approximately 130 kW and the reactive power consumption was about 76 kVAr. Such a high reactive power consumption was due to a lack of one of the 50 kVAr capacitor bank steps at the time.

A fault occurred in the grid at $t = 0.92$ s and was cleared at $t = 1.18$ s while the voltage continued to oscillate due to the breaker switching (opening), before the voltage oscillations finally died out at $t = 1.8$ s. The voltage oscillations were characterized by the presence of dc-components due to discharging earth capacitance, which was charged during earth-fault, and formed an oscillation circuit with the line inductance.
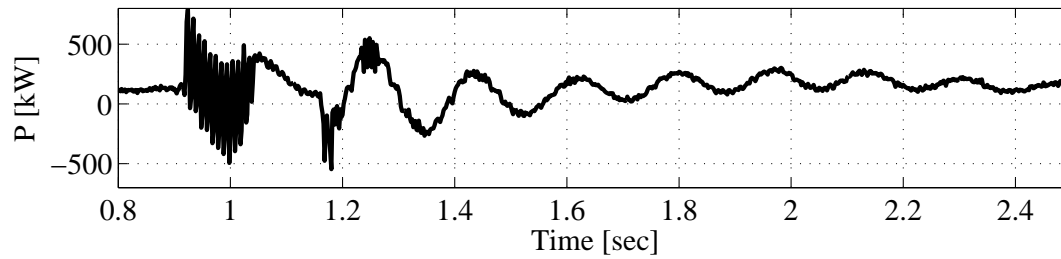
(a) Active power
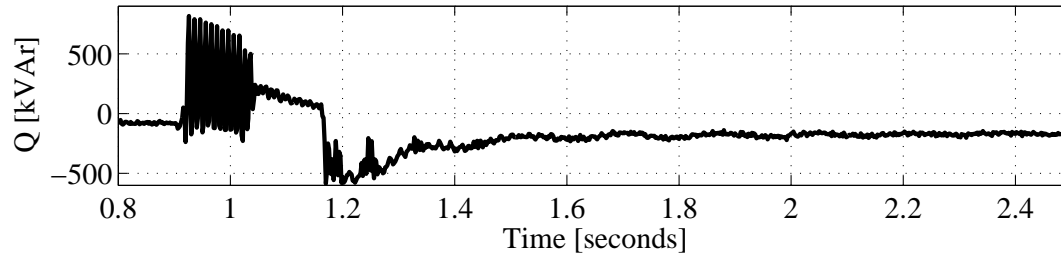
(b) Reactive power

Figure 4.13: Calculated active and reactive power of single turbine at Olos wind farm with 500 Hz sampling frequency.

Meanwhile, the current oscillations were sustained for a longer time. Unlike the voltage oscillations, the current oscillations are likely to be caused by the natural frequency of the drive train and the generator. Using spectrum analysis, the oscillation frequency was found to be 5.8 Hz.

The current oscillations affected the active power, as shown in Figure 4.13a, whereas the reactive power was hardly affected by the oscillations, as shown in Figure 4.13b. This is because the grid was strong enough for the terminal voltage to be relatively insensitive to active power oscillations. The reactive power was highly influenced by the voltage and was loosely correlated with the behavior of active power. Furthermore, this indicates that the active power oscillations were related to drive-train dynamics.

As a typical response of an induction generator, a large amount of reactive power was absorbed by the generator during voltage recovery, as shown in Figure 4.13b. Additionally, the figure shows that the reactive power before and after the fault was not the same and instead the reactive power consumption increased by nearly 100 kVAr. The reason for this is a disconnection of the capacitor bank. The reactive power of the capacitor bank is strongly dependent on voltage, and as in this case when the voltage is below the nominal, the reactive power production of the bank is less than nominal. Thus, a 100 kVAr drop in reactive power production at 0.98 pu voltage responds quite well to the disconnection of capacitors of 112.5 kVAr reactive power production at the nominal voltage.

Another finding was a relatively high transient current during the fault clearing, which was initiated by the opening of the breaker. Although the opening of the breaker occurred at the zero crossing point, a sudden voltage magnitude change and voltage angle jump were still present on the generator terminal, and a high transient current response of the generator could not be avoided. Hence, the fault-clearing transient cannot be neglected.

3.7 kHz measurement data

The same event as discussed earlier was also measured at a sampling frequency of 3.7 kHz. Such a high resolution data, offer the potential to observe the events encountered during fault. In detail, the measurement data can be described as follows: The measured phase voltages and currents of wind turbine 2 are shown in Figure 4.14. Note that the voltage data were measured at the end of the collector line of the wind farm shown in Figure 4.11, which was practically the same as the voltage at the point where the current was measured. The active and reactive power of WT-2 were calculated as shown in Figure 4.15.
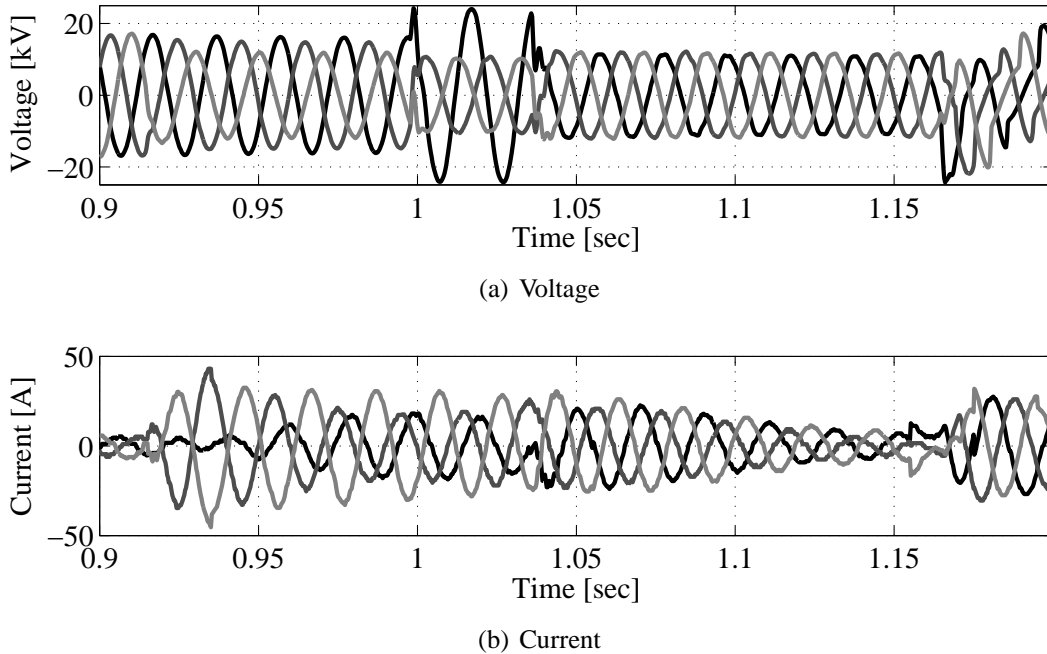

(a) Voltage

(b) Current

Figure 4.14: Measured voltage and current of single turbine at Olos wind farm with 3.7 kHz sampling frequency.

There were 100 Hz oscillations in the 3.7 kHz active and reactive power data before the fault. Power oscillations at a frequency of twice the fundamental frequency signify that there is an unbalance between the phases. In this case, it most likely means that the unbalance is in the measurements (i.e. scaling of some line currents), as the phenomenon is not seen in the 500 Hz measurement data. The 500 Hz data give reasonable active and reactive power values, of which the 3.7 kHz data power values differ (active power less, and the reactive power, which is more sensitive to unbalance, more).

The 3.7 kHz measurement data provide detailed information on events during the fault. A two-phase fault occurred in the grid at $t = 0.92$ s lasting for 0.083 s. The fault then turned into a two-phase to ground and lasted for 0.038 s before it finally became a three-phase fault at $t = 1.04$ sec, which caused the voltage to drop to 0.7 pu. The fault was cleared at $t = 1.18$ s.

Note that transient current was encountered at $t = 1.154$ s, in which there was a sudden change in current magnitude and phase angle. This event was due to the disconnection of the compensating capacitors as indicated earlier.

The presence of negative sequence components in the voltages and currents during the asymmetrical fault resulted in 100 Hz oscillations of active power during $t = 0.92$-1.04 s.
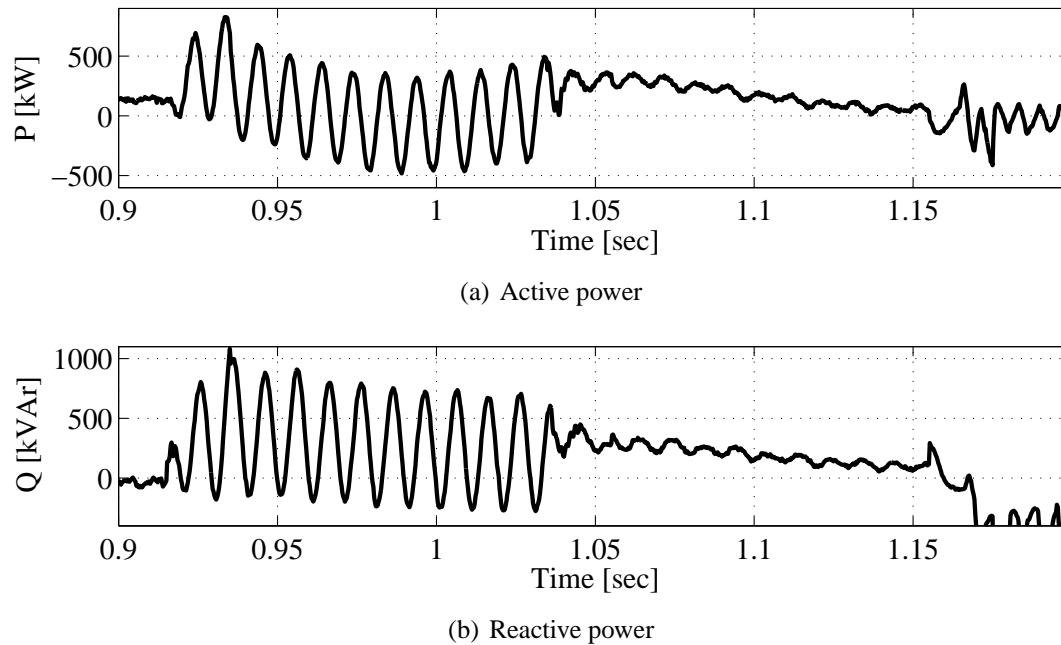
(a) Active power

(b) Reactive power

Figure 4.15: Calculated active and reactive power of a single turbine at Olos wind farm with 3.7 kHz sampling frequency.

It is important to mention again that the reactive power calculated during this unbalanced condition should be interpreted with caution, as explained earlier.

4.2.2 Simulation

The simulation was performed using the simulation tool SimPowerSystem. In the simulation, the generator is represented by the fifth-order model. The third-order model of an induction generator is not possible to simulate the case appropriately owing to its inability to simulate unsymmetrical conditions during fault. The drive-train is represented by the two-mass model.

The mechanical input power of the turbine model was set so that the generator produced the same level of active power as before the fault, which was equivalent to 130 kW, and remained constant during the simulation.

As shown in Figure 4.16a, the simulated currents agree well with the measured ones (see Figure 4.14 for comparison). The model predicts a higher transient current for the first cycle, but the prediction is better for the rest of the cycles. The same conformity applies to active and reactive power, as shown in Figure 4.16b and 4.16c, respectively.

As shown in Figure 4.16b, during the first cycle after the fault, the two-mass model and the one-mass model of the drive train do not differ in predicting the peak transient power. This shows that the accuracy of the mechanical drive train parameters is not essential for this short period of study. During the first few cycles of transient, the responses of wind turbine were characterized by the dynamics of the generator and other electrical components of the wind turbine. This occurred because the mechanical system time constants are usually much larger than the electrical system time constants.

Based on these facts, it can be said that for an over current protection design, and more

60
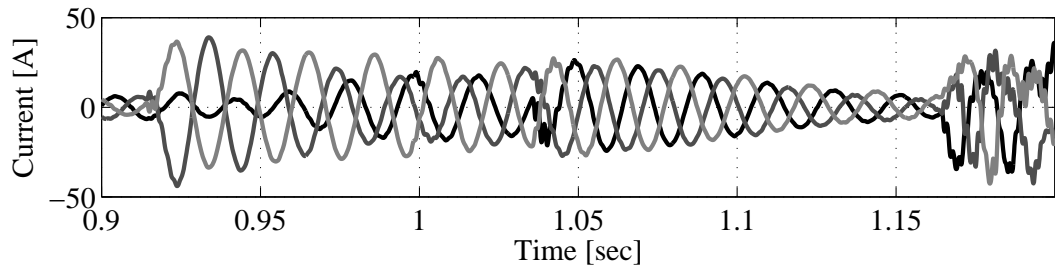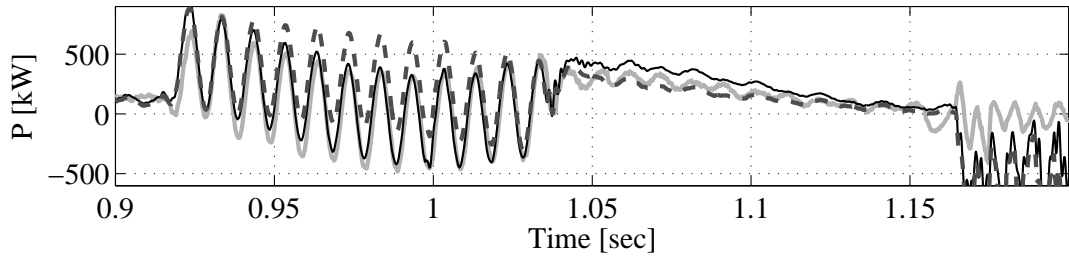
(a) Current

(b) Active power: two-mass model (solid-black), one-mass model (dash) and measured (solid-grey)

(c) Reactive power: two-mass model (solid-black), one-mass model (dash) and measured (solid-grey)

Figure 4.16: Simulated current, active and reactive power of single turbine at Olos wind farm with voltage from 3.7 kHz sampling frequency data as input.

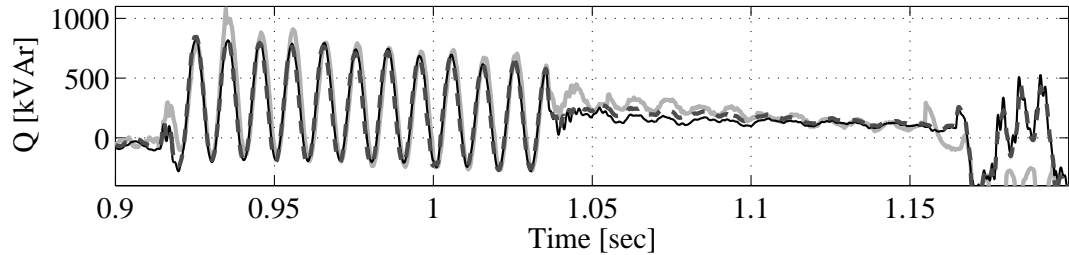specifically, for an instantaneous over current protection design, the accuracy of the generator model is the most important factor.

Differences between the measured and simulated results at the end of the active and reactive power curves in Figure 4.16b and 4.16c are caused by an inaccuracy of the model to simulate switching events. Therefore, the simulation results of this event can be disregarded.

The simulation results for a longer time frame are shown in Figure 4.17. The figure shows an agreement between the measured and the simulated reactive power despite a 50 Hz ripple due to the presence of the dc-offset in the input voltage, which was not perfectly filtered. The drive train dynamics can be clearly observed in the active power oscillations.

4.3   Conclusion

Measurement data taken from the Alsvik and Olos wind turbines show the validity of the fifth order model of an induction generator and the two-mass model of a drive train for simulating responses of the wind turbine. This shows that the fifth-order model is adequate

(a) Active power
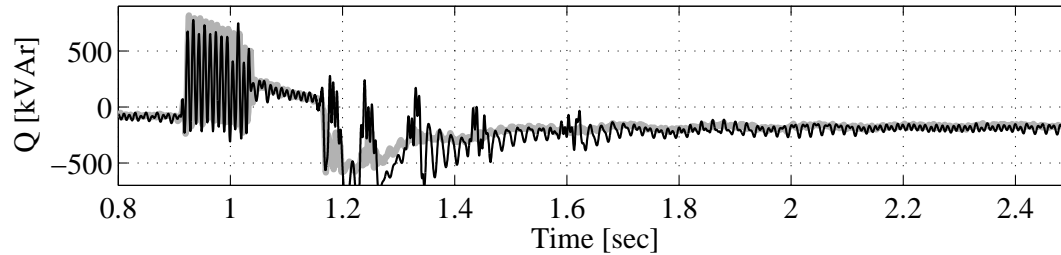
(b) Reactive power

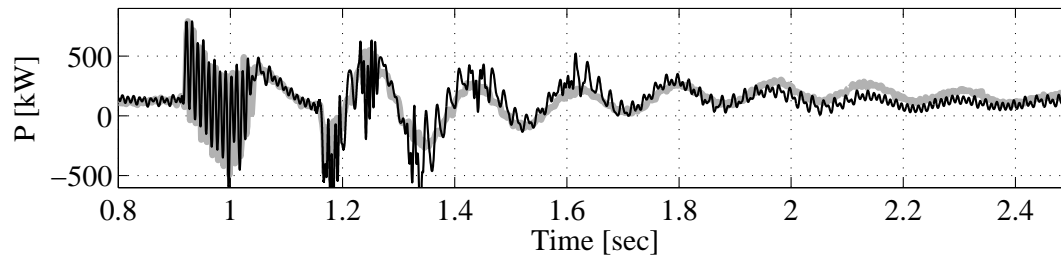Figure 4.17: Simulated active and reactive power of a single turbine at Olos wind farm with voltage from 500 Hz sampling frequency data as an input (black) compared with measurement data (grey).

as a reference model. Accordingly, less detailed models can be sufficiently validated against the fifth-order model.

The third-order model is also proven to accurately simulate the behaviors of a wind turbine subjected to a symmetrical fault event if the fast transient current, which usually occurs following switching, is not of interest. The validation results also emphasize the importance of the drive-train model being represented by using at least the two-mass model.

Nevertheless, it was found from experience that there is a need to have information on reactive power compensator status during the measurement in order to explain the phenomena more accurately.

Chapter 5

Simulation of Fixed Speed Wind Turbines

The simulations are intended to examine the response of wind turbine models subjected to a number of disturbances. Four different cases are simulated:

- A wind gust that causes a small voltage disturbance due to a rapid increase in power production.

- A fault in the grid that causes short-term voltage stability phenomena.

- Long-term voltage stability phenomena, which are initiated by a loss of line followed by a slow acting on-load tap changer (OLTC).

- A frequency deviation, which is initiated by the trip of a generating unit.

The simulations are performed in PSS/E with a 10 ms time step. The fifth-order model used in the simulation refers to the modified fifth-order model as described in 3.1.7.

5.1   Wind gust simulation

In this simulation, effects of a wind gust on voltage stability are studied. This phenomenon can be explained briefly as a rapid increase in wind speed, which results in an increase in the active power output of a wind turbine. The aerodynamic part is modeled using $C_p(\lambda, \beta)$ lookup table.

To simulate the case, a simple test grid was developed. The test grid consisted of two buses, which were connected to each other with two lines as depicted in Figure 5.1. The wind turbine was connected to the first bus and an infinite generator was connected to the other bus.

The wind turbine capacity rating was 2 MW, the parameters for which was derived from wind turbine data given in Appendix F after scaling up the rating to 2 MW. Initially, the wind turbine was operating at less than half of nominal power when the wind gust was applied. The wind gust was simulated as a rapid increase in wind speed from 8 m/s to almost 20 m/s within 2 seconds, which can be considered to be a very strong gust.
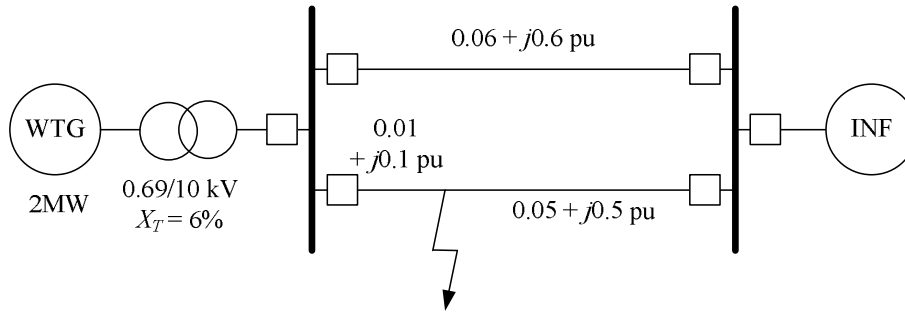
Figure 5.1: Test-grid model. The values of the impedances are on a 10 MW basis.

Three different models of an induction generator were studied: the first-order, the third-order and the fifth-order model. In this case, the two-mass model of a drive train was employed. Simulation results are shown in Figure 5.2.

The results show that the active power of the wind turbine increased as a result of an increase in wind speed. Subsequently, the terminal voltage of the turbine decreased by 2%. However, when the wind speed exceeded a certain value, the turbine started to operate in stall mode, which limited the output power at a certain level. Note that, due to the passive stall design of the wind turbine, the power does not rise wildly following a cubic relation of the wind flow, despite a considerably high wind gust.

In general, the three different induction generator models provide a similar response for the case of wind gust. This is because the dynamics of wind speed are considered to be slower than the electrical dynamics.

The effect of the drive train model was investigated. The results show that the wind turbine model with the one-mass model of a drive train predicted slightly more optimistic results where oscillations in the wind turbine response due to shaft oscillations were omitted.

It can be concluded that if the wind speed is considered as the only dynamic input of a study, the first-order model of an induction generator with the two-mass model of a drive train can be adequately used to represent the wind turbine for the study.

5.2 Fault simulation

The simulation in this section was performed in order to investigate the response of the wind turbine subject to a severe fault in the grid.

The 2 MW wind turbine was simulated. A fault was applied to one of the transmission lines close to the wind turbine bus (see Figure 5.1) leading to a voltage drop of 0.2 pu. The fault was then cleared after 100 ms by tripping the corresponding line. Simulation results are shown in Figure 5.3.

The first-order model predicts a higher value for speed deviation. This is because of the absence of electric torque once the fault is initiated. As the main flux in the third- and the fifth-order models does not drop instantaneously, this causes a slower decay of the electric torque, which subsequently suppresses the speed deviation at a lower value.

During the fault, the active power of the first-order model dropped directly to nearly zero, which corresponds to the magnitude of the terminal voltage. For the third- and the fifth-order models, the active power stayed at a higher value due to rotor dynamics.

(a) Wind speed

(b) Generator terminal voltage

(c) Active power

(d) Reactive power

(e)Generator speed deviation

Figure 5.2:
Response of fixed-speed wind turbine to wind gust: fifth-order (solid-grey), third-order (dash-dotted) and first-order (dash) model of induction generators with two-mass model of drive train; and third-order model of induction generator with one-mass model of drive train (solid-black).

(a) Terminal voltage

(b) Current magnitude

(c) Active power

(d) Reactive power
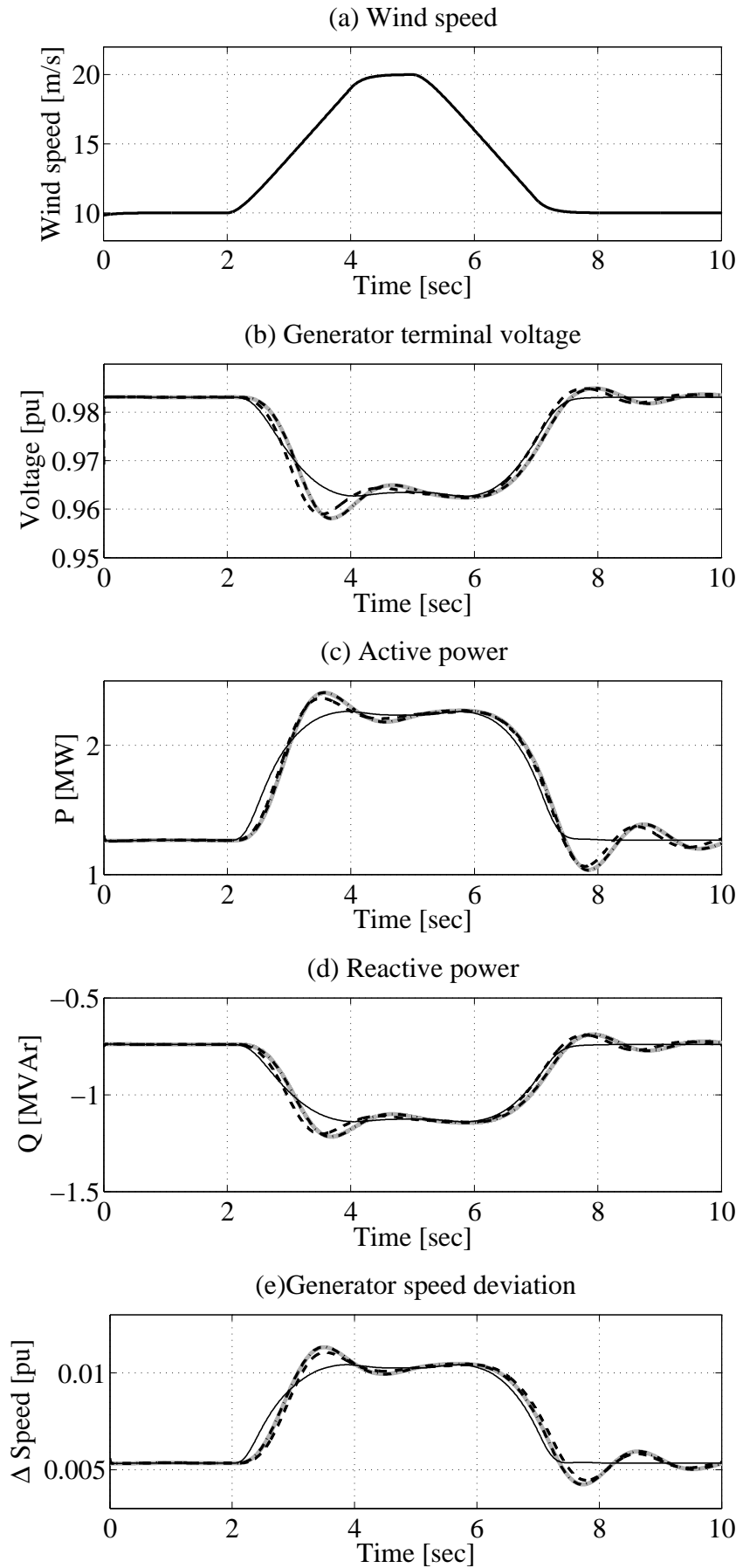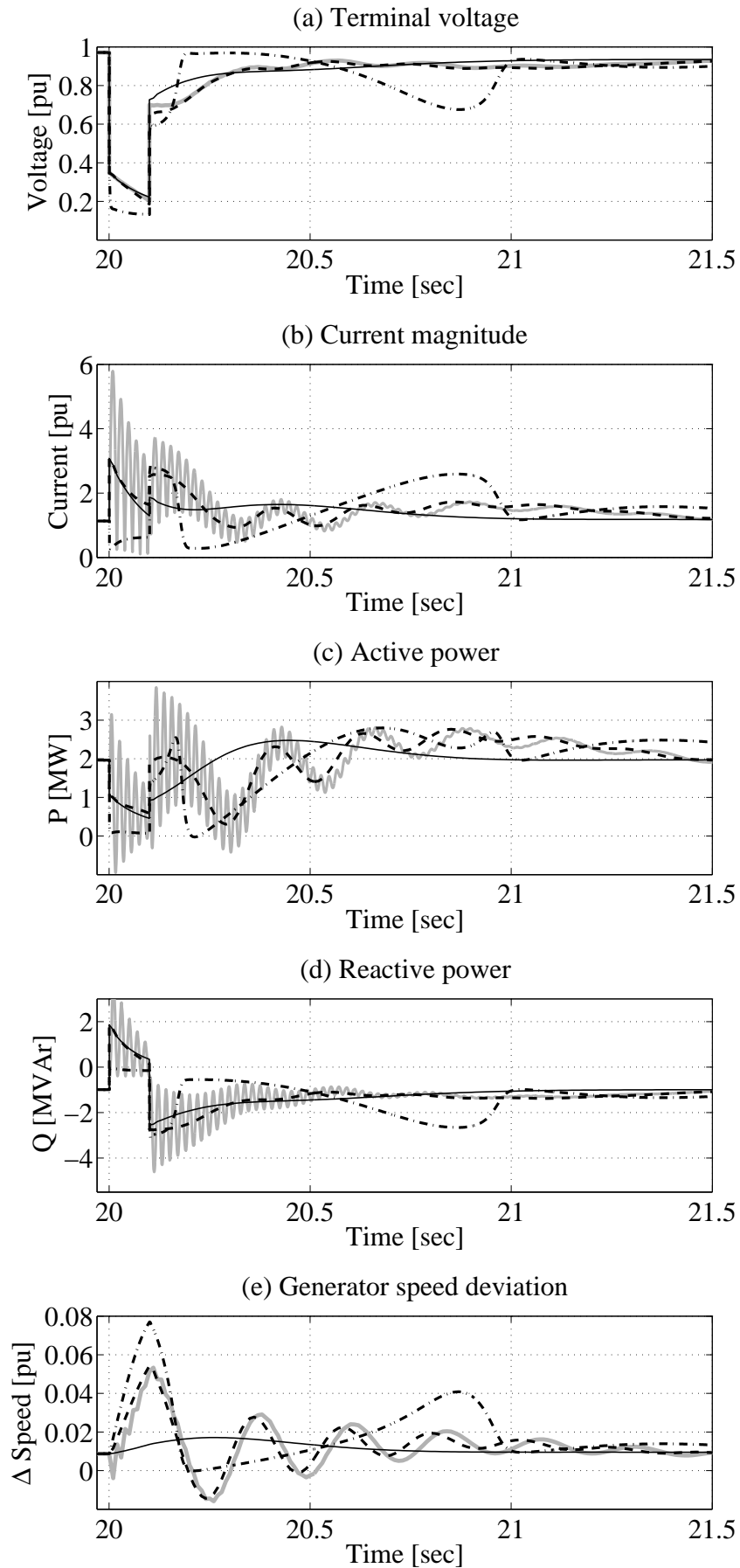
(e) Generator speed deviation

Figure 5.3: Response of fixed-speed wind turbine to grid fault with: fifth-order (solid-grey), third-order (dash-dotted) and first-order (dash) model of induction generators with two-mass model of drive train; and third-order model of induction generator with one-mass model of drive train (solid-black).

An injection of reactive power during the fault in the third-order and the fifth-order models was encountered due to demagnetization of the magnetizing inductance.

The third- and the fifth-order models show similar oscillations following the fault. These 5 Hz oscillations are governed by the dynamics of the drive-train.

Despite the inability to trace the first peak transient current, the third-order model can generally offer a sufficiently accurate estimation of wind turbine behaviors during the fault.

Regarding the drive train model, the results show that the use of the one-mass model of a drive train cannot accurately predict the wind turbine response during faults. The high inertia of the generator-turbine provides less speed deviation, which results in more optimistic results.

5.3   Long-term voltage stability

Long-term voltage stability was simulated by incorporating the slow action of OLTC. The test-grid used for the simulation is shown in Figure 5.4. To initiate the long-term voltage stability phenomena, one of the transmission lines was tripped. Two different models were then simulated: the fifth-order model of an induction generator with a two-mass model of a drive train (detailed model) and the first-order model of an induction generator with a one-mass model of the drive train (simplified model). The two models represent the most and the least detailed representations of wind turbine models.
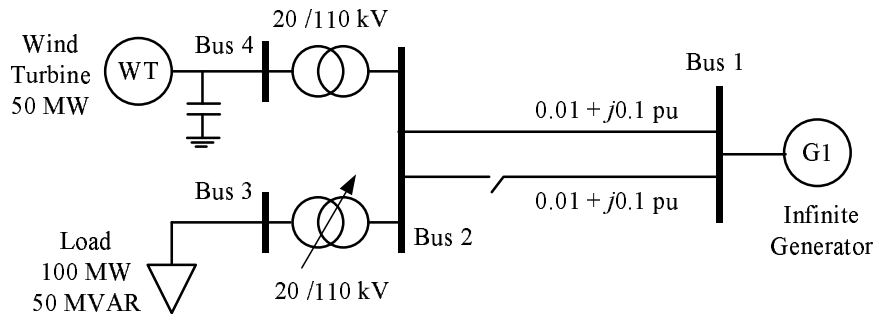
Figure 5.4: Test-grid model for long term voltage stability. The values of the impedances are on a 100 MW basis.

The response of the system and the wind turbine in the two different models is shown in Figure 5.5. Immediately after the line tripping, the voltage at bus 2 dropped to approximately 0.91 pu due to an increase in effective impedance between bus 1 and bus 2. The OLTC acted by adjusting the tap changer, with a certain time delay, to maintain the voltage at the load bus (bus 3) within a predefined range. This resulted in a higher current flowing through the transmission line. As a consequence, a further voltage drop was encountered at bus 2.

A sharp transient was encountered at the instance of the line disconnection. The active power of the wind turbine fell for 2 seconds before it recovered following line disconnection. Small oscillations in the active power of the detailed model due to shaft dynamics were observed, while no power oscillation was encountered in the simplified model. Generator speed increased marginally, caused by a lower terminal voltage.

Simulation results show that, despite minor differences occurring during the event of tap changing/switching, the two different models provide similar results. This suggests that

a detailed level of wind turbine dynamic models is not required for a long-term voltage stability study.

(a) Terminal voltage

(b) Active power

(c) Generator speed deviation
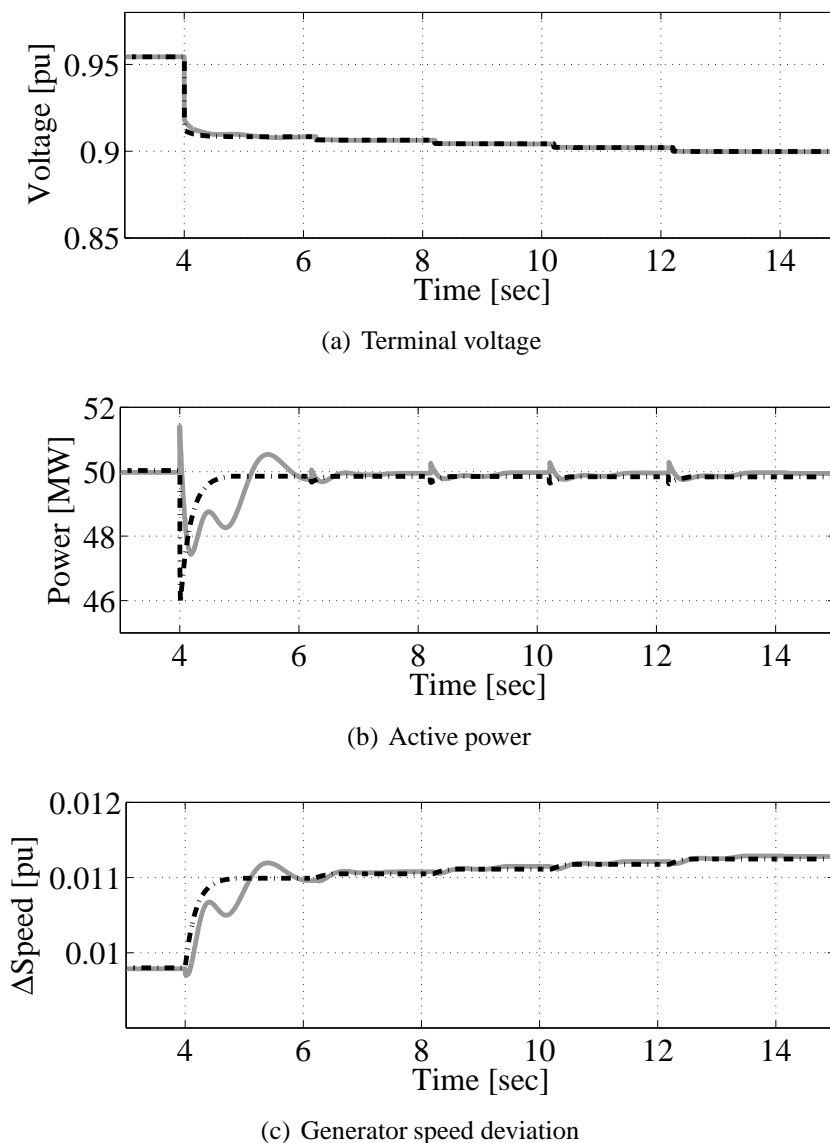
Figure 5.5: Response of induction generator models for long-term stability study: fifth-order model of induction generator in combination with two-mass model of drive train (solid-grey) and first-order model of induction generator in combination with one-mass model of drive train (dash-dotted).

5.4 Frequency deviation

In this section, the validity of the wind turbine models subjected to a frequency deviation is investigated. Figure 5.6 shows the test-grid used to simulate the effect of frequency deviation on the behavior of the wind turbine model. The test system consisted of 4 busses: an infinite bus (bus 1), a substation bus (bus 2), a load bus (bus 3) and a wind turbine bus (bus 4).
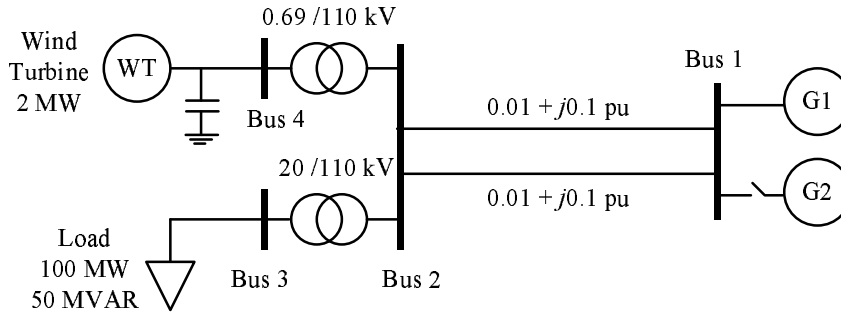
Figure 5.6: Test-grid model for frequency deviation. The values of the impedances are on a 100 MW basis.

The two generators at the infinite bus represent conventional power plants, which are hydro power plants in this case.

The load was a composite load consisting of large and small size motors (40%), current exciter transformers (5%), lightings (30%) and constant MVA loads (25%). The total active and reactive power consumption of the load were 100 MW and 50 MVAR, respectively.

A 2 MW wind turbine with the same parameters as the wind turbine used in the previous section was connected at bus 4. Bus 4 was connected to bus 2 through a step up transformer 0.69/110 kV. The size of the wind turbine was chosen to be small enough in relation to the total system size, so that the turbine virtually had no influence on the dynamics of the power system. This was because this study examines how the frequency deviation may influence behaviors of the wind turbine model rather than the effects of the wind turbine on the rest of the system.

Simulation results are shown in Figure 5.7. In the beginning of the simulation, two synchronous generators G1 and G2 supplied the load with an output power of 90 MW and 10 MW, respectively.

At $t = 20$ s, the G2 unit was tripped. This resulted in an unbalance between load and generation which lead to a frequency drop of 5% (equivalent to a 2.5 Hz frequency drop). After some time, the action of the hydro governor at G1 was able to recover frequency closer to the nominal value.

At $t = 20$ - 26 s, the system frequency constantly decreased. During this period, a fraction of the mechanical energy contained in the rotor was released into the grid. As the mechanical input was constant throughout the simulation, by neglecting losses, the sum of the mechanical power used to decelerate the rotor and electrical power delivered to the grid was virtually constant.

In contrary, at $t = 26$ - 43 s, when the frequency increased, the mechanical rotor required more power to accelerate speed. This resulted in a lower electric power output (see Figure 5.7c). Once the frequency became stable, the active power returned to its nominal value.

The active power of the two models was different during the frequency deviation. This difference was caused by the disregard of the stator flux component $d\psi/dt$ in the third-order model as was explained in Subsection 3.1.5. Ignoring the stator flux component also caused a higher reactive power consumption in the third-order model than in the fifth-order model. As a consequence, the voltage response of the generator was also different in the two models. Nevertheless, 1 - 3% of a maximum difference in voltage and reactive power result during the transient may be still acceptable.

(a) Bus voltage

(b) Bus frequency deviation

(c) Active power

(d) Reactive power

(e) Speed deviation

Figure 5.7: Response of induction generator models to frequency deviation with low wind power penetration ($\pm 2\%$): fifth-order (dash-dotted), third-order (solid-grey) and first-order (dotted) model.

As shown in Figure 5.7c, 5.7d and 5.7e, the first-order model of an induction generator is practically unaffected by the frequency deviation. This is because the generator reactances are constant irrespective of the grid frequency. That is why traces of the active and reactive power and generator speed are constant throughout the simulation.

Based on a simulation, which is not shown here, the effect of a drive train model was also investigated. Simulation results suggest that the drive-train model is insignificant for

this type of study.

High wind power penetration

With a higher penetration of wind power into the power system, the accuracy of the model becomes more essential. In order to simulate this case, the capacity of the wind power generation in the previous case was increased to 20 MW, which corresponds to around 20% of power penetration. The same event was applied to the power system, i.e. one of the synchronous generators was tripped. Simulation results are presented in Figure 5.8.

There is a slight difference between the fifth-order model and the third-order model of induction generator in respect to the frequency deviation response. According to simulation results, the third-order model provides a more optimistic estimation of the frequency response. The figure shows that the third-order model provides a 0.4% lower maximum frequency deviation than the fifth-order model. The reasons for this difference are the same as in the previous simulation. Nevertheless, the overall discrepancy of the frequency is not obvious.

It can be concluded that the use of a third-order model of an induction generator with the one-mass model of a drive train is adequate for a frequency stability study. For a large frequency deviation (more than 10%) with high wind power penetration (more than 20%), however, the use of a fifth-order model is recommended.

5.5 Conclusion

Different stability study cases of power systems with a fixed-speed wind turbine were simulated in this chapter. The result fidelity of a simulation is determined by the level of detail of the model being used. However if only a single model is to be used for different studies, and the validity of the results and simulation efficiency are of primary concerns then the turbine with a third-order model of an induction generator and a two-mass model of a drive-train is the best compromise. This is because the use of the fifth-order model of an induction generator posses incompatibility with the network model. Although the incompatibility problem can be eased by some modifications, the increase in accuracy (in the peak transient current estimation) is not critical for typical stability studies. If the peak transient current must be taken into account, an estimation using an analytical method in parallel with a third-order model is preferable.

For a frequency deviation study, however, the conclusion above is to be interpreted with caution, since it is only valid for a moderate frequency deviation. For a large frequency deviation, the result validity of the third-order model of induction generator can no longer be held. The decision of whether or not to include the possibility of a large frequency deviation in a study must be decided by the investigator by considering the nature of the system to be investigated.

The choice of aerodynamic model is determined by the purpose of the study and the type of the fixed-speed wind turbine. If fast wind fluctuations are included and an active stall wind turbine is used in the study, then the aerodynamic model should be at least modeled using the $Cp(\lambda, \beta)$ lookup table. This configuration is only relevant for a short-term voltage stability study. For other studies with a longer time frame (and lower frequency bandwidth) the aerodynamic model is sufficient to be represented using the wind speed-mechanical power

(a) Bus voltage

(b) Bus frequency deviation

(c) Active power

(d) Reactive power

(e) Speed deviation
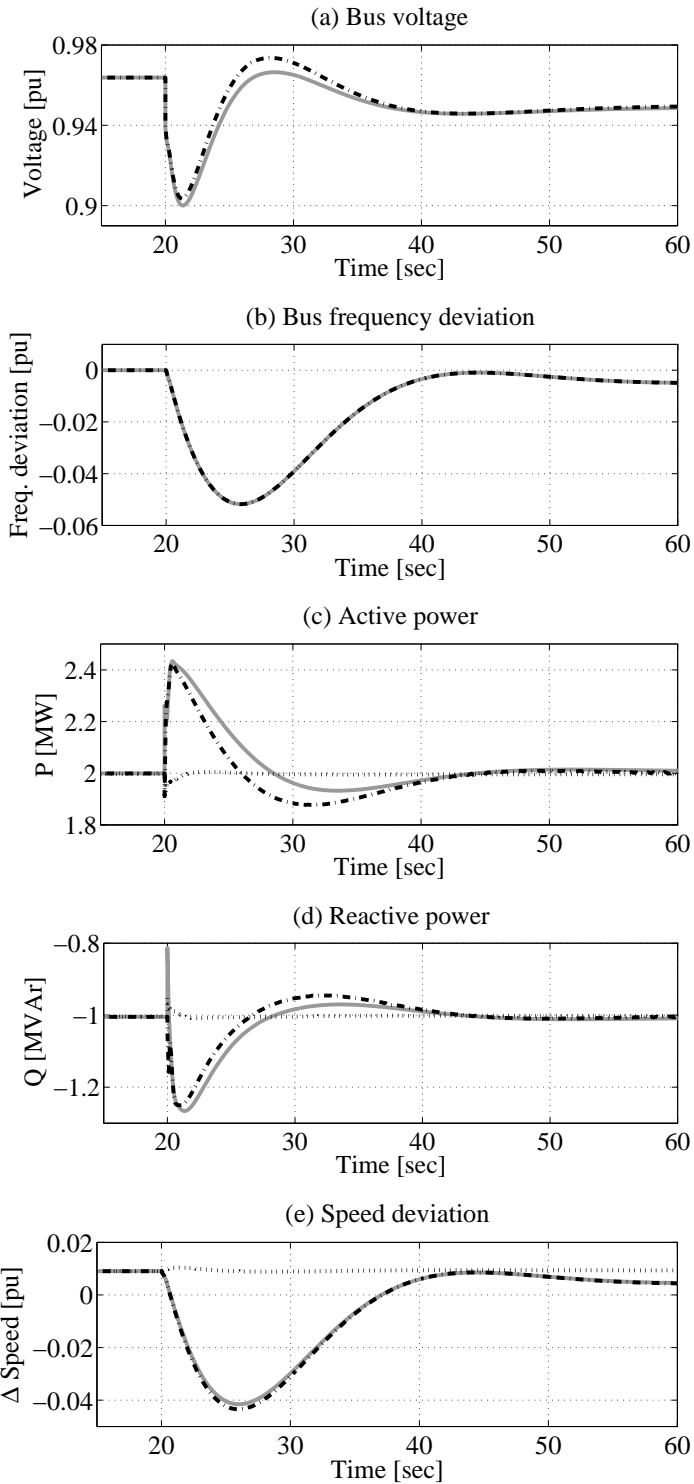
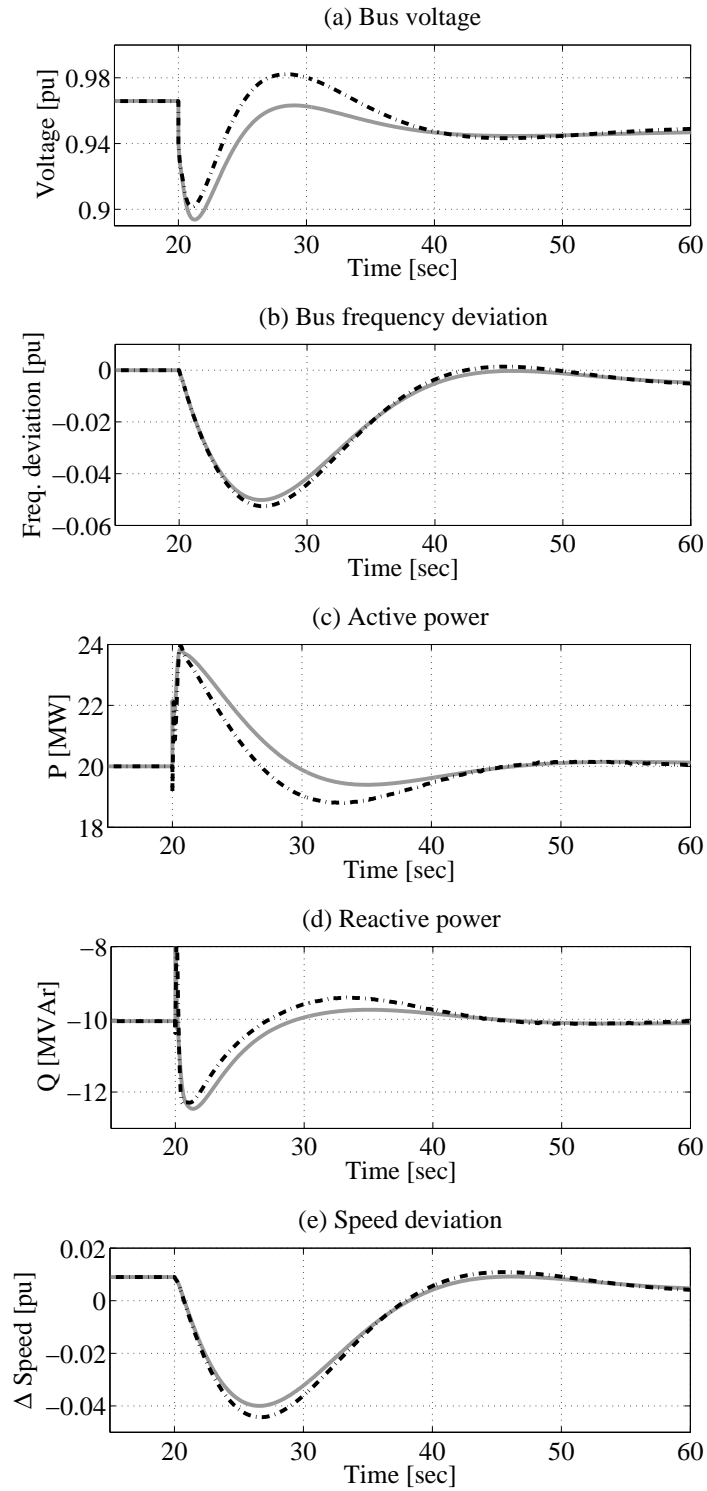Figure 5.8: Response of induction generator models to frequency deviation for high wind power penetration (20%): fifth-order (dash-dotted) and third-order (solid-grey) model.

lookup table. An increased in detail of the aerodynamic model does not significantly affect overall simulation efficiency, if we assume that the $Cp(\lambda, \beta)$ lookup table model is the most detailed model in this context.

Chapter 6

Aggregated Modelling of Wind Turbines

The content of this chapter was presented in Paper 4 [37].

Typical utility-scale wind farms may consist of tens to hundreds of identical wind turbines. As a consequence, representing wind farm with individual wind turbines for power system stability studies increases the complexity of the model and thus requires time-consuming simulation. Hence, simplification of wind farms consisting of a large number of wind turbines is essential. However, this simplification must not result in incorrect predictions of wind farm behaviors, especially under fault conditions.

In a study of a normal operation, it is essential for the equivalent model of the wind farm to represent the smoothing effect of wind power fluctuation [39]. This implies that a model of wind plays the most significant role in the model, while the electrical and the mechanical parts of the wind turbine are of secondary importance.

In contrast, an appropriate model of the mechanical and the electrical systems of wind turbines are highly important for dynamic stability studies of power systems. Different methods for aggregating a wind farm are proposed in [7, 8, 26]. Nevertheless, until now, validation of wind turbine aggregated models during a fault event against field measurement data has not been treated in any paper.

The main goal of this chapter is to present an aggregated model of a wind farm with fixed-speed wind turbines validated against field measurement data. The study emphasizes transient events of a wind farm due to a grid fault.

6.1   Aggregation method

For identical machines, principally, a single-machine aggregated model of a wind farm can be simply made by summing all machine ratings. Hence the equivalent generator rating is given by

$$S_{eq} = \sum_{i=1}^{n} S_i \tag{6.1}$$

where S_i is the $i-$th generator rating and n is the number of turbine units. Since all parameters are given in per unit, this implies that all parameter values remain the same.

Among the other electrical parts of a wind farm, the transformers and the compensating capacitors are of importance in modelling. This is because these components have relatively high impedances and admittances, respectively. Other quantities, such as farm cable

impedances, can be neglected. Similar to the generator, the equivalent representation of the transformers is derived by summing up the rating of the transformer by means of (6.1).

It is important to mention that an aggregation of a wind farm is somewhat different from the aggregation of a typical induction machine, for several reasons:

- The presence of a gearbox and a relatively soft shaft mean that the wind turbine drive train cannot be considered as a stiff shaft. This factor causes an oscillation in the output power of the turbine when subjected to disturbances. Drive train dynamics dominate the response of the wind turbine rather than the electrical properties of the generator. This is even more critical since the inertia of the turbine is much larger than inertia of a typical induction machine and each turbine is likely to deliver a varying mechanical power to the generator.

- During a grid fault, induction motor speed normally slows down. However, the consequence is the opposite in case of a wind turbine, where the decrease in voltage due to the grid fault accelerates the generator rotor speed.

6.2 Simulation of an aggregated model

In order to comprehend the problem of wind turbine aggregation, this section presents a comparison between a wind farm modeled as individual wind turbines (a detailed model) and a wind farm modeled as a single equivalent wind turbine (an aggregated model).

This simulation uses a wind farm consisting of 24 x 2 MW wind turbines. The layout of the turbine is shown in Figure 6.1. The wind turbine data is given in Appendix F, with the exception of the power rating that is scaled up to 2 MW. The wind turbines are modelled using the third-order model of induction generators and the two-mass model of drive train. The simulation is performed using the simulation tool PSS/E.

The wind speed was assumed to be distributed unevenly during the simulation, which results in a difference in the output power of the turbines. By assuming that the first row turbines produce the rated value, the second row was set at 80%, the third row was set at 60% and the last row was set at 40% of the rated output, the total output of wind farm was 33.6 MW. Note that the power distribution is given to provide an extreme condition. This is because, in more realistic cases, the difference in the output power of the turbines would be smaller.

For the aggregated model, a single generator was used to represent all the turbines on the farm. The output power of the generator was equal to the total output power of the farm, which was 33.6 MW. The transformers and the compensating capacitors were lumped together into a single transformer and a single compensating capacitor.

The voltage, active and reactive power response of the detailed and the aggregated model are shown in Figure 6.2. Basically, there was no significant difference between the two models of the wind farm.

Examination of the individual turbines, however, shows that the behavior of each wind turbine was not the same. For example wind turbine 24 experienced the best conditions, since it suffered a less severe voltage dip and produced less power output during the fault. The worse case was encountered by wind turbine 1, which endured the most severe voltage dip at the rated power output. This resulted in a difference in speed deviation, as shown in Figure 6.3. During the transient even, the maximum speed deviation of the wind turbine
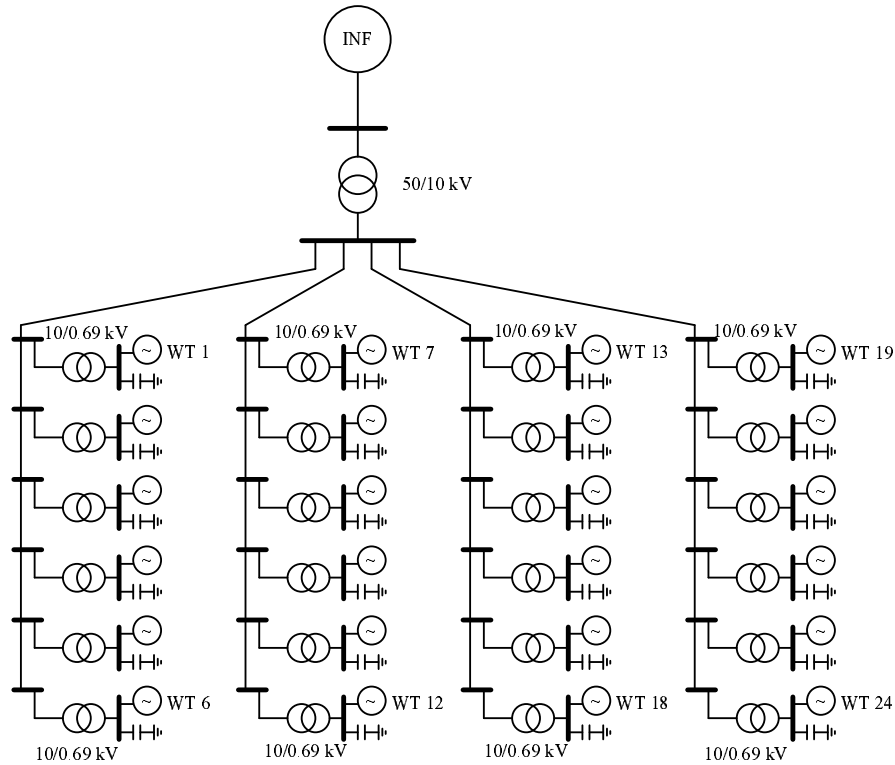
Figure 6.1: Layout of wind farm.

1 was 40% higher than the maximum speed deviation of the single equivalent turbine. In contrast, wind turbine 24 had a speed deviation 40% lower than the equivalent wind turbine. In more severe conditions, this may lead to a trip of wind turbines in the first row, while the rest of the turbines remain intact.

A more accurate representation of a wind farm can be achieved by representing the wind farm with several wind turbine units according to wind speed distribution. However, the representation of multi machines for aggregated wind turbines conflicts with the idea of aggregation. Moreover, a trip of some wind turbines in a wind farm due to uneven wind distribution will not end up as the worst case anyway. In fact, the worst case is obtained if all wind turbines are operating at rated value. In such a case, the speed estimation of each wind turbine will be practically the same as the estimation provided by a single equivalent wind turbine model. Hence, the representation of a wind farm as a single machine is sufficient to predict the best and the worst scenarios.
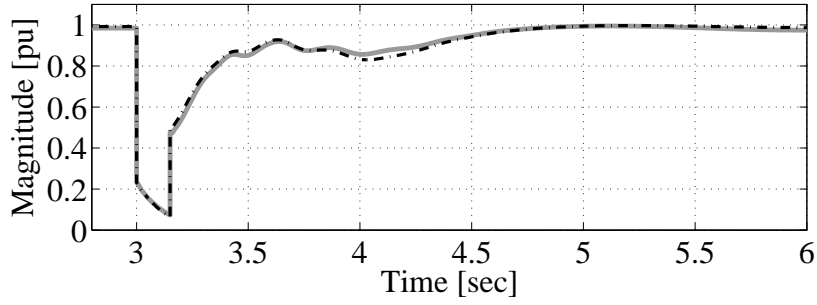
(a) Voltage at collector bus
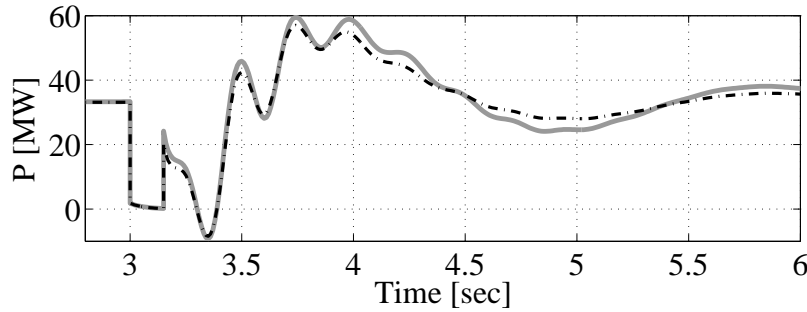
(b) Active power
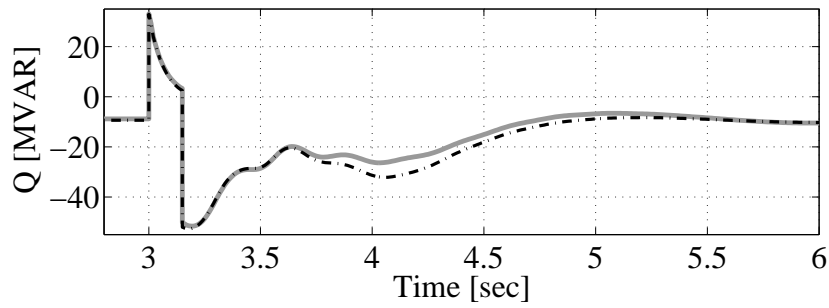
(c) Reactive power

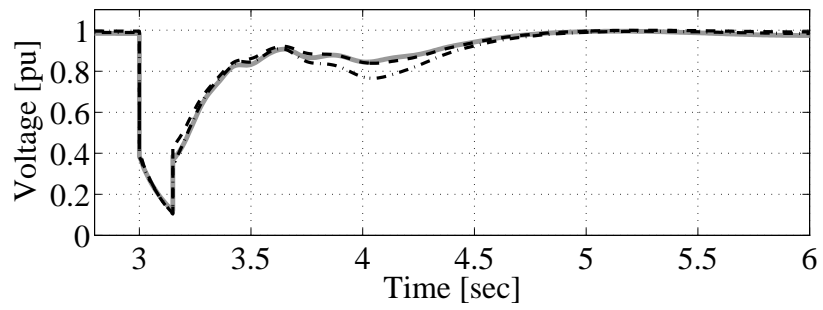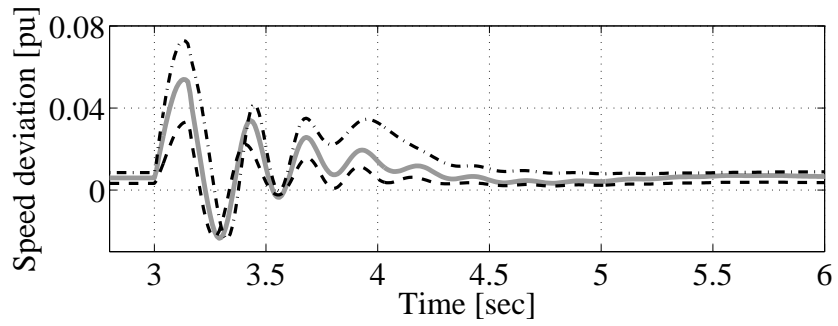Figure 6.2: Voltage, active and reactive power at collector bus: detailed model (dash-dot) and single machine aggregated model (solid-grey).

(a) Voltage

(b) Speed

Figure 6.3: Voltage and speed of wind turbines: single turbine model (solid-grey), turbine 1 (dash-dot) and turbine 24 (dash).

6.3 Validation

In the following, the model is validated against the field measurement data obtained from Olos wind farm.

6.3.1 Measurement location and data

A detailed description of wind turbines in the Olos wind farm is presented in Subsection 4.2.1. The farm was connected to a substation bus through a single three-phase overhead line. Observe that there was a load connected to the same feeder where the farm is connected.

 The farm measurements were taken at the wind farm collector bus. Another measurement system was located in the substation feeder where the farm is connected. The location, sampling frequency and the measured parameters of each measurement system are shown in Figure 6.4. More detailed information on the wind turbines and the farm network parameters are provided in D.
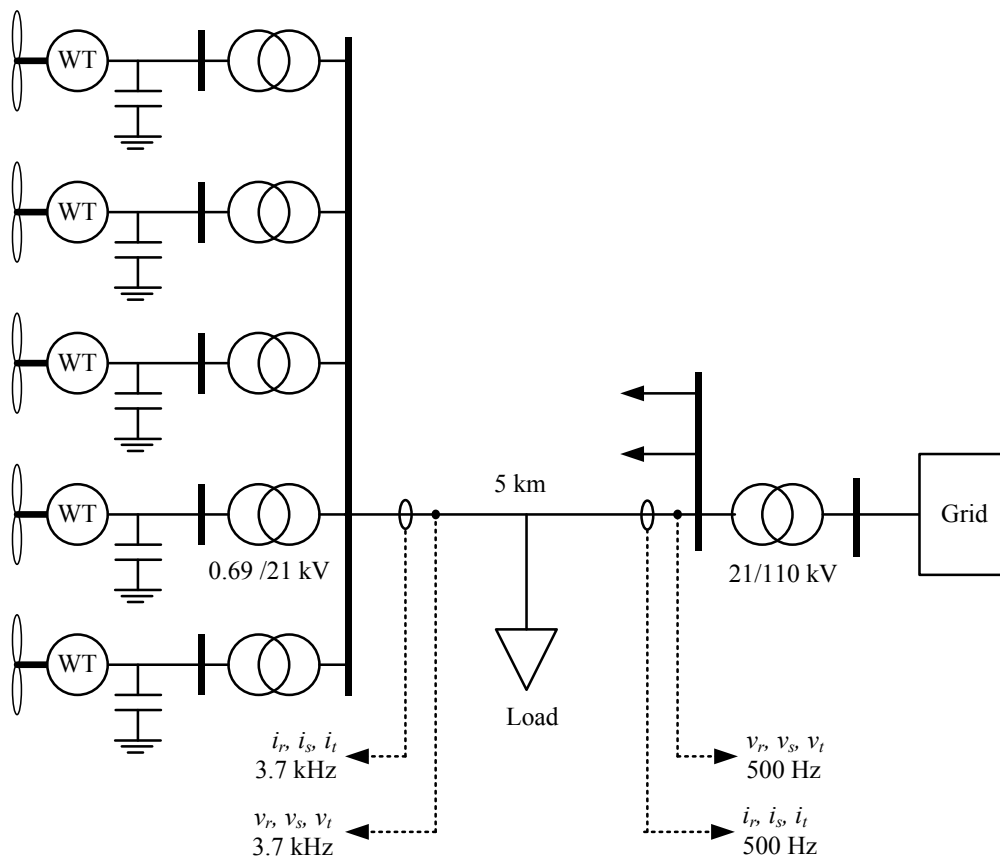

Figure 6.4: Olos wind farm measurement set up.

3.7 kHz measurement data

The voltage and current from a 3.7 kHz measurement at the collector bus are shown in Figure 6.5. From these quantities, the active and reactive power output of the farm can be obtained, as shown in Figure 6.6.
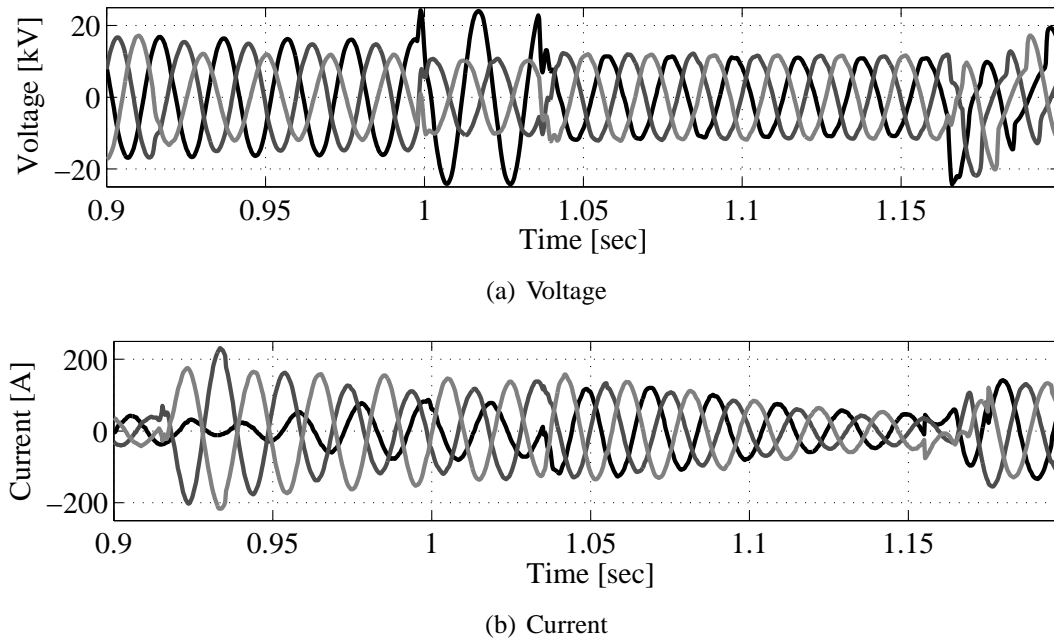

(a) Voltage

(b) Current

Figure 6.5: Measured voltage and current of at wind farm collector with 3.7 kHz sampling frequency.

500 Hz measurement data at substation

The voltages and currents along with the calculated active and reactive power from 500 Hz measurement data of the wind farm feeder at substation are shown in Figure 6.7. As mentioned earlier, the presence of a load in the same feeder where the farm is connected makes the current at the wind farm collector and the wind farm feeder at the substation significantly different.

As shown in Figure 6.8, the total production of the farm measured at the wind farm collector before the fault was approximately 932 kW and the reactive power consumption was 430 kVAr.

It should be noted that one of the compensating capacitors at wind turbine 2 was out of operation, and thus the turbine took the corresponding lacking reactive power from the grid. From the substation 500 Hz data, the change in reactive power in pre- and post-fault situations, mainly due to a disconnection of capacitor banks in the wind farm, can be calculated. The calculated change in reactive power is about 500 kVAr.

Known from continuous 1 Hz measurement data (not shown in this paper), the active power production and the reactive power consumption of the other turbines are presented in Table 6.1.

Reactive power consumption values suggest that all three steps of the capacitor banks in turbines 1, 3 and 4 are in operation. In turbine 5, only 2 steps of the capacitor banks are in
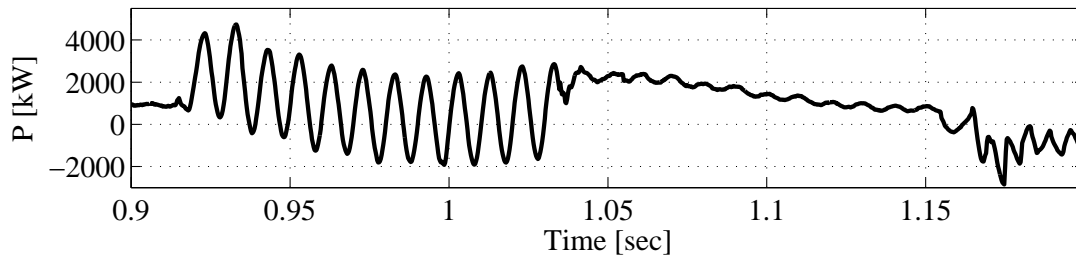
(a) Active power
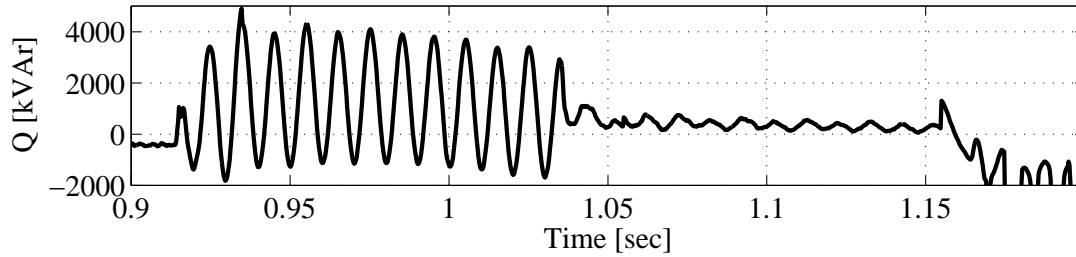
(b) Reactive power

Figure 6.6: Calculated active and reactive power of wind farm with 3.7 kHz sampling frequency.
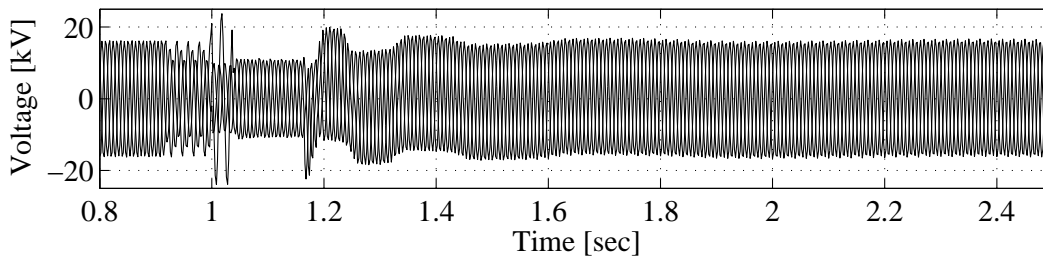
(a) Voltage
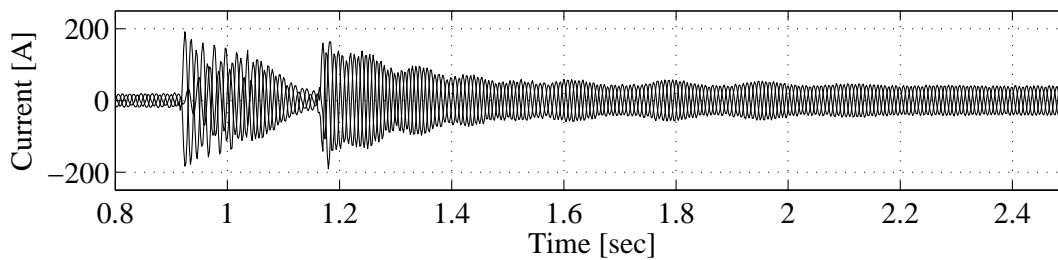
(b) Current

Figure 6.7: Measured voltage and current of wind farm feeder at the substation with 500 Hz sampling frequency.

operation. The change in reactive power between pre-fault and post-fault stages (based on 1 Hz continuous data) suggests that all the operating capacitors were disconnected during the grid fault.

The active and reactive power flow at the substation feeder measurement point towards
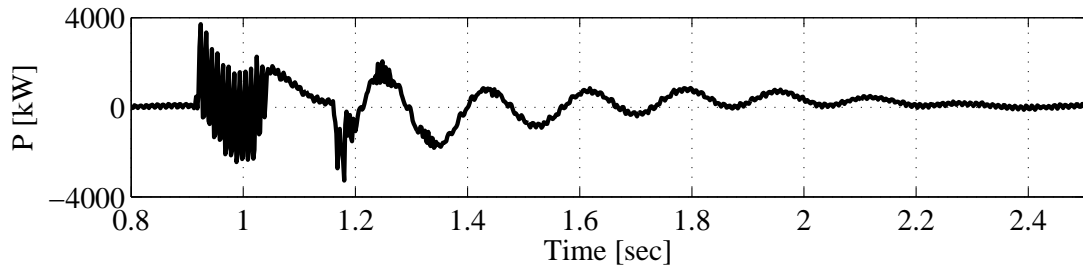
(a) Active power
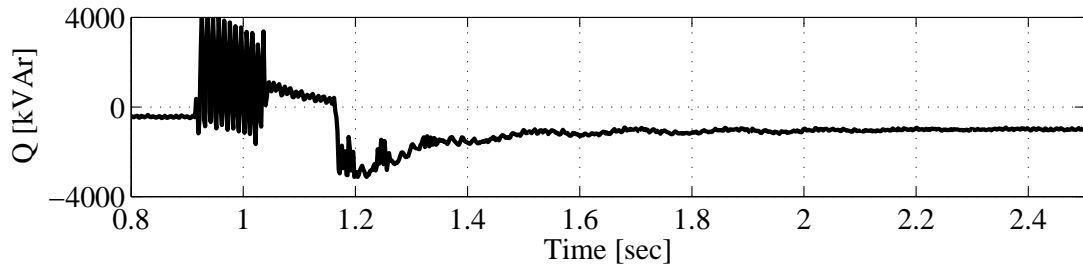
(b) Reactive power

Figure 6.8: Calculated active and reactive power of wind farm feeder at the substation with 500 Hz sampling frequency.

Table 6.1: Initial wind turbines active power output and reactive power consumption recorded before fault.

Turbine	P (kW)	Q (kVAr)
1	200	50
3	250	60
4	200	50
5	200	90

the substation was about 50 kW and -450 kVAr, respectively. As shown in the measurement data, despite differences in magnitude, profiles of the measurement data at the collector bus and at the substation feeder are similar to the single turbine measurement data presented in Section 4.2. It should be emphasized that this similarity indicates that all wind turbines in the farm respond synchronously (in-phase).

Although the measurement point at the substation feeder does not exactly represent farm quantities, wind farm dynamics can be clearly seen in the substation feeder measurement due to the following conditions:

- No influential dynamics of the load occurred during the fault, in other words the load can be treated as a constant impedance.

- The line impedance connecting the wind farm to the substation is relatively small. Therefore the current response of the load insignificantly influences the voltage at the

81

point of measurement.

6.3.2   Simulation

Simulation of 3.7 kHz measurement data at wind farm collector

The farm was modeled as a single equivalent turbine with a rated power of $5 \times 600 \, \text{kW} = 3 \, \text{MW}$. The mechanical power input was set at a constant value that produced electric power output of 930 kW, as given by the measurement data. The fifth-order model of an induction generator and the two-mass model of a drive train were used in the model.

The simulation results from the equivalent aggregated model of the wind farm and the comparison with corresponding measurement data are presented in Figure 6.9. Note that the simulated current in Figure 6.9a is comparable to the measured current shown in Figure 6.5b.

(a) Current

(b) Active power

(c) Reactive power

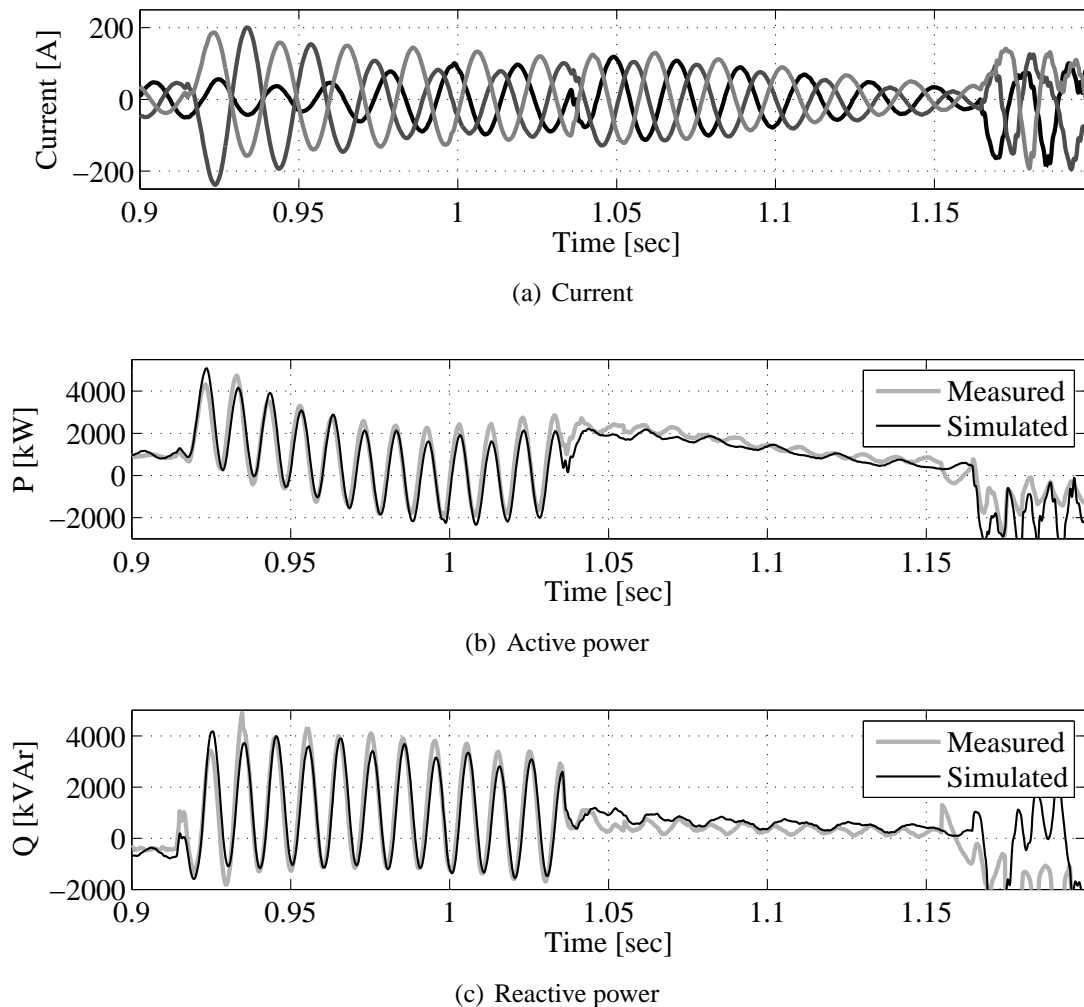Figure 6.9: Simulated current, active and reactive power of wind farm with 3.7 kHz sampling frequency voltage data as an input.

Simulation of the 500 Hz measurement data of the wind farm feeder at the substation

Results of the wind farm simulation based on the 500 Hz measurement data are shown in Figure 6.10. There is a slight difference in the active power magnitude between the simulation and the measurement data at the substation feeder measurement point after $t = 1.4$ sec. This is because a constant mechanical input power was assumed in the model, while in reality there may be power fluctuations, as well, due to wind speed variation. The slight difference in the oscillation frequency was likely due to inaccurate mechanical parameters used in the simulation. The dynamics of the load also contribute to this discrepancy, although not significantly.

(a) Active power
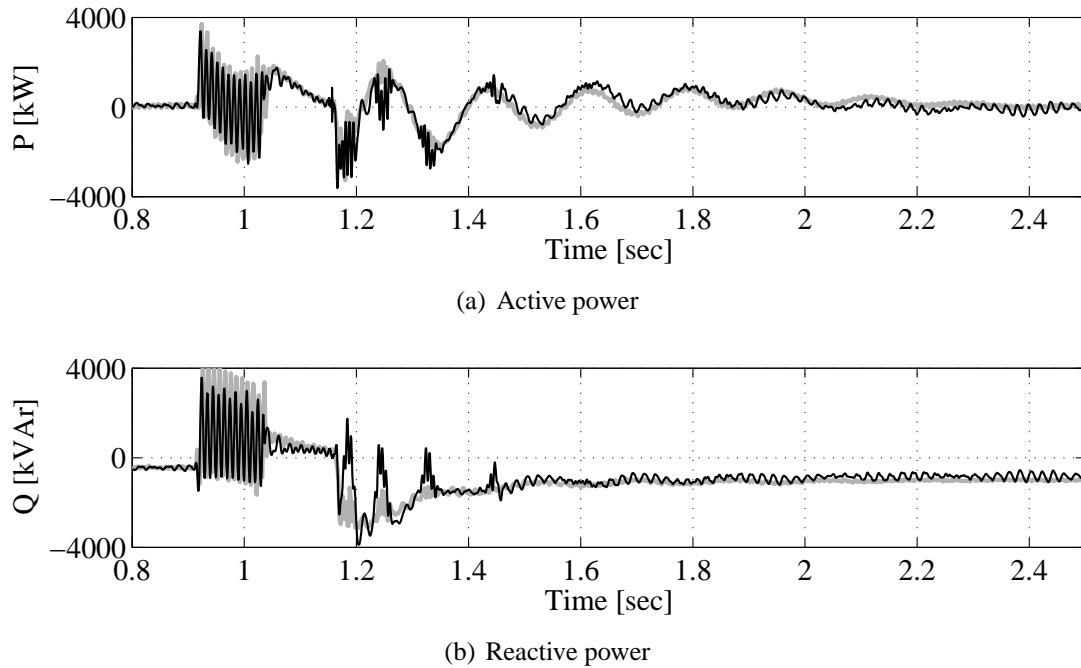
(b) Reactive power

Figure 6.10: Active and reactive power of wind farm feeder at substation: simulated (black), the 500 Hz measurement data (grey).

From the short- and long-time frame simulations, it can be concluded that the behaviors of the wind farm subjected to a fault can be accurately modeled as a single equivalent wind turbine. It should be kept in mind that the error of the aggregated model becomes larger as a difference in the operating points of the wind turbines increases.

6.4   Conclusion

In aggregating wind turbines as a single equivalent wind turbine, the electrical components that should be taken into account are the generators, the compensating capacitors and the transformers. In contrast, effects of the wind farm cables have no significant influence on the modelling. Hence, these effects can be excluded from the aggregated model.

Modelling a small wind farm with a single equivalent wind turbine adequately represents the wind farm behaviors during a grid fault. Simulation result showed that all turbines in the wind farm respond in phase to the fault.

For a large wind farm, the speed response of individual wind turbines may not be the same due to an uneven distribution of wind speed. This may lead to tripping of wind turbines in the farm. This situation cannot be simulated by a single machine representation of the wind farm. Nevertheless, the single machine representation is capable of representing the worse and the best scenarios.

Chapter 7

Fault Ride-through Capabilities of Wind Turbines

7.1   Fault ride-through requirements in grid codes

Following recent growth of wind power generation at a level where the influence of the wind turbine dynamics cannot be neglected, power system operators have imposed requirements for grid-connected wind turbines to assure the stability of the system. One of the requirements is to provide fault ride-through capabilities. This means that the wind turbines must not be disconnected during grid faults. Svenska Kraftnät (Swedish Transmission Company), for example, has stated that wind farms with installed capacity of more than 100 MW are not allowed to be disconnected within the range of a certain voltage level criteria as depicted in Figure 7.1 [40]. This means that the turbine must stay connected to the grid as long as the grid voltage above the criteria limit. A similar requirement is also imposed by other system operators, such as presented in [41, 42, 43].
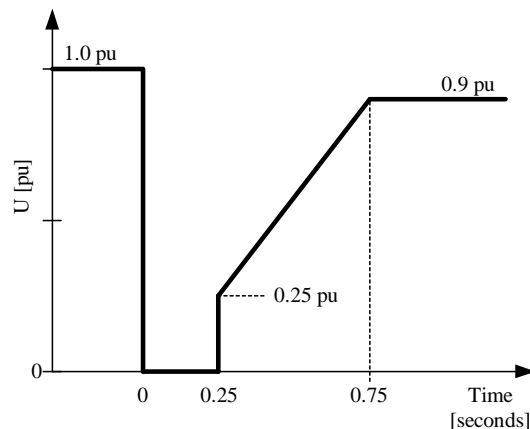
Figure 7.1: Voltage limit criteria according to Svenska Krafnät's grid code.

7.2 Fault ride-through schemes

Each type of wind turbine has specific vulnerabilities when subjected to grid faults. In order to fulfill the requirement imposed by grid utilities, the turbine must be equipped with the ability to ride-through in case of faults in the grid.

7.2.1 Fixed-speed wind turbines

The phenomena that occur in an induction generator without fault ride-through capability during a grid fault are described first. Later, the fault ride-through capability of an active stall wind turbine is presented.

A model of a 10 MW fixed-speed wind turbine with the third-order model of an induction generator and the two-mass model of a drive train, which represents a small wind farm, is used in the following simulations. The simulations are performed in the simulation tool PSS/E with the standard simulation time step. The parameters of the wind turbine are scaled-up from model parameters given in Appendix F .

Speed instability due to fault event

According to simulation results shown in Figure 7.2, the sequence of events can be described as follows:

When the fault occurs in the grid at $t = 5$ s, the terminal voltage drops rapidly. The magnitude of the voltage drop is dependent on the fault distance from the generator. Due to a reduced terminal voltage, the machine looses electric torque, which leads to a rotor acceleration. If the speed deviation is too large, the generator already exceeds the pullout slip at the event when the fault is cleared and the voltage is recovered. Meanwhile, the mechanical torque applied to the rotor can be considered constant during the event. If the electric torque at this point is higher than the mechanical torque, the generator will be eventually back to the normal operating point. However, when the electric torque is lower than the mechanical torque, the speed will continuously increase. This continued speed increase could result in electric torque reduction leading to an unstable situation.

In the case of the two-mass model of a drive train, the situation is even worse. This is because in the instance of voltage recovery, although the generator speed is able to recover back to the normal operating point, turbine speed does not decrease instantaneously because some amount of energy in the mechanical shaft is stored in the twisted shaft, instead of directly utilized to decelerate the turbine speed. This allows the turbine speed to continuously increase for a short time.

During the next period, the energy is released from the twisted shaft and creates the opposite effect. This charge and discharge of twisted shaft energy creates oscillations in the generator and turbine speed. In reality, the electrical torque also suffers oscillations due to terminal voltage variation caused by active and reactive power fluctuations. At the same time, the turbine torque also fluctuates slightly due to a small variation in the C_p value. All these factors interacting with each other create composite oscillations as shown in Figure 7.2e. This event, clearly indicates that there is not only instability which may occur due to the fault event, but there is also considerably high mechanical stress in the shaft.

86
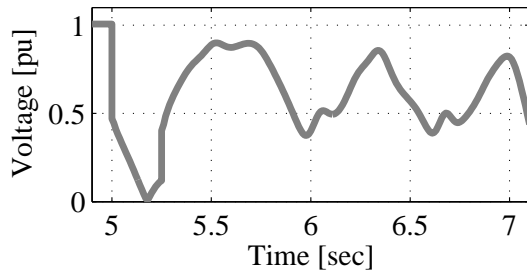
(a) Terminal voltage
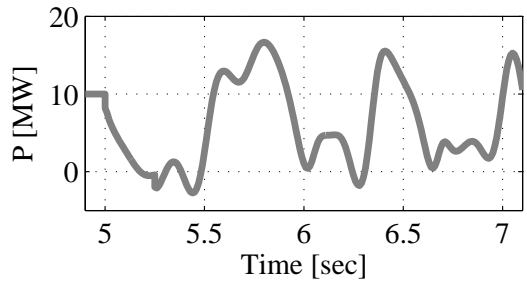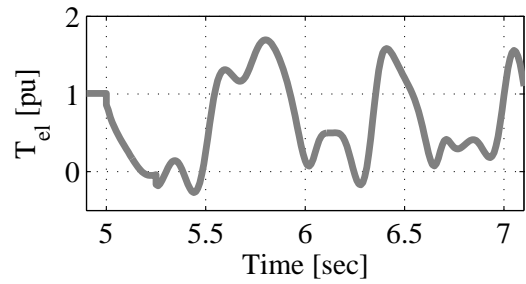
(b) Active power

(c) Electric torque
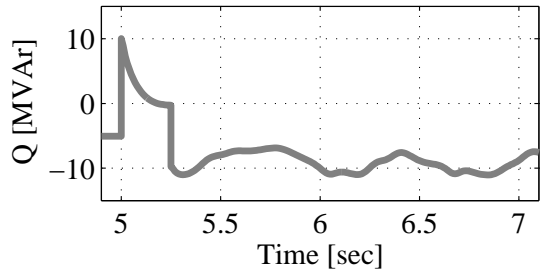
(d) Reactive power
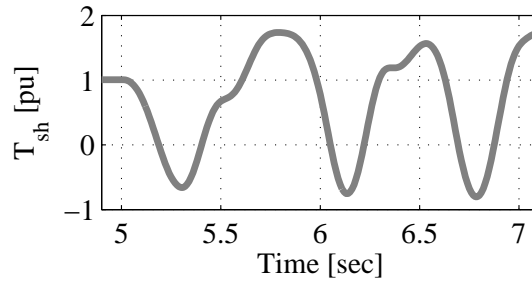
(e) Shaft torque
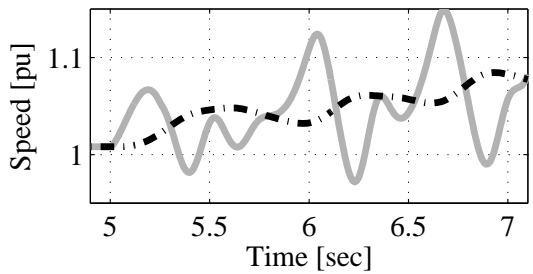
(f) Generator speed (solid) and turbine speed (dash-dot)
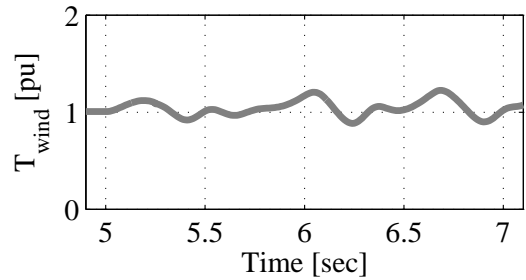
(g) Wind turbine rotor torque

Figure 7.2: Speed instability of passive stall fixed-speed wind turbine without fault ride-through capability following grid fault.

Fault ride-through scheme

The sequence of the scheme for a wind turbine equipped with fault ride-through capability is shown in Figure 7.3. A fault occurring at $t = 5$ s causes the terminal voltage to go down to nearly zero. The generator speed increases due to loss of electric torque. The pitch is regulated toward a stall mechanism (active-stall) in order to reduce the mechanical torque from the turbine rotor. Note that the active-stall regulation can reduce C_p faster than the pitch regulation (shown in Figure 3.22). Due to mechanical restrictions of the actuator, the pitch rate is limited to 8°/sec.

At the event when the fault is cleared, the voltage starts to recover. At the same time the electric torque is built up. As the generator starts to magnetize, there is a need to absorb a large amount of reactive power. Subsequently, this causes a prolonged voltage recovery. As the electric torque is recovered, the generator speed decreases. At around 1 sec the pitch has reached a value that is able to reduce the C_p at a relatively low level (0.6 pu), which means less stress on the shaft.

When the voltage is recovered, the pitch angle does not move directly to the normal value. Instead, it is held constant until the grid status returns to normal. The grid status is determined by the terminal voltage level. In this case, the voltage level threshold for the grid status is set at 0.8 pu. This means that if the voltage is below the threshold, the grid is considered as abnormal. Once the grid status is normal, there is a 2-second time delay to assure that the grid is fully stable to avoid rapid voltage oscillations following a fault clearing being registered by the controller. Two seconds later, the pitch angle increases gradually back to normal operation.

In the event of a fault that results in a steady low voltage and leads to an increase in slip, excessive reactive power consumption is unavoidable (see Figure 3.7), unless some other measures such as the utilization of SVC or STATCOM is considered.

7.2.2   Wind turbines with DFIG

This subsection provides a brief description of a fault ride-through scheme for a wind turbine with DFIG. Different schemes of a fault ride-through are proposed in literature [12, 13, 14]

In a fault situation, the rotor converter of a wind turbine with DFIG is the most exposed component since it can only handle a fraction of generator power. Consequently, this part is not allowed to endure excessive transient current. Additionally, there is a risk of over voltage on the dc-link capacitor during this situation. Hence, it must be equipped with a fast over current protection to protect the power electronic valves and an over voltage protection to protect the dc-link capacitor. If the fault is not severe, the DFIG control operates as usual.

Typical responses of a wind turbine with DFIG without ride-trough capability when subjected to a severe fault during sub- and super-synchronous operation are described in Paper 5 [44]. In general, the sequence of events can be described as follows: When the rotor current or dc link voltage hit their limits, the over current or over voltage protection is activated, respectively. This is followed by an activation of the rotor crowbar. Subsequently, the converter is deactivated. Eventually, the generator is disconnected from the network.

However, in order to fulfill grid requirements, the generator must stay connected during such a situation. This means that when the fault occurs and the rotor converter is deactivated, the generator stator must remain connected to the grid. The pitch is regulated in such a way to reduce mechanical torque in order to avoid over-speeding of the rotor. When the fault

(a) Terminal voltage

(b) Electric toque

(c) Active power

(d) Shaft torque

(e) Reactive Power

(f) Turbine torque

(g) Pitch Angle

(h) Generator speed (solid) and turbine speed (dash-dot)
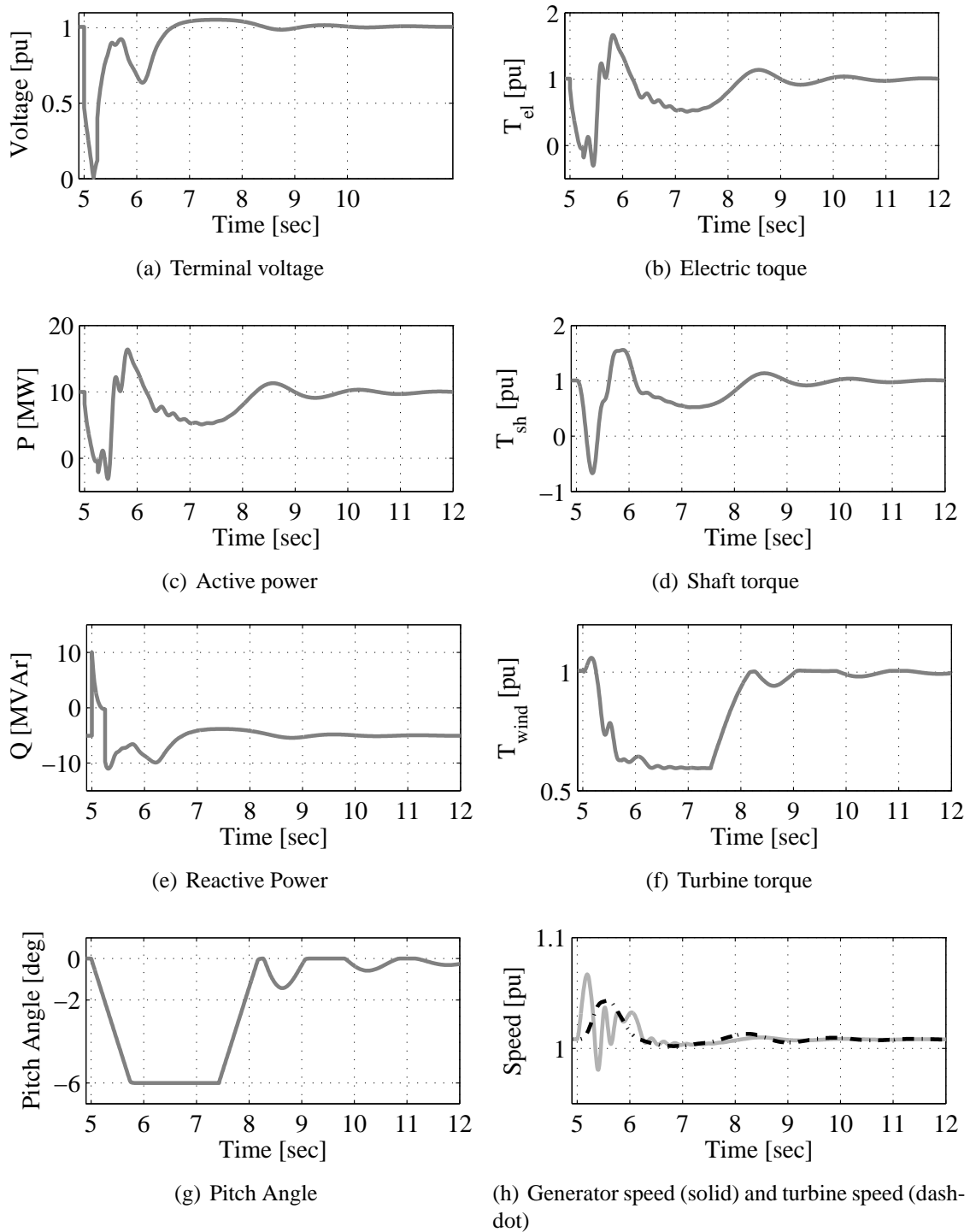
Figure 7.3: Fault ride-through response of active stall fixed-speed wind turbine.

is cleared and the rotor current goes down to a relatively low value, the rotor converter is restarted. The reference power is then ramped up.

7.2.3 Wind turbines with full power converter

A variable speed wind turbine with a full converter is relatively insensitive to faults compared to the other types. Hence, the turbine is able to ride-through without requiring significant modifications. During a fault, however, the capability of the converter to deliver active power from the turbine to the grid is reduced significantly. If no action is taken, this will lead to a dc-link over voltage due to an excess of energy from the generator. Several remedies can be implemented to overcome this problem, such as pitching out the blade, using a braking chopper, an over-dimensioned dc-link capacitor, or installing a battery and employing an over-dimensioned converter to allow more current flows during a fault. All these alternatives are governed by cost and requirements. The response of the converter to different types of fault is reported in [45].

Chapter 8

Conclusion and Future Work

8.1 Conclusion

The validation results suggest that the fifth-order model of an induction generator is sufficient to accurately represent the behaviors of an induction generator for power system studies. This reinforces the argument that the effect of saturation, core losses, skin effect and other more detailed representations of an induction generator can be neglected for such a study.

Incompatibility with the fundamental frequency network model and requirements for a small simulation time step are the main challenges in implementing the fifth-order model of an induction generator into typical power system stability studies. In this thesis, a modified model was proposed as an alternative solution. Compatibility with the fundamental frequency network model was achieved by excluding the dc-offset in the stator current that is injected to the grid. The problem with the simulation time step was overcome by an implementation of an internal integration loop. Different cases simulated in this thesis showed the feasibility of using the modified model in the fundamental frequency network model with a typical simulation time step: half of the system period.

As an alternative to the fifth-order model, the thesis proposed the use of an analytical method to estimate the peak transient current of an induction generator during faults, which is important in respect to the over current protection system, without necessarily using a detailed model such as the fifth-order model. This enables the use of the third-order model to provide more efficient simulations while the model is still capable of predicting the peak transient current.

The selection of an appropriate model of a wind turbine for power system stability studies shall be determined by the type of stability study. In other words, there is no single model of wind turbines that satisfies all types of stability studies, as by nature, there are always conflicts between desired accuracy and simulation efficiency. Requirements for different types of stability studies can be summarized as follows:

- **Short-term voltage stability study:** In general, a short-term voltage stability study requires a detailed representation of the wind turbine. The mechanical model must be represented at least by the two-mass model. For a passive stall wind turbine, the aerodynamic model is sufficient to represent the constant mechanical power or the constant mechanical torque. However, for an active stall wind turbine, the use of $C_p(\lambda, \beta)$ curve together with a pitch controller is required. This is because the action of the pitch controller must be taken into account.

Although the third-order model of an induction generator is less accurate in speed and peak current prediction, the use of the model is still considered as an optimum option. This is due to the fact that the overall inertia of the wind turbine is considerably large, as a consequence, the speed deviation during fault events between the fifth-order and the third-order model of an induction generator is insignificant. While the lack of ability of the third-order model to estimate the peak transient current can be overcome by using the analytical estimation method.

- **Long-term voltage stability study:** The first-order model of an induction generator in combination with the one-mass model of a drive train is the bottom limit for modelling a wind turbine for the study. However, the use of the third-order model of an induction generator with the two-mass model is recommended since the two-mass model of a drive train does not significantly influence simulation efficiency. While the use of the fifth-order model of an induction generator does not contribute to result accuracy.

- **Frequency stability study:** For a temporary and small frequency deviation ($\pm 5\%$) with a medium wind power penetration (less than 20%), the induction generator model can be adequately represented by the third-order model. However, when the penetration is higher and the frequency is significantly large for a long period, the use of the fifth-order model of an induction generator can be considered as a better option in order to achieve a more accurate prediction of active and reactive power response and energy production. The influence of the mechanical and aerodynamic model can be disregarded.

It should be recognized, however, that there is a need to provide a single model of a fixed-speed wind turbine that is able to perform different types of stability studies. A compromised solution can be using the model as proposed for a short-term voltage stability study, at the expense of slightly poor simulation efficiency for the other types of study, which require a longer simulation time frame.

Concerning the aggregated model of wind turbines, the thesis has shown that a wind farm consisting of a relatively small number of turbines can be practically represented as a single turbine model without any doubt. A representation of a large wind farm as a single turbine is fully acceptable to predicts the worse case scenario with all wind turbines tripped during fault, or the best case scenario with all wind turbines remaining intact during fault.

The fault ride-through capability of an active stall wind turbine was demonstrated. The scheme was able to maintain the turbine connected during the fault without leading to voltage instability. However a relatively high reactive power consumption during the ride through is unavoidable, unless some other measures, such as utilization of SVC or STATCOM, are considered.

8.2   Future work

One of the important topics for future work is to provide generic models for other common wind turbine technologies, such as the wind turbine with a doubly fed induction generator and the wind turbine with a full power converter. The main issue should focus on providing generalized models rather than on manufacturer specific models. This should be included in

efforts to develop more standardized wind turbine models for power system stability studies, especially an aggregated model of wind turbines, which do not currently exist.

From a system perspective, an investigation of cluster control of wind farms can be of important. Hence, rather than performing control schemes for an individual wind turbine, the control can be performed collectively comprising several wind turbines or wind farms. The type of control may extend from an active and reactive power control as well as a frequency control. A cluster power control is expected to ease problems of power balance, which is typical for areas with high wind power penetration. A reactive power control may consider advantages of utilizing wind turbine technology with reactive power capability, such as a wind turbine with a full power converter. Another possibility would be the application of a centralized reactive power control using SVC or STATCOM. As a consequence, more work is required to economically justify the feasibility of these schemes.

Bibliography

[1] "The Windicator," *WindPower Monthly*, vol. 22, no. 7, p. 66, July 2006.

[2] C. Ender, "International Development of Wind Energy Use - Status 31.12.2004," *DEWI Magazine*, no. 27, pp. 36–43, Aug. 2005.

[3] "IEA Wind Energy Annual Report 2005," International Energy Agency (IEA), Tech. Rep., June 2006.

[4] H. Holttinen, J.Pedersen, "The Effect of Large Scale Wind Power on a Thermal System Operation," in *Proc. of 4th International Workshop on Large-scale Integration of Wind Power and Transmission Networks for Offshore Wind Farms*, Stockholm, Sweden, Oct. 2003, p. 7.

[5] V. Akhmatov, "Analysis of Dynamic behavior of Electric Power System with Large Amount of Wind Power," Ph.D. dissertation, Technical University of Denmark, 2003.

[6] J. G. Slootweg, "Wind Power, Modelling and Impact on Power System Dynamics," Ph.D. dissertation, TU Delft, Netherland, Dec. 2003.

[7] V. Akhmatov, "An Aggregate Model of a Grid-Connected, Large-Scale, Offshore Wind Farm for Power Stability Investigations - Importance of Windmill Mechanical System," *Electrical Power and Energy Systems*, vol. 24, pp. 709–717, 2002.

[8] L.M. Fernandez, J.R. Saenz, F. Jurado, "Dynamic Models of Wind Farms with Fixed-Speed Wind Turbines," *Renewable Energy*, vol. 31, pp. 1203–1230, 2006.

[9] M. Poller, S. Achilles, "Aggregated Wind Park Models for Analyzing Power System Dynamics," Available: http://www.digsilent.de/Consulting/Publications.

[10] C. Jauch, P. Sørensen, B. B. Jensen, "Simulation Model of a Transient Fault Controller for an Active-Stall Wind Turbine," *Wind Engineering*, vol. 29, no. 1, pp. 33–47, 2005.

[11] V. Akhmatov, A. H. Nielsen, "Fixed-speed active-stall wind turbines in offshore applications," *Euro. Trans. Electrical Power*, vol. 15, pp. 1–12, Aug. 2004.

[12] T. Sun, "Power Quality of Grid-Connected Wind Turbines with DFIG and Their Interaction with the Grid," PhD Thesis, Aalborg University, Aalborg, Denmark, May 2004.

[13] J. Niiranen, "Voltage Dip Ride-Through of a Doubly Fed Generator Equipped with an Active Crowbar," in *Proc. of Nordic Wind Power Conference 2004*, Gothenburg, Sweden, Mar. 2004.

[14] A. Petersson, "Analysis, Modeling and Control of Doubly-Fed Induction Generators for Wind Turbines," Ph.D. dissertation, Chalmers University of Technology, 2005.

[15] P. Kundur, J. Paserba, V. Ajjarapu, G. Andersson, A. Bose, C. Canizares, N. Hatziargyriou, D. Hill, A. Stankovic, C. Taylor, T. Van Cutsem, V. Vittal, "Definition and Classification of Power System Stability IEEE/CIGRE Joint Task Force on Stability Terms and Definitions," *Power Systems, IEEE Transactions on*, vol. 19, no. 3, pp. 1387 – 1401, Aug. 2004.

[16] E. Hagstrom, I. Norheim, K. Uhlen, "Large-Scale Wind Power Integration in Norway and Effect on Damping in the Nordic Grid," in *Proc. Nordic Wind Power Conference*, March 2004.

[17] O. Carlson, A. Perdana, N. R. Ullah, M. Martins, E. Agneholm, "Power System Voltage Stability Related to Wind Power Generation," in *Proc. European Wind Energy Conference and Exhibition*. European Wind Energy Association, 2006.

[18] S.K. Salaman, A.L.J. Teo, "Windmill Modeling Consideration and Factors Influencing the Stability of a Grid-Connected Wind Power-Based Embedded Generator," *Power Systems, IEEE Transactions on*, vol. 18, no. 2, pp. 793–802, May 2003.

[19] G. Lalor, A. Mullane, M. O'Malley, "Frequency Control and Wind Turbine Technologies," *Power Systems, IEEE Transactions on*, vol. 20, no. 4, pp. 1905–1913, Nov. 2005.

[20] *PSS/E-29 Program Application Guide: Volume I*, Siemens PTI Ltd, 2002.

[21] "Dynamic Modelling of Wind Generation in Ireland," ESB National Grid, Ireland, Progress and Status Report, Jun. 2005.

[22] *PSS/E-29 Program Application Guide: Volume II*, Siemens PTI Ltd, 2002.

[23] *Advanced User's Manual DigSILENT Powerfactory version 12.1*, DigSILENT GmbH, Gomaringen, Germany, 2001.

[24] H. Antia, *Numerical methods for Scientists and Engineers*, 2nd ed. Basel, Switzerland: Birkhäuser Verlag, 2002.

[25] P. Kundur, *Power System Stability and Control*. New York: Elsevier, 1984.

[26] M. Pöller, M. Schmieg, "Exploiting Multiple Time Scale Properties for Fast Simulation Algorithms," in *Proc. 13th Power Systems Computation Conference*, 1999.

[27] T. Thiringer, "Grid-friendly Connecting of Constant-Speed Wind Turbines Using External Resistors," *Energy Conversion, IEEE Transactions on*, vol. 17, no. 4, pp. 537–542, Dec. 2002.

[28] ——, "Measurements and Modelling of Low-Frequency Disturbances in Induction Machines," PhD Thesis, Chalmers University of Technology, Gothenburg, Sweden, Nov. 1996.

[29] P.K. Kóvacs, *Transient Phenomena in Electrical Machine*. New York: McGraw-Hill, 1994.

[30] S. Heier, *Gid Integration of Wind Energy Conversion System*. England: John Wiley & Sons, 1998.

[31] T. Burton, D. Sharpe, N. Jenkins, *Hanbook of Wind Energy*. England: John Wiley & Sons, 2001.

[32] C. Jauch, A.D. hansen, P. Sørensen, F. Blaabjerg, "Simulation Model of an Active-Stall Fixed-Speed Wind Turbine Controller," *Wind Engineering*, vol. 29, no. 1, pp. 33–47, 2005.

[33] A.G. Gonzales Rodriguez, M. Burgos Paydn, C. Izquierdo Mitchell, "PSCAD Based Simulation of the Connection of a Wind Generator to the Network," in *Power Tech Proceedings, 2001 IEEE Porto*, vol. 4, Sept. 2001, p. 6.

[34] S.M. Bolik, "Modelling and Analysis of Variable Speed Wind Turbines with Induction Generator during Grid Fault," PhD Thesis, Aalborg University, Aalborg, Denmark, Oct. 2004.

[35] D. Ruiz-Vega, T. I. A. Olivares, D. O. Salinas, "An Approach to the Initialization of Dynamic Induction Motor Models," *Power Systems, IEEE Transactions on*, vol. 17, no. 3, pp. 747–751, Aug. 2002.

[36] M. Martins, A. Perdana, O. Carlson, E. Agneholm, P. Ledesma, "Validation of fixed-speed wind turbine dynamic models with measurement," *Accepted for publication in journal of Renewable Energy*, 2006.

[37] A. Perdana, S. Uski, O. Carlson, B. Lemström, "Validation of Aggragte Model of Wind Farm with Fixed-speed Wind Turbines against Measurement," in *Proc. of Nordic Wind Power Conference 2006*, Espoo, Finland, May 2006.

[38] J.O.G. Tande, I. Norheim, O. Carlson, A. Perdana, J. Pierik, J. Morren, A. Estanqueiro, J. Lameira, P. Sørensen, M. O'Malley, A. Mullane, O. Anaya-Lara, B.Lemström, S. Uski, E. Muljadi, "Benchmark test of dynamic wind generation models for power system stability studies," *Submitted to IEEE Transactions on Power Systems*.

[39] P. Nørgaard, H. Holttinen, "A Multi-Turbine Power Curve Approach," in *Proc. of Nordic Wind Power Conference*, Gothenburg, Sweden, Mar. 2004.

[40] *Affärsverket svenska kraftnäts föreskrifter och allmänna råd om driftsäkerhetsteknisk utformning av produktionsanläggningar*, Svenska Kraftnät, Sweden, Jan. 2004.

[41] C. Jauch, P. Sørensen, B. Bak-Jensen, "International Review of Grid Connection Requirements for Wind Turbines," in *Proc. of Nordic Wind Power Conference 2004*, Gothenburg, Sweden, Mar. 2004.

[42] J. Matevosyan, T. Ackermann, S. Bolik, L.Söder, "Comparison of International Regulations for Connection of Wind Turbines to the Network," in *Proc. of Nordic Wind Power Conference 2004*, Gothenburg, Sweden, Mar. 2004.

[43] A. Dummer, B. I. Kozma, P. Mortensen, H. Abildgaard, M. Luther, J. L. Javerzac, J. M. Rodríguez-García, T. B. Scirocco, W. Kling, W. Winter, "Wind Power in the UCTE Interconnected System," Union for the Co-ordination of Transmission of Electricity (UCTE)," Technical Report, 2004, Available: http://www.ucte.org.

[44] A. Perdana, O. Carlson, J. Person, "Dynamic Response of Wind Turbine with DFIG During Disturbances," in *Proc. of IEEE Nordic Workshop on Power and Industrial Electronics (NORpie)*, Trondheim, Norway, Jun. 2004.

[45] R. Ottersten, A. Petersson, Pietiläinen, "Voltage Sag Response of PWM Rectifiers for Variable-Speed Wind Turbines," in *Proc. of IEEE Nordic Workshop on Power and Industrial Electronics (NORpie)*, Trondheim, Norway, Jun. 2004.

Appendix A

Formula Derivation of an Induction Machine Model as a Voltage Source behind a Transient Impedance

The stator and rotor equations of induction machine can be written as

$$\mathbf{v_s} = \mathbf{i_s}R_s + j\omega_s \boldsymbol{\psi_s} + \frac{d\boldsymbol{\psi_s}}{dt} \tag{A.1}$$

$$\mathbf{v_r} = \mathbf{i_s}R_r + js\omega_s \boldsymbol{\psi_r} + \frac{d\boldsymbol{\psi_r}}{dt} \tag{A.2}$$

The stator and rotor flux are given by

$$\boldsymbol{\psi_s} = \mathbf{i_s}L_s + \mathbf{i_r}L_m \tag{A.3}$$

$$\boldsymbol{\psi_r} = \mathbf{i_r}L_r + \mathbf{i_s}L_m \tag{A.4}$$

where

$$L_s = L_{\sigma s} + L_m \tag{A.5}$$

$$L_r = L_{\sigma r} + L_m \tag{A.6}$$

$$\mathbf{i_r} = \frac{\boldsymbol{\psi_r} - \mathbf{i_s}L_m}{L_r} \tag{A.7}$$

Substitution of (A.7) into (A.3) yields

$$
\begin{aligned}
\boldsymbol{\psi_s} &= \mathbf{i_s}L_s + \frac{L_m}{L_r}\boldsymbol{\psi_r} - \frac{{L_m}^2}{L_r}\mathbf{i_s} \\
&= \mathbf{i_s}\left(L_s - \frac{{L_m}^2}{L_r}\right) + \frac{L_m}{L_r}\boldsymbol{\psi_r}
\end{aligned} \tag{A.8}
$$

Now, the transient reactance is introduced as

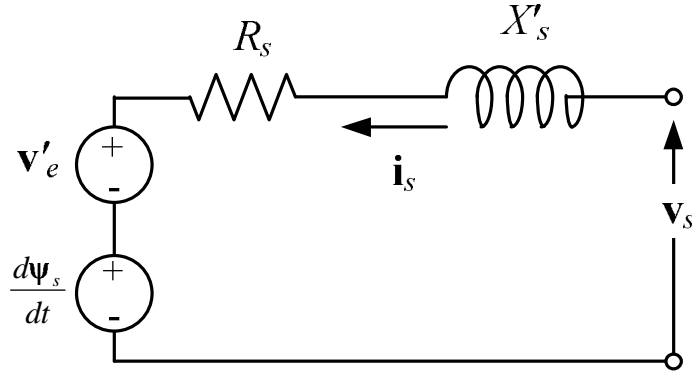$$X' = \omega_s\left(L_s - \frac{{L_m}^2}{L_r}\right) \tag{A.9}$$

Figure A.1: Transient representation of the fifth-order induction generator.

Substituting (A.9) into (A.8)

$$\boldsymbol{\psi_s} = \mathbf{i_s}\frac{X'}{\omega_s} + \frac{L_m}{L_r}\psi_r \tag{A.10}$$

Introducing voltage components defined as

$$\mathbf{v_e} = j\frac{\omega_s L_m}{L_r}\boldsymbol{\psi_r} \tag{A.11}$$

Substituting (A.11) into (A.10)

$$\boldsymbol{\psi_s} = \mathbf{i_s}\frac{X'}{\omega_s} - j\frac{\mathbf{v_e}}{\omega_s} \tag{A.12}$$

Substituting (A.12) into (A.1) while keeping the last derivative unchange we obtain

$$\mathbf{v_s} = R_s\mathbf{i_s} + jX'\mathbf{i_s} + \mathbf{v_e} + \frac{d\boldsymbol{\psi_s}}{dt} \tag{A.13}$$

The transient representation of (A.13) can be depicted as shown in Figure A.1

By eliminating the rotor current and expressing the rotor flux in term of $\mathbf{v_e}$, the rotor equation will be

$$\frac{d\mathbf{v'_e}}{dt} = \frac{1}{T_o}[\mathbf{v'_e} - j(X_s - X')\mathbf{i_s}] + js\mathbf{v'_e} + j\frac{X_m}{X_r}\mathbf{v_r} \tag{A.14}$$

By removing derivative in the stator voltage equation the third order model of the machine can be obtained. Subsequently, the transient representation is shown in Figure A.2

The torque equation can be expressed as

$$T_e = \Im\left[\boldsymbol{\psi_s}\mathbf{i_s}^*\right] \tag{A.15}$$

Substituting (A.7) into (A.15), we have

$$T_e = \Im\left[\left(\mathbf{i_s}\frac{X'}{\omega_s} + j\frac{\mathbf{v_e}}{\omega_s}\right)\mathbf{i_s}^*\right] \tag{A.16}$$

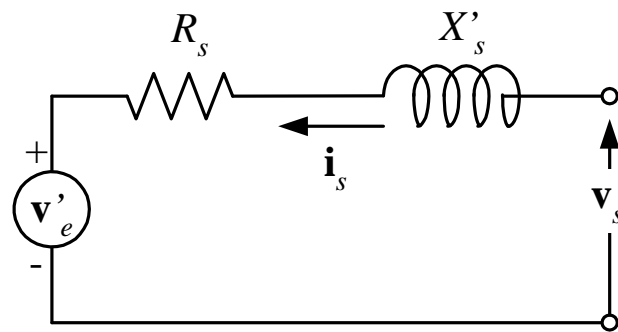$$T_e = \Im\left[j\frac{\mathbf{v_e}}{\omega_s}\mathbf{i_s}^*\right] \tag{A.17}$$

Figure A.2: Transient representation of the third-order induction generator.

Appendix B

Blade Element Method

According to the blade element method (sometimes called the blade element theory or the blade element momentum) [30, 31] a turbine blade is divided into several cross-sections along the radius. The total forces applied to the blade are the sum of force on each section. Two major force components that act on each blade segment are (see Figure B.2): (1) lift force, which occurs because of the pressure difference between the upper and the lower side of the blade, the force direction is orthogonal to the equivalent wind speed, and (2) drag force, which acts on the same direction of the equivalent wind speed.
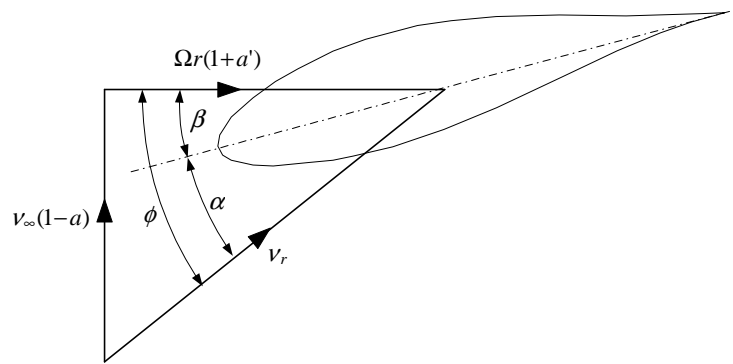
Figure B.1: Wind velocity components in blade element method.

The relative wind velocity is

$$\nu_r = \sqrt{\nu_\infty^2(1-a)^2 + \Omega^2 r^2 (1+a')^2} \tag{B.1}$$

Consider an N blade turbine with cord length c, the axial rotor torque is given by

$$T = \int \frac{1}{2}\rho\nu_r^2 Nc(C_L sin\phi - C_D cos\phi)r\partial r \tag{B.2}$$

Typical value of lift and drag coefficient for different angle of attack is shown in Figure B.3.
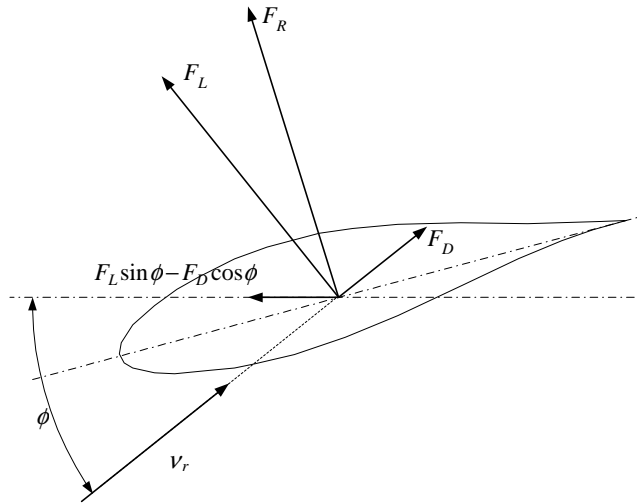
Figure B.2: Forces act on a turbine rotor blade segment in blade element method.

Notation

ν_∞ is the far upstream wind velocity or the undisturbed wind velocity.

a is the axial flow induction factor, this constant represent fractional reduction in wind velocity at the rotor plane (actuator disc) compared to the undisturbed wind velocity.

a' is the tangential flow induction factor.

ν_r is the relative wind velocity at the blade.

α is the angle of attack.

β is the pitch angle.

ϕ is the angle of relative wind velocity v_r to the rotor plane.

Ω is the rotational speed of the turbine rotor.

r is the radial position of the blade section.

C_L is the lift coefficient.

C_D is the drag coefficient.

F_L is the lift force.

F_D is the drag force.
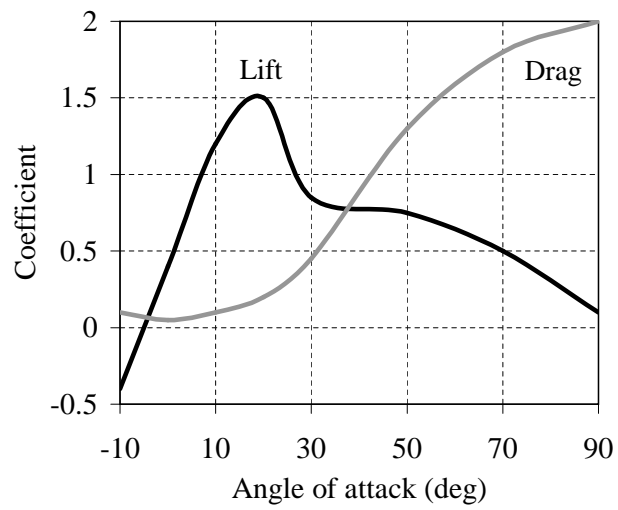
F_R is the resultant force.

Figure B.3: Lift and drag coefficient for a typical blade.

Appendix C

Alsvik Wind Turbine Parameters

Table C.1: Wind turbine parameters.

Parameter	Value	Units
Hub height	30	m
Rotor diameter	23.2	m
Rotor rated speed	42	r.p.m.
Gearbox ratio	23.75	
Turbine inertia constant H_t	2.6	s
Generator inertia constant H_g	0.22	s
Stiffness constant K	141.0	p.u.
Damping factor (when applied) D	3.0	p.u.

Table C.2: Generator parameters.

Parameter	Value	Units
Rated power	210	kVA
Rated voltage	415	V
Stator resistance R_s	0.0121	p.u.
Stator leakage inductance X_s	0.0742	p.u.
Mutual inductance X_m	2.7626	p.u.
Rotor resistance R_r	0.0080	p.u.
Rotor leakage inductance X_r	0.1761	p.u.

Table C.3: Compensating capacitor parameters.

Parameter	Value	Units
Grid rated voltage	400	V
Capacitor bank susceptance B	0.11	p.u.

Appendix D

Olos Wind Farm Parameters

Table D.1: Generator parameters.

Parameters	Values	Units
Power rating (P_n)	600	kW
Voltage rating	690	V
Stator resistance (R_1)	0.0642	pu
Stator reactance (X_1)	0.0067	pu
Magnetizing reactance (X_m)	2.79	pu
Rotor resistance (R_2')	0.0799	pu
Rotor reactance (X_2')	0.0920	pu

Table D.2: Mechanical shaft parameters.

Parameters	Values	Units
Turbine inertia (J_t)	210	kgm2
Generator inertia (J_g)	16	kgm2
High speed shaft and gearbox inertia (estimated)	8	kgm2
Spring constant (k)	7965	Nm/rad
Gear ratio (gr)	55	

Table D.3: No-load reactive power compensator.

Parameters	Values	Units
High-speed mode	162.5	kVAr
Low-speed mode	62.5	kVAr

Table D.4: Transformer data.

Parameters	Values	Units
Type	21/0.69 kV Dyn11	
Power rating (S_n)	800	kVA
Short-circuit impedance (Z_k)	4.8	%
Short-circuit power (P_k)	6730	W
Power at no-load (P_o)	934	W

Table D.5: Rising cable to the generator.

Parameters	Values & Units
Impedance (Z)	$0.0138\Omega/7.8°$

Table D.6: Grid data (21 kV side of the wind turbine step-up transformer.)

Parameters	Values & Units
Impedance (Z_k)	$8.27\Omega/60°$

Table D.7: Line from wind farm to the substation.

Parameters	Values & Units
Impedance (Z)	$4.08\Omega\angle25°$

Appendix E

Parameters Used for Simulation of Frequency Deviation

Table E.1: Synchronous generator (GENSAL) parameters.

Parameters	Values	Units
T'_{do}	5	sec
T''_{do}	0.05	sec
T''_{qo}	0.1	sec
Inertia (H)	3	pu
Speed damping (D)	0	pu
X_d	1.1	pu
X_q	0.7	pu
X'_d	0.25	pu
$X''_d = X''_q$	0.2	pu
X_l	0.15	pu
$S(1.0)$	0.1	pu
$S(1.2)$	0.3	pu

Table E.2: Hydro governor (HYGOV) parameters.

Parameters	Values	Units
Permanent droop (R)	0.04	
Temporary droop (r)	0.8	
Governor time constant (T_r)	5	sec
Filter time constant (T_f)	0.05	sec
Servo time constant (Tg)	0.2	sec
Gate velocity limit (VELM)	0.1	
Maximum gate limit (GMAX)	0.95	
Minimum gate limit (GMIN)	0	
Water time constant (TW)	1	
Turbine gain (A_t)	1	
Turbine damping (D_{turb})	0	
No load flow (q_{NL})	0	

Appendix F

Wind Turbine Parameters

Table F.1: Generator parameters.

Parameters	Values	Units
Power base (S_{base})	781	kVA
Voltage base (U_{base})	690	V
Stator resistance (R_s)	0.00539	pu
Stator leakage reactance (X_{sl})	0.09062	pu
Magnetizing reactance (X_m)	3.31065	pu
Rotor resistance (R_r)	0.007616	pu
Rotor leakage reactance (X_{rl})	0.100718	pu
Generator rotor inertia constant (H_g)	0.53273	s

Table F.2: Drive-train parameters.

Parameters	Values	Units
Power base (S_{base})	781	kVA
Turbine rotor and low speed shaft inertia constants (H_t)	5.8	s
Shaft stiffness (K_s)	0.5603	